Hemoglobin nanoparticles equipped with antioxidant coatings as a novel type of therapeutic oxygen carriers

Chen, Jiantao

Publication date:
2023

Document Version
Publisher's PDF, also known as Version of record

DTU

DTU Health Tech

Hemoglobin nanoparticles equipped with antioxidant coatings as a novel type of therapeutic oxygen carriers

Jiantao Chen (陈健涛)

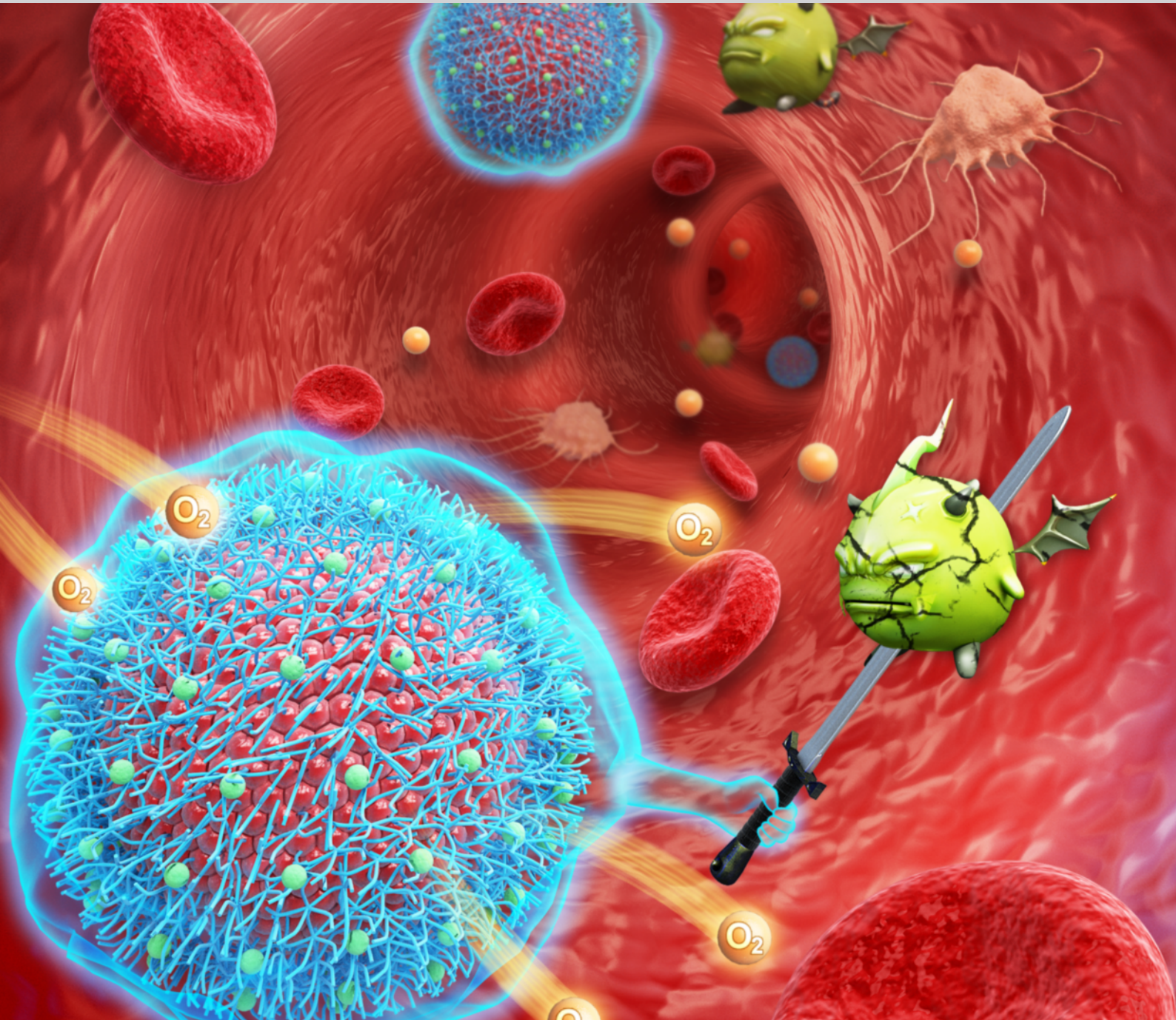

University: Technical University of Denmark

Department: Department of Health Technology

Author: Jiantao Chen

Title: Hemoglobin nanoparticles equipped with antioxidant coatings as a novel type of therapeutic oxygen carriers

Supervisors: Leticia Hosta-Rigau (Associate Professor, Technical University of Denmark)

Xiaoli Liu (Researcher, Technical University of Denmark)

Assessment Committee:

Yi Sun (Associate Professor, Technical University of Denmark)

Lene Jørgensen (Associate Professor, University of Copenhagen)

Yunlu Dai (Associate Professor, University of Macau)

Preface

This thesis is written in fulfillment of the requirements for the Ph.D. degree set by the Technical University of Denmark (DTU). The work described in this thesis was performed at the Biomimetics, Biocarriers and Bioimplants Group (The 3Bs) headed by Associate Professor Leticia Hosta-Rigau, which is part of the Centre for Nanomedicine and Theranostics, and the Department of Health Technology, at DTU.

The work presented was carried out from October 2019 to January 2023, under the supervision of Associate Professor Leticia Hosta-Rigau and Researcher Xiaoli Liu.

This work has been supported by the Danish Council for Independent Research (Grant No. 6111-00298B).

Jiantao Chen

Copenhagen, January 2023

Acknowledgments

First and foremost, I would like to express my heartfelt gratitude to my main supervisor Associate Professor Leticia Hosta-Rigau. Thank you for giving me the chance to study in this group and thank you for the very valuable guidance and kind help throughout my PhD project. Moreover, I would like to thank my co-supervisor Xiaoli Liu, thank for your kind help especially the very valuable help in the 2nd part of my PhD project.

Then, I would like to thank Associate Professor Peter Waaben Thulstrup (Department of Chemistry, University of Copenhagen), thank for your guidance in using circular dichroism and for giving me access to this equipment.

Furthermore, I would like to thank my colleagues in 3Bs group. I especially appreciate Michelle for joining my PhD project and your very kind and valuable help in the trouble shooting during my PhD project. Also, my gratitude goes to Clara and Marta for the help in SEM images taking; and to Shahana, thank you for your encouragement and help. Next, I would like to thank Max, Aurelie, Eva, Gizem, Weiguang, Fatemeh, and Sadegh for being great colleagues, and to thank Christina and Christian for being great office mates.

Last but not the least, I would like to thank my family and friends, especially my wife Xingli, my daughter Kangyi, and my parents, I am very grateful for your supporting and understanding in my PhD.

Abstract

The transfusion of red blood cells (RBCs) is a well-established clinical procedure for patients experiencing acute blood loss. However, there are several challenges associated with blood transfusions. These include the need for blood typing and matching, particular storage conditions, a short shelf-life, potential risks of virus transmission, and a global shortage in blood availability. As such, there is an imminent demand for the development of RBCs substitutes to overcome these challenges and supplement blood transfusions. Prominent advances in the development of hemoglobin (Hb)-based oxygen carriers (HBOCs) as RBC substitutes have been made in the past decades. Nonetheless, several shortcomings of the reported HBOCs still need to be addressed, including the preservation Hb's functionality and achieve a high Hb content to obtain a high oxygen (O_2) delivering capacity.

In the current thesis, these challenges have been addressed to obtain HBOCs not only with a high Hb content, but also with remarkable antioxidant properties that shield this Hb from autoxidation into non-functional methemoglobin (metHb). For this, a desolvation technique and different functional surface coating techniques were employed.

Desolvation techniques have previously been used for the fabrication of protein particles both in nano- and micro-sizes. Here, the assembly of nanoparticles (NPs) fully made of Hb (Hb-NPs) by the desolvation technique was demonstrated. For this, several desolvation-related parameters were optimized (i.e., Hb concentration, the ratio of organic phase/water phase, and sonication intensity/time) to obtain Hb-NPs with a size of ~568 nm and a polydispersity index of ~0.2. Next, a surface functionalization with a polydopamine (PDA) coating was performed to further stabilize the Hb-NPs and, more importantly, provide them with antioxidant properties. The resulting PDA-coated Hb-NPs (Hb/PDA-NPs) were able to scavenge reactive oxygen species such as superoxide radical anion and hydrogen peroxide. Most importantly, PDA's antioxidant features protected the encapsulated Hb from autooxidation into metHb. Furthermore, the biocompatibility and ability of the Hb/PDA-NPs to reversibly bind O_2 were also demonstrated.

Next, for better preservation of Hb functionality within the Hb-NPs, process optimizations were performed. These included the desolvation being carried out at 4 °C and the use of a different metal phenolic network (MPN) coating consisting of tannic acid and iron (III) ions. The resulting MPN-

coated Hb-NPs (MPN@Hb-NPs) were spherical NPs with a size of ~250 nm and a polydispersity index of ~0.1. The encapsulated Hb well maintained its O_2 delivery capacity in the MPN@Hb-NPs. Furthermore, these modified Hb-NPs could scavenge multiple reactive oxygen and nitrogen species due to the MPN coating. This was demonstrated also in the presence of donor RBCs, macrophages, and endothelial cells. Moreover, Hb protection by the antioxidant MPN coating was suggested by a decreased metHb conversion. Lastly, the MPN@Hb-NPs were also remarkably biocompatible, suggesting their great potential as HBOCs.

Overall, these reported HBOCs with an antioxidant surface coating and a high Hb content are a step forward towards the development of a new generation of improved HBOCs.

Dansk resumé

Transfusion af røde blodlegemer (RBC'er) er en udbredt og anerkendt klinisk procedure til patienter, der får akut blodtab. Der er dog adskillige udfordringer forbundet med blodtransfusioner. Disse omfatter behovet for blodtypebestemmelse og matchning, særlige opbevaringsforhold, kort holdbarhed, potentielle risici for virusoverførsel og en global mangel på blod. Derfor er der en imminent efterspørgsel efter udvikling af RBC-erstatninger for at overvinde disse udfordringer og supplere blodtransfusioner. Store fremskridt i udviklingen af hæmoglobin (Hb)-baserede oxygenbærere (HBOC'er), som RBC-erstatninger, er blevet gjort i de sidste årtier. Ikke desto mindre skal flere mangler/svagheder ved de rapporterede HBOC'er stadig løses, herunder bevarelsen af Hb's funktionalitet og høje hæmoglobinindhold, for at opnå en høj ilt (O_2) leveringskapacitet.

I den aktuelle afhandling er disse udfordringer blevet behandlet for at opnå HBOC'er ikke kun med et højt Hb-indhold, men også med bemærkelsesværdige antioxidantegenskaber, der beskytter dette Hb fra autoxidation til ikke-funktionelt methæmoglobin (metHb). Til dette blev der anvendt en desolvationsteknik og forskellige funktionelle overfladecoatningsteknikker.

Desolvationsteknikker er tidligere blevet brugt til fremstilling af proteinpartikler både i nano- og mikrostørrelser. Her blev samlingen af nanopartikler (NP'er) lavet af Hb (Hb-NP'er) ved desolvationsteknikken demonstreret. Til dette blev adskillige desolvatiseringsrelaterede parametre optimeret (dvs. Hb-koncentration, forholdet mellem organisk fase/vand fase og sonikeringsintensitet/tid) for at opnå Hb-NP'er med en størrelse på ~568 nm og et polydispersitetsindeks på ~0,2. Dernæst blev en overfladefunktionalisering med en polydopamin (PDA) belægning udført for yderligere at stabilisere Hb-NP'erne og endnu vigtigere, give dem antioxidantegenskaber. Disse egenskaber gjorde det således muligt for de PDA-coatede Hb-NP'er (Hb/PDA-NP'er) at opfange reaktive oxygenarter såsom superoxid radikal anion og hydrogenperoxid. Derudover beskyttede PDA's antioxidantegenskaber Hb mod oxidation til metHb. Desuden blev biokompatibiliteten og evnen af Hb/PDA-NP'erne til reversibelt at binde O_2 også demonstreret.

Dernæst, for bedre bibeholdelse af Hb-funktionalitet inden for Hb-NP'erne, blev procesoptimeringer udført. Disse omfattede desolveringen, der blev udført ved 4 °C og brugen af en alternativ metal-phenoliske netværk (MPN) belægning, bestående af garvesyre og jern(III)-ioner. De resulterende MPN-coatede Hb-NP'er (MPN@Hb-NP'er) var faste (solide) NP'er med en størrelse på ~250 nm og

et polydispersitetsindeks på ~0,1. Hb'et bibeholdt sin oxygenleveringskapacitet i MPN@Hb-NP'erne godt. Desuden kunne disse modificerede Hb-NP'er opfange flere reaktive O_2- og nitrogenarter på grund af MPN-belægningen. Dette blev demonstreret ikke kun i opløsninger, men også i tilstedevær af donor-RBC'er, makrofager og endotelceller. Desuden blev Hb-beskyttelse af antioxidanten MPN-belægningen begrundet af en reduceret metHb-omdannelse. Endelig var MPN@Hb-NP'erne også bemærkelsesværdigt biokompatible, hvilket indikerer at de har stort potentiale som HBOC'er.

Samlet set er disse rapporterede HBOC'er med en antioxidantoverfladebelægning og et højt Hb-indhold et skridt fremad mod udviklingen af en ny generation af forbedrede HBOC'er.

List of Publications

The thesis is based on the article contributions listed below.

Coll-Satue, C. †; Bishnoi, S. †; **Chen, J. †**; Hosta-Rigau, L. Stepping Stones to the Future of Haemoglobin-Based Blood Products: Clinical, Preclinical and Innovative Examples. *Biomater Sci* 2021, 9 (4), 1135–1152. https://doi.org/10.1039/D0BM01767A
(† These authors contributed equally)

Chen, J.; Jansman, M. M. T.; Liu, X.; Hosta-Rigau, L. Synthesis of Nanoparticles Fully Made of Hemoglobin with Antioxidant Properties: A Step toward the Creation of Successful Oxygen Carriers. *Langmuir* **2021**, *37* (39), 11561–11572. https://doi.org/10.1021/acs.langmuir.1c01855

Chen, J.; Liu, X.; Jansman, M. M. T.; Thulstrup, P. W.; Hosta-Rigau, L. Metal-Phenolic Networks as Broad-Spectrum Antioxidant Coatings for Hemoglobin Nanoparticles Working as Oxygen Carriers. *Chemistry of Materials* **2022**, *34* (20), 9200–9211. https://doi.org/10.1021/acs.chemmater.2c02190.

Materials reproduced from publications

This thesis contains three original manuscripts listed above under permission. As such, the figures and textual parts are copyrighted by Royal Society of Chemistry (2021), American Chemical Society (2021), and American Chemical Society (2022). The styles were adjusted to fit the thesis.

Contents

List of Abbreviations

Abs	Absorbance
ABTS	2,2’-azino-bis(3-ethylbenzothiazoline-6-sulfonic acid) diammonium salt
BCA	Bicinchoninic acid
BSA	Bovine serum albumin
CA	Carbonic anhydrase
$CaCO_3$	Calcium carbonate
CAT	Catalase
CD	Circular dichroism
CeO_2-NPs	Cerium oxide nanoparticles
CO_2	Carbon dioxide
DA	Dopamine
Deoxy-Hb	Deoxygenated Hb
DIC	Differential interference contrast
DLS	Dynamic light scattering
DMEM	Dulbecco’s Modified Eagle’s medium-high glucose
DOX	Doxorubicin
$DPPH^{\bullet}$	2,2-diphenyl-1-picrylhydrazyl
ECM	Endothelial cell medium
EDTA	Ethylenediaminetetraacetic acid
EtOH	Ethanol absolute
FBS	Fetal bovine serum
Fe_3O_4	Iron oxide
$FeCl_3 \cdot 6H_2O$	iron (III) chloride hexahydrate
FI	Fluorescence intensity
FTIR	Fourier-transform infrared spectroscopy
GPx	Glutathione peroxidase
GSH	Glutathione
GA	Glutaraldehyde

H_2O	Water
H_2O_2	Hydrogen peroxide
Hb	Hemoglobin
HBOC	Hb-based oxygen carrier
HbV	Hemoglobin vesicle
HCl	Hydrochloric acid
HIV	Human immunodeficiency virus
HRP	Horseradish peroxidase
HSA	Human serum albumin
HUVEC	Human umbilical vein endothelial cell line
KO_2	Potassium dioxide
MetHb	Methemoglobin, ferric Hb
$MnCO_3$	Manganese carbonate
MOF	Metal-organic framework
MPN	Metal phenolic network
MPS	Mononuclear phagocyte system
MW	Molecular weight
MQ	Milli-Q, ultrapure water
N_2	Nitrogen
nAbs	Normalized absorbance
NaCl	Sodium chloride
$NADP^+$/ NADPH	Nicotinamide adenine dinucleotide phosphate
nCV	Normalized cell viability
nFI	Normalized fluorescence intensity
NO	Nitric oxide
NPs	Nanoparticles
O_2	Oxygen
$O_2^{\bullet-}$	Superoxide radical anion
ODC	Oxygen dissociation curve
Oxy-Hb	Oxygenated Hb

p50	pO_2 at which Hb is 50% saturated with oxygen
PBS	Phosphate buffer saline
pCO_2	Partial pressure of carbon dioxide
PDA	Polydopamine
PDI	Polydispersity index
PEG	Poly(ethylene glycol)
PFC	Perfluorocarbon
PLA	Poly(lactide)
PLGA	Poly(lactide-co-glycolide)
pO_2	Partial pressure of oxygen
Pt-NP	Platinum nanoparticle
RBCs	Red blood cells
ROS	Reactive oxygen species
R-state	Relaxed state
SDT	Sodium dithionite
SOD	Superoxide dismutase
TRIS	Tris(hydroxymethyl) aminomethane
T-state	Tense state
TA	Tannic acid
XO	Xanthine oxidase
ζ-potential	Zeta-potential

Chapter 1

Introduction

The information in Section 1.1-1.2 in Chapter 1 was directly taken or slightly adapted (both in Arial format) from: Coll-Satue, C.; Bishnoi, S.; **Chen, J.**; Hosta-Rigau, L. Stepping Stones to the Future of Haemoglobin-Based Blood Products: Clinical, Preclinical and Innovative Examples. *Biomater Sci* 2021, 9 (4), 1135–1152. https://doi.org/10.1039/D0BM01767A

1.1. Background

The transfusion of whole blood but also of various isolated components (e.g., packed red blood cells (RBCs), platelet concentrates or plasma) is an indispensable and common clinical procedure. Specifically, blood transfusions are widely employed in conditions of serious blood disorders such as anemia, hemophilia or for patients receiving tumour chemotherapy.[1] In addition, blood transfusions are also extensively used in the context of traumatic injuries and surgical operation (e.g., transplants).[2] Despite its many advantages, the use of donor blood has several limitations and risks. For example, there is a limited availability since only 10% of eligible donors actually donate blood.[3] Unfortunately, this short supply of blood is expected to get worse due to increased population growth and aging. What is more, only 7% of the donors have blood that can be immediately used in emergencies (i.e., "universal" O-negative blood).[3] Thus, before blood can be transfused, there is a need for crossmatching and blood group typing which can cause fatal delays in emergency situations. Blood-based products have a short storage lifetime of a maximum of 42 days under refrigerated conditions and 1 day at room temperature. This short shelf-life makes it impossible to create large stockpiles to be used in acute disasters (e.g., earthquakes, plane crashes or terrorist attacks). Furthermore, the need for refrigerated conditions creates major logistical challenges when donor blood is needed in austere and remote battlefield or civilian locations.[4–6] In addition, both RBCs and platelets develop storage lesions over time affecting their stability, physiology and their in vivo circulation time.[7,8] For example, while RBCs can circulate in the bloodstream for about 120 days, this time is reduced to only 28 days for donor RBCs. Blood products are also a transmission vector for infectious diseases such as human immunodeficiency (HIV) virus, Zika virus and hepatitis B or C. This results in extensive and costly screening prior to transfusion.[3] Lastly, of the 75 million units of RBCs that are collected worldwide, 13 million are currently not being tested for HIV.[9] While research efforts have been focused on resolving these issues to enhance the availability and applicability of donor-derived blood products,[10–13] in parallel, a robust volume of research has been devoted to creating semi- or fully synthetic artificial oxygen (O_2) carriers. It is envisioned that such an approach will revolutionize the practices in blood banking and transfusion medicine.[14] Artificial O_2 carriers are specifically designed to substitute and even amplify the functions of endogenous blood components. Additionally, such a (semi)-synthetic platform will have several advantages over donor blood including: sufficient availability, since it can be produced at a large scale; prolonged storage across a wide range of environmental conditions, thus having easy storage and portability; absence of disease transmission, since they

could be sterilized without compromising their functionality; universal application since blood group antigens are absent thus avoiding the need for typing and cross-matching.[15,16]

For the artificial O_2 carriers, two promising candidates have developed: perfluorocarbon (PFC)-based emulsions and hemoglobin (Hb)-based oxygen carriers (HBOCs). PFC-based emulsions were developed by making use of the remarkable ability to dissolve gasses (e.g., O_2 and CO_2) of PFC, however, obvious drawbacks such as low emulsion stability, weak O_2-carrying interactions, as well as activation of the mononuclear phagocyte system (MPS) limited the development of PFC-based emulsions. Meanwhile, HBOCs, which make use of the excellent O_2-carrying/releasing properties of native Hb (mainly obtained from either bovine blood or outdated donor blood), have been also widely investigated. Thus, I focus on developing the most promising HBOCs in this thesis.

1.1.1. Hemoglobin.

1.1.1.1. The structure and functionality of Hb.

The transportation of O_2 in the body is conducted by Hb, which is the main component of RBCs (Scheme 1.1A). Hb is responsible for the transport of 98% of all the O_2 while the remaining 2% is dissolved in blood plasma. In an adult human, around 250 million Hb molecules with a weight of 27-31 pg can be found in each RBC. This accounts for one third of the total volume of an RBC. In fact, to allow for a high Hb loading, mature human RBCs do not have a nucleus and are missing most of the organelles present in other eukaryotic cells (e.g., mitochondria or Golgi apparatus). Hb is a tetrameric protein with a molecular weight (MW) of 64.5 kDa. As suggested by its name, Hb is constituted of “heme groups” (non-protein part) and “globins” (protein part). Specifically, Hb is composed of two alpha and two beta subunits (α1β1α2β2) and each subunit contains a heme group and a polypeptide globulin chain (Scheme 1.1B). The alpha globulin chains consist of 141 amino acid residues and the beta chains are slightly bigger with 146 amino acids.[17] The heme group is comprised of a protoporphyrin ring with an iron ion bound to the centre, which is responsible for O_2 transport. Since each iron ion can carry one O_2 molecule, a total of four O_2 can be transported by each Hb. Importantly, for O_2 transport, the iron ion must be in the reduced state (ferrous form: Fe^{2+}).

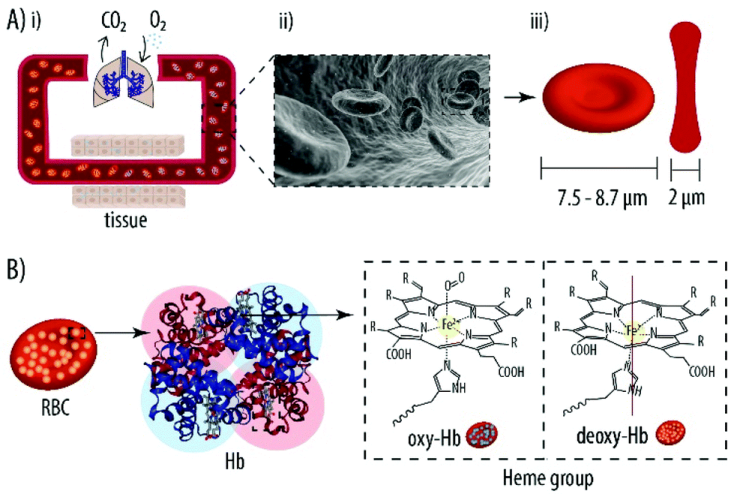

Scheme 1.1. (A) (i) Schematic illustration of red blood cells (RBCs) travelling from the lungs (oxygen (O_2)-loading site) to the tissues where O_2 is released. The RBCs also carry carbon dioxide (CO_2) from the tissues and to the lungs for excretion. Schematic representation of RBCs circulating within a blood vessel (ii) and showing their diameter and thickness (iii). (B) Multi-scale representation of RBCs and hemoglobin (Hb). Hb is composed of two alpha (red) and two beta (blue) subunits constituting the "globins" (protein part). Each globin contains a heme group in the centre (non-protein part), which changes conformation from an oxygenated (oxy-Hb) to a deoxygenated (deoxy-Hb) state.

Throughout the bloodstream, Hb is exposed to different partial O_2 pressures (pO_2) and the O_2 binding kinetics to Hb is positively cooperative. This means that, a small variation in pO_2 results in a large change in the amount of O_2 captured or released by Hb. Thus, in the lungs, where there is high pO_2, Hb predominates in the relaxed state (R-state) displaying a high affinity for O_2 (Scheme 1.2A). In this R-state, Hb readily binds to O_2 (oxy-Hb). As a result, within the lung capillaries, Hb is nearly saturated with approximately 98% of its O_2-binding sites occupied. However, as blood transits from the lungs to the tissues with a lower pO_2, Hb changes its conformation to the tense state (T-state). In the T-state, also known as the unbound state (deoxy-Hb), Hb has a low affinity towards O_2, thus promoting its release into the tissues.[18] An O_2 dissociation curve (ODC) is obtained by plotting the percentage of saturated Hb (y) versus pO_2 (x) (Scheme 1.2B). Such a curve displays a sigmoidal shape highlighting that O_2 binding takes place in a positively cooperative fashion. The ODC shows a plateau for high pO_2 indicating complete saturation of Hb. Several physiological factors can influence the O_2 binding kinetics to Hb and this will result in shift for the ODC. Specifically, an increase in the CO_2 partial pressure (pCO_2), the concentration of the allosteric effector 2,3-diphosphoglycerate (2,3-DPG), the temperature or a decrease in pH (acidity) promote the T-state and the release of O_2 into the

tissues. In contrast, lower pCO_2, 2,3-DPG concentration, temperature or higher pH (alkalinity) will result on a leftward shift, promoting the R-state and consequently enhancing the O_2 binding.[19] The p50, which is defined as the pO_2 at which Hb is 50% saturated with O_2, is a good indication of Hb's affinity for O_2. Thus, for high p50 values, Hb's affinity for O_2 decreases while low p50 values result in a left shift of the ODC and the corresponding high O_2 affinity. The p50 of Hb encapsulated within RBCs corresponds to 26.6 mmHg.[20,21]

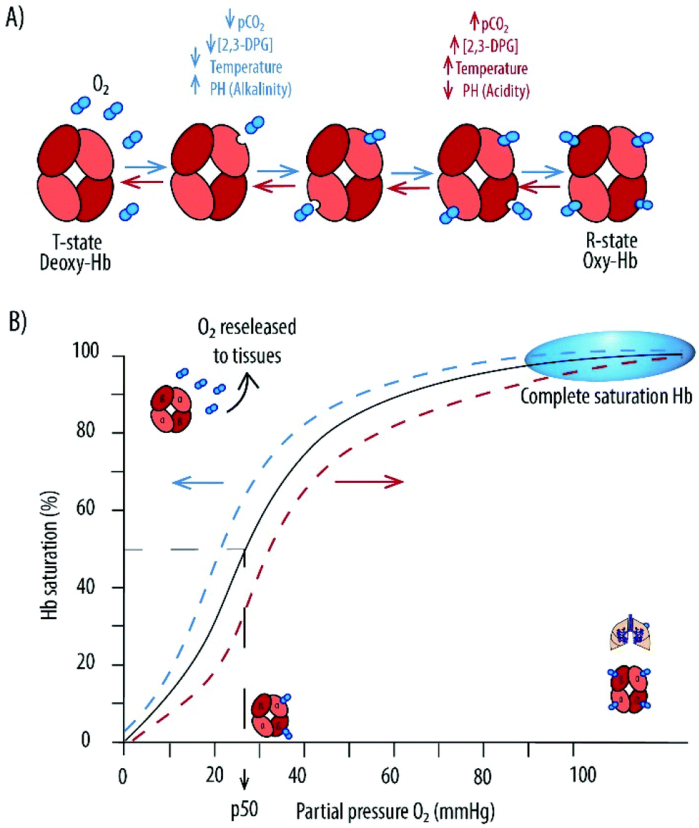

Scheme 1.2. (A) Schematic representation of the different conformations of hemoglobin (Hb) depending on the partial oxygen (O_2) pressure (pO_2). In the tense state (T-state) or unbound state (deoxy-Hb), Hb has a low affinity towards O_2 promoting its release into the tissues. However, when the first molecule of O_2 binds to Hb, a conformational change in the Hb's structure increases the O_2 affinity favouring the binding of more O_2 molecules and facilitating the transition to the relaxed state (R-state) where Hb binds to O_2 (oxy-Hb). Several physiological factors such as temperature (T), pH, concentration of 2,3-diphosphoglycerate (2,3-DPG) or partial carbon dioxide pressure (pCO_2) facilitate either the T- or the R-state. (B) Representation of the Hb O_2 dissociation curve with the characteristic sigmoidal shape highlighting Hb's positive cooperativity. The plateau reached at high pO_2 indicates complete saturation of Hb. p50 indicates the pO_2 at which Hb is 50% saturated with O_2.

1.1.1.2. Native protection system for maintaining Hb's function.

Within RBCs (Scheme 1.3), Hb is exposed to different endogenous and exogenous agents oxidizing it to methemoglobin (metHb). Within metHb, the heme iron is in its oxidized ferric state (Fe^{3+}) and is not able to bind O_2.[22] Every 24 hours, 3% of all Hb is oxidized into metHb producing reactive oxygen species (ROS) as by-products. However, this process is accelerated under oxidative stress conditions or in the setting of increased O_2 delivery. In particular, H_2O_2 can react with both Fe^{2+} and Fe^{3+}-Hb, resulting in heme degradation and the subsequent release of the free iron ions. These free iron ions can take part, together with H_2O_2, in the Haber–Weiss or Fenton reaction generating hydroxyl radicals ($OH^{\bullet -}$).[23] These resulting ROS have a very short life since they rapidly participate in a wide variety of reactions increasing toxicity. As an example, ROS can react with nitric oxide (NO) producing metHb and nitrate (NO_3^-).[24] NO being an important signalling molecule and a natural vasodilator, its depletion from the bloodstream results in vasoconstriction and subsequent cardiovascular complications.[25] Fortunately, natural RBCs are well equipped with mechanisms to prevent oxidation. In particular, cytochrome-b5 reductase using NADH as a cofactor, maintains metHb levels below 1%.[26] The enzyme metHb reductase, which also uses the NADH co-factor, has the ability to revert Hb's auto-oxidation. Antioxidant enzymes such as superoxide dismutase (SOD), catalase (CAT) and glutathione peroxidase (GPx) prevent ROS generation and thus contribute to RBC function and integrity. RBCs also present high concentrations of antioxidant vitamins (ascorbic acid, α-tocopherol) and other antioxidant compounds such as reduced glutathione (GSH) or ferritin, which can scavenge free iron ions preventing the formation of $OH^{\bullet -}$. Importantly, failure to reverse metHb formation not only diminishes the O_2-carrying capacity of RBCs but also impairs Hb's positive cooperativity resulting in an increased affinity for O_2 for the remaining ferrous heme groups. This also leads to dysregulated vascular tone and inflammatory reactions.[2]

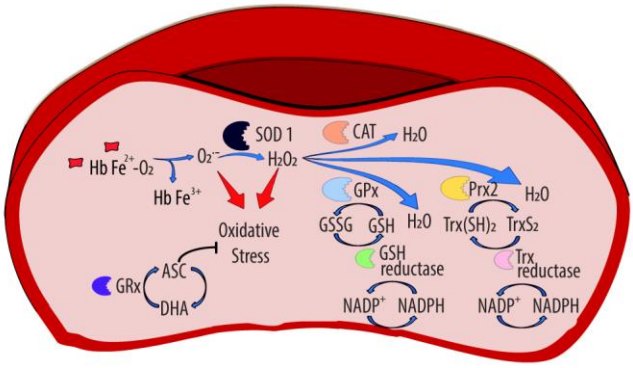

Scheme 1.3. Redox regulation in RBCs. Redox regulation in RBCs. Oxyhemoglobin (OxyHb or Hb-Fe^{2+}-O_2) is oxidized into methemoglobin (metHb or Hb-Fe^{3+}) in RBCs by oxidant events naturally occurring in RBCs. If metHb (Hb-Fe^{3+}) is not converted back into Hb-Fe^{2+} by Cytb5 reductase (not shown), Hb-Fe^{3+} undergo further autoxidation reactions producing superoxide anion radical ($O_2^{\bullet-}$) and other reactive oxygen species. The enzyme superoxide dismutase (SOD)-1 reduce $O_2^{\bullet-}$ into hydrogen peroxide (H_2O_2). H_2O_2 can be further reduced into water by catalase (Cat), glutathione peroxidase (GPx) and peroxiredoxin (Prx)-2. The activity of GPx depends on reduced glutathione (GSH) and its recycling enzymes glutathione reductase (GR), which on turn depends on NADPH. Prx2 is associated to membrane of RBCs and its recycling depends on the oxidation of thioredoxin ($Trx(SH)_2$) into dimeric ($TrxS_2$); $TrxS_2$ is on turn recycled by the Trx reductase using NADPH as source for reducing equivalents. The only source of energy (ATP) or redox equivalents (NADPH) in RBCs is glucose. Glucose is taken up by the Glut-1 transporter and then channeled into the glycolytic pathway and (via glucose-6-phosphate) into the pentose phosphate pathway, which is the source NADPH. NADPH is used as a co-factor of GR to recycle oxidized GSH (GSSG) back into reduced GSH. Glutaredoxin (GRx) depends on the ascorbate (ASC)/dehydroascorbate (DHA) redox couple, which is also very abundant in RBCs. Adapted with permission from Cortese-Krott et al.[22] Copyright ©2019, Elsevier B.V.

1.2. Hemoglobin-based oxygen carriers

HBOCs are semi-synthetic systems that make use of the excellent O_2 carrying and delivering properties of natural Hb's. The idea is to eliminate the toxic effects of free Hb to create a RBC surrogate to be used when donor RBCs are not available. The toxicity of acellular Hb mainly results from the tetramer dissociation into dimers and monomers, which can then permeate in between the endothelial cells lining our blood vessels into smooth muscle tissue.[27,28] There, they rapidly scavenge NO promoting the subsequent cardiovascular problems resulting from vasoconstriction.[29] Additionally, free Hb affects the osmolarity of blood thus leading to alteration of blood volumes and associated side effects. Therefore, as a result of all these shortcomings, a substantial amount of research has been devoted to stabilizing the Hb molecule while also optimizing its functionality. The two main approaches developed until now involve the chemical modification of Hb or its encapsulation within a protective carrier shell. Both strategies aim at eliminating, or at least minimizing, Hb's dissociation and extravasation as well as its rapid

clearance by the kidneys. At the same time, extended blood circulation lifetimes should also be achieved. Importantly, Hb's modification should not compromise its O_2 loading–releasing abilities.

1.2.1. Chemical-modification strategies.

The chemical-modification approaches developed so far involve: Hb cross-linking, polymerization and conjugation to polymers. The different Hb subunits can be cross-linked intramolecularly while polymerized Hb can be fabricated by employing bifunctional cross-linking reagents. Using bifunctional crosslinkers, the Hb molecules are linked to each other increasing the overall molecular size. Chemically modified HBOCs can also be obtained by conjugation to biocompatible polymers such as poly(ethylene glycol) (PEG) or poly(oxyethylene).

After decades of research, only two HBOCs based on the chemical-modification are currently on the market. Hemopure (HbO_2 Therapeutics, USA), clinically approved in South Africa (in 2001) and in Russia (in 2012) for the treatment of acutely anemic patients,[30,31] is a type of polymerized Hb (polyHb) created using glutaraldehyde (GA) as the bifunctional crosslinking agent. Each polyHb is constituted of four or five Hb molecules yielding a total MW of 250 kDa and a p50 value of 38 mm Hg.[32] The other product called Oxyglobin, an analogous product to Hemopure, also produced by the same company (HbO_2 Therapeutics, USA). While both products are chemically identical, Hemopure has undergone thorough purification steps to remove the majority of low MW products from the solution.[33,34] Oxyglobin is currently approved for veterinary use in both the USA and the EU.[2]

Despite only two market products of HBOCs being developed so far, several promising HBOCs were reached to clinical development. For example, by conjugating human Hb to PEG with a maleimide linker,[21,35] MP4 (previously known as Hemospan, Sangart Inc., San Diego, CA) was developed. As one of the bioconjugation of Hb, MP4 was being developed as an O_2carrier to improve the supply of O_2 rather than a blood surrogate for the full replacement of blood,[36] the clinical trials that have been conducted so far have shown that MP4 is an efficient O_2 delivery system well tolerated in humans.[37,38] Moreover, PEGylated Hb has also been employed to develop Sanguinate, a HBOC with a MW of 120 kDa and a p50 value of 7-16 mm Hg. Sanguinate is currently in phase I and II clinical trials for sickle cell disease and in phase I for the treatment of acute anemia. Other than the Hb derived from bovine or human, the $HemO_2$ Life, employs Hb extracted from lugworms and not packed within RBCs or any other type of membrane.

Interestingly, HemO_2Life has been evaluated both in pre-clinical animal models and clinical trials but in the context of organ transplantation.

However, some of the chemical-modification-based HBOCs were discontinued following clinical evaluation. For instance, HemAssist (Baxter, USA), consists of intramolecular crosslinked human Hb, while HemAssist had been extensively evaluated in preclinical models and also phase I and II clinical studies, phase III clinical trials were discontinued due to a 72% increase in mortality rate for the treatment groups as compared to the saline control.[39,40] Moreover, PolyHeme (Northfield Laboratories, Evanston, IL), is a polyHb-based product that employs pyridoxylated human Hb instead of bovine Hb. However adverse effects were observed and attributed to vasoconstriction and oxidative stress,[41] resulting in the rejection by the FDA.

As a result of the failure in clinical trials of the abovementioned chemical-modified HBOCs, research efforts have been focused on refining their design to address the toxicity issues. There are HBOCs that have been evaluated in preclinical animal models. For example, HemoTech is fabricated by co-polymerizing Hb together with pharmacologically active compounds (i.e., adenosine triphosphate (ATP), adenosine, and GSH). While GSH was incorporated to protect the heme group from NO and ROS, open-ring ATP was introduced to regulate the vascular tone through purinergic receptors. Open-ring adenosine was incorporated to counteract the potential vasoconstriction promoted by Hb. Preclinical studies in several animal models have shown the ability of HemoTech to reduce vasoconstriction following a hemorrhage. Additionally, after administration, no adverse nephrotoxic, neurotoxic, oxidative or inflammatory reactions could be detected.[42,43] Moreover, polyHb-SOD-CAT, that is cross-linked the CAT and SOD enzymes to polyHb was developed.[44] Preclinical evaluation was also conducted on a rat model of intestinal ischemia–reperfusion injury, which demonstrated that polyHb-SOD-CAT decreased the formation of O_2 radicals as compared to polyHb only. Other chemical-modified HBOCs under preclinical studies were also evaluated, such as OxyVita (consists of inter- and intra-molecularly crosslinked bovine Hb), VitalHeme (consists of carboxylated PEG-Hb containing nitroxide moieties), and HemoAct (human serum albumin (HSA) is conjugated to human Hb). Interestingly, as an innovative approach, the HemoAct product consisting of Hb–HSA core–shell nanoclusters was also equipped with antioxidant platinum nanoparticles (Pt-NPs).[45] The PtNPs were incorporated within the clefts of the HSA units of the clusters where they acted as reductive catalytic entities and were able to deplete $O_2^{\bullet-}$ radicals and H_2O_2 which, in turn, prevented the formation of metHb.

While two of the HBOCs based on the chemical-modification strategies reached the market and serval promising chemical-modified HBOCs are under clinical or preclinical evaluation, the

development of HBOCs based on encapsulation strategies is essential in order to expect HBOCs with better performance.

1.2.2. Encapsulation strategies.

Encapsulation strategies aim to mimic the in vivo situation, where Hb is encased in a protective RBC membrane. Specifically, Hb entrapment within micro- or nano-sized (up to 500 nm) encapsulation platforms has emerged as a promising strategy. Hb encapsulation offers several advantages. Firstly, it mimics more closely the physiological encapsulated state of Hb within biological RBCs. Secondly, by preventing Hb from being in direct contact with plasma, increased circulation times, reduced hypertensive response and uptake by the MPS can be achieved. Lastly, encapsulation platforms offer the possibility of incorporating other functional compounds such as antioxidant enzymes or allosteric effector molecules within the same carrier. In fact, the concept of Hb encapsulation was presented in the 1950s and 1960s in a pioneering work by Chang and collaborators.[2,46] The authors were able to encapsulate, not only Hb, but also reductive enzymes within a polymeric micron-sized carrier shell. While, on a first study, cellulose nitrate was used to fabricate the carrier shell, in a follow-up work, PEG-poly(lactide) was used as a biocompatible and biodegradable material.[47,48] With such a carrier, the authors were able to co-encapsulate not only SOD, CAT and CA enzymes but also the 2,3-DPG allosteric effector.[49,50] However, these Hb-loaded microcarriers, which were termed “hemoglobin corpuscles”, were rapidly removed from the circulation by the MPS. Regrettably, reducing the size of the microcarriers to about 1 μm in diameter resulted in only a slight improvement in the vascular residence time.[46] Since then, much work has been conducted towards improving the circulation lifetime by making use of different polymers, phospholipids or surface coatings. Few systems have undergone pre-clinical evaluation and some novel designs of HBOCs based on encapsulation strategies will be discussed below.

For instance, ErythroMer (KaloCyte, St Louis MO, USA), consists of toroidal-shaped NPs of approximately 200 nm in diameter. Such nanoparticles (NPs) are fabricated by the self-assembly of an amphiphilic polymeric system of polyethylene imine (PEI) grafted to palmitic acid. Leuko-methylene blue encapsulation provides a reductive environment able to retard the rate of metHb conversion. The pH-sensitive allosteric modifier 2-[4-[[(3,5-dimethylanilino) carbonyl]methyl]phenoxy]-2-methylpropionic acid (also known as RSR-13) was incorporated too.

RSR-13 promotes the O_2 release of Hb at lower pH, thus increasing O_2 availability to hypoxic tissues.[51] ErythroMer has been evaluated in murine models of hemorrhagic shock and in a hemodilution model of 70% blood exchange. The results have shown promising O_2 transport in vivo.[21,52] Additionally, ErythroMer can be efficiently lyophilized and reconstituted in saline prior to administration. Despite the progress, biocompatibility, vascular residence time and immunotoxicity still need to be thoroughly evaluated. Moreover, Hb vesicles (HbVs), as liposome-encapsulated Hb with a size of 250–280 nm in diameter, are structures with a core of concentrated Hb wrapped in a phospholipid membrane.[38] Extra PEG modification has rendered HbVs with extended circulation times of approximately 60 h in some animal models.[53–55] HbVs have been extensively studied in preclinical animal models such as the animal models of hemorrhagic shock or for the oxygenation of ischemic tissues.[53,56] Despite the promising results as therapeutic O_2 carriers, issues with pharmacokinetics and complement-mediated immune responses still need to be addressed.[57] There are other Hb encapsulation platforms that have been fabricated to serve as O_2 carriers, such as Hb-loaded polymersomes with higher stability both in storage and in vivo,[58] Hb-entrapped polymeric micelles,[59] and Hb-loaded Manganese carbonate ($MnCO_3$) microparticles followed by the immediate addition of HSA for encapsulation and stabilization of the particles.[60] However, due to early developments, a preclinical evaluation still remains to be conducted.

Interestingly, there are few novel designs of HBOCs based on the rapid development of encapsulation strategies recently. For instance, several studies have focused on encapsulating Hb within a polydopamine (PDA) shell. In particular, Wang et al. coated single Hb molecules rendering Hb-PDA.[61] Such a PDA coating was able to inhibit metHb formation as well as heme oxidation to ferryl (Fe^{4+}) Hb. Furthermore, the Hb-PDA particles were able to scavenge free radicals and ROS. They were, in addition, able to suppress intracellular ROS generated by incubating cardiomyocytes with H_2O_2. Micron-sized Hb particles fabricated by co-precipitation have been also successfully coated with PDA.[62] In this study, the PDA-coated particles showed twice as much functional Hb content than their uncoated counterparts. This was attributed to PDA's antioxidant properties, which minimized metHb conversion. Moreover, metal-organic frameworks (MOFs) are another interesting material for the fabrication of HBOCs since they display well-defined, crystalline pore structures.[63–65]. Specifically, a first report employed the so-called zeolitic imidazole framework-8 (ZIF-8).[66] Due to this ZIF-8 coating, the encapsulated Hb exhibited enhanced stability upon exposure to several harsh conditions such as alkaline treatment, oxidation, high temperature or even an enzymatic environment. Furthermore, following evaluation in a murine model, the Hb-loaded ZIF-8 NPs displayed extended circulation times and reduced

nonspecific distribution in normal organs as compared to free Hb. The ZIF-8 NPs were also evaluated in a mice model of hemorrhagic shock where enhanced survival time was observed for the treatment group. Our group also employed MOF-NPs for Hb encapsulation. Specifically, we used the so-called porous coordination network (PCN)-333(Al), which is composed of trivalent metal species (i.e., Al^{3+}) coordinated to the organic linker triazine-2,4,6-triyl-tribenzoic acid.[67] PCN-333 was chosen since such a MOF-NP displays one of the highest void volumes and largest cages. As a result, PCN-333 acts as a single molecule trap for Hb thus minimizing Hb's aggregation and leaching.[68] We demonstrated preservation of the excellent O_2 binding and releasing properties of Hb following encapsulation within MOF-NPs. Additionally, to achieve extended circulation lifetimes in the blood stream, the Hb-loaded MOF-NPs were camouflaged within erythrocyte-derived cell membranes. Such an approach is based on the "self-marker" biomolecules embedded within the lipid bilayer of natural RBCs.[69] Successful coating by the cell membranes was demonstrated by the decreased protein adsorption and cell uptake by mouse macrophages for the coated MOF-NPs. In all, these innovative designs bring new potential for the future development of HBOCs.

1.3. Characteristics of HBOCs

1.3.1. Size.

Particle size is an important factor when designing a long-circulating carrier for biomedical applications. This is because small particles with a size of less than 10 nm are more easily filtered out by the kidney, thereby being eliminated from the circulation. Meanwhile, NPs with a size between 10 nm ~ 100 nm can avoid renal filtration, but have more opportunity to be recognized by macrophages and, as a result, they are mainly eliminated by the liver.[70–73] On the other hand, particles with a size larger than 100 nm will generally display a longer time of circulation. However, there is a big difference when the size goes up to the micrometer level, where particles with a size of 1-3 μm are easily phagocytosed by the MPS, and extremely large particles (larger than 5 μm) can result in microcirculation blockage when the particle concentration is high.[74,75] Consequently, the renal filtration of small particles (< 10 nm) and the strong macrophage uptake of large particles (> 1 μm) can both decrease the in vivo circulation time of particles, then it is crucial to develope a proper size of particles which can minimize both of the renal filtration and the macrophage uptake.

In terms of the size of HBOCs, in addition to the factors mentioned above, small-sized HBOCs (< 100 nm) or free Hb will face some other challenges. Firstly, they can penetrate the endothelial gaps of the vascular lining and be a potent NO scavenger, which will result in various side effects, including vasoconstriction. Thus, it has been shown that the size of HBOCs is inversely proportional to vasoconstriction and hypertension.[76,77] Secondly, accumulation of small-sized HBOCs (< 100 nm) or free Hb in the bloodstream can result in an overload of the renal filtration system, causing cytotoxicity and oxidative damage in the kidneys.[78] On the other hand, HBOCs with large size (> 1 μm) are rarely explored due to their decreased circulation time, and thus they are mainly used for tissue engineering purposes, such as O_2 depots.[79] Consequently, to avoid the drawbacks, the fabrication of HBOCs with a size between 100 nm and 1 μm is performed in this thesis.

1.3.2. Hb content.

In native RBCs, the Hb content is 92% (in dry weight),[80] which gives the RBC its potent O_2-carrying ability. Since a high Hb content indicates a greater O_2 delivery potential, designing HBOCs with a high Hb content is very important. For the aforementioned chemically modified HBOCs, several approaches have been performed to control the Hb content. For example, both the diaspirin cross-linked Hb and GA cross-linked Hb can reach a Hb content as high as 100% since these HBOCs are almost fully made of Hb, with little amount of the cross-linker present (Table 1.1).[24,81] But one of the important disadvantages of the cross-linked HBOCs is the toxicity of the cross-linker. Therefore, even though a 100% Hb content has been reached within these HBOCs, they have not been approved for human use by FDA so far.[82] Other HBOCs based on chemical modification displayed lower Hb contents. For example, by conjugating the human Hb (hHb) onto the surface of a biocompatible gelatin microparticle, Paciello et al. reported a Hb content of only 3.92–4.49%. Thus, such microparticles were used for tissue engineering applications to implement controlled perfusion cultures.[83] Furthermore, two Hb-polymer conjugates were developed, Bu et al. reported a Hb conjugated to the amphiphilic block copolymer poly[2-(methacrylamido) glucopyranose]-*block*-poly(methacrylic acid)-*block*-poly(butylmethacrylate) (PMAG-b-PMAA-b-PBMA)) for the therapy of hypoxia in tumors, where the PMAG-b-PMAA-b-PBMA polymer

was used for Hb conjugation and cancer cell recognition via the glucose transporter isoform 1.[84] And Hb conjugated dextran (Dex) nanogels (DexHb-SA-DA-Dex, succinic anhydride (SA) and dopamine (DA) contained) for the fabrication of functionalized Dex nanogels were reported, where the Dex was served as the building block of the nanogel, the DA was used for hydrophobic moieties, and SA can control the process of the self-assemble system.[85] Hb was act as the oxygen carrier in these Hb-polymer conjugates, but unfortunately, both of these two Hb-polymer conjugates reached a relatively low Hb content of 10.7% and 25–55% (conjugation ratio: $C_{Hb}/ (C_{total} – C_{Hb}) *100\%$), respectively.[84,85] In all, most of the chemically-modified HBOCs have not reached a remarkable Hb content compared to the Hb amount in native RBCs, while the ones with a remarkable Hb content face the drawbacks of using toxic crosslinkers (e.g., GA) and having small diameters (<100 nm).

	Formulation	Size	Hb content	p50 (mmHg)
	Hb in RBC	2 × 7 μm	92%[a]	24–30
	Free hHb	~65 kDa	100%[a]	15
Chemically modification of Hb	– Nanoarchitectures			
Cross-linked Hb	Diaspirin cross-linked Hb	69 kDa	100%[a]	33
Polymerized Hb (polyHb)	GA polymerized Hb	100–500 kDa	100%[a]	38
	polyHb-SOD-CAT-CA	N450 kDa	–	19.92
	polyHb-Rbr	≤600 kDa	–	8.9
	polyHb-ATP-AD-GSH	b500 kDa	–	20
Hb-polymer conjugates	Hb-PEG	~120 kDa	–	10–20
	Hb-SA-DA-Dex	320 nm[d] 260 nm[e]	25–55%[b] 7–33%[c]	14
	Hb-Dex-g-PNIPAAm	~50 nm[d] ~30 nm[e]	–	–
	PMAG-b-PMAA-Hb-b-PBMA	147 nm[d] 73 nm[e]	10.7%[b]	–
	Hb-(HSA)3 clusters	65 kDa	25%[a]	9
Chemical modification of Hb	- Microarchitectures			
	Gelatin-encapsulated poly(Hb-PEG)	1.37 μm[d]	25.0%[c]	–
	Gelatin-hHb microparticles	75–150 μm[e]	3.9–4.5%[a] 60–70%[c]	–

Table 1.1. Several examples of chemically modified hemoglobin-based oxygen carriers. Hb: hemoglobin, RBC: red blood cell, hHb: human Hb, p50: partial pressurewith 50% oxygenated Hb, GA: glutaraldehyde, SOD: superoxide anhydrase, CAT: catalase, CA: carbonic anhydrase,MAP:mean arterial blood pressure, pCO2: partial pressure of carbon dioxide, Rbr: ruberitrin, ATP: adenosine-5'-triphosphate, AD: adenosine, GSH: reduced glutathione, TTUHSC: Texas Tech Uni. Health Sc. Center, PEG: poly(ethylene glycol), Dex: dextran, SA: succinic anhydride, DA: dopamine, PNIPAAm: poly(N-isopropylacrylamide), PMAG-b-PMAA-b-PBMA: poly[2-(methacrylamido) glucopyranose]-block-poly(methacrylicacid)-block-poly(butylmethacrylate), HSA: human serum albumin, O_2: oxygen. ([a] Weight content. [b] Conjugation ratio: C_{Hb}/ (C_{total} – CHb) *100%. [c] Encapsulation efficiency: (Hb_{total} − Hb_{free}) / Hbtotal *100%. [d] Hydrodynamic size. [e] Size by electron microscopy.) Adapted with permission from Jansman et al.[24] Copyright ©2018, Elsevier B.V.

Accordingly, encapsulation strategies were developed to reach a relatively high Hb content and, at the same time, minimize the side effects of free Hb or chemically modified HBOCs. Li et al.

synthesized particles containing hetero triblock co-polymer (PEG-P (CL-co-LA)-PEG, with a PEG, a PCL (poly(ε-caprolactone)), and a PLA (poly-lactide) chain), and optimized the ratio between polymers and Hb, resulting in more than 60% Hb content.[86] In a different study, by using the shirasu porous glass membrane emulsification technique, Lai et al. prepared Hb-albumin microparticles with a higher Hb content (up to 70%).[87,88] In order to reach a higher Hb content for the HBOCs based on encapsulation strategy, serval techniques were developed. One of the promising ways is the so-called co-precipitation technique. For example, by co-precipitating the Hb together with Dex and calcium hydroxide ($Ca(OH)_2$), followed by cross-linking with GA, Yu et al. fabricated biconcave Hb-loaded $Ca(OH)_2$ microparticles with a Hb content corresponded to 68% of the Hb content in natural RBC.[89] In another example, Xiong et al. reported the fabrication of Hb particles (HbPs) where the Hb was co-precipitated together with $MnCO_3$ and a HSA corona was absorbed on the surface of this particle to avoid further aggregation. Then the Hb and HSA in the particle were cross-linked by GA and the $MnCO_3$ template was removed by EDTA solution. This final HSA-coated HbPs reached 80% of the Hb content of the natural RBCs.[60] Another way of increasing the Hb content in HBOCs is by combining electrospray and surface coating technique. Liu et al. prepared NPs fully made of Hb by using electrospray, with subsequent PDA and PEG coating, which resulted in a HBOC with a high Hb content and low-fouling surface.[90] Despite the high Hb content that can be reached when using co-precipitation and electrospray techniques, the poor size control of co-precipitation and low yield of electrospray may prevent their application for fabricating clinically relevant amounts. The desolvation technique, which is widely applied in albumin NPs fabrication for drug delivery systems, was another promising method to fabricate HBOCs with a high Hb content. In this case, we can expect a particle fully made of Hb as well, but with an easier protocol, lower cost, and higher possibility of scaling up. Thus, this technique will be further discussed in Section 1.4.1 and is finally used in this thesis for HBOCs fabrication.

	Formulation	Size	Hb content	p50 (mmHg)
Encapsulation strategies for Hb-Nanoarchitectures				
Polymeric nanoparticles	PLA-PEG	100–200 nm[c]	71–88%[b]	–
	PLGA-PEG	200 nm[c]	48%[b]	14.2
	PEG-PCL-PLA-PEG	800 nm[c]	N60%[a]	21.6
	PEG-PAGE(MPA)-PCL	200–300 nm[c]	–	20.4
	PDA-coated Hb	6–8 nm[c]	–	13.9
	Hb-catalase nanotubes	300–420 nm × 10 μm[d]	–	–
Liposomes	hHb, DPPC, Chol, DHSG, DSPE-PEG5K	250–280 nm	10 g dL^{-1}	20.2
	hHb, DPPC, Chol, VitE, HDAS, HDAS-PEG2K	215 nm[c]	7.2 g dL^{-1}	31.9
Encapsulation strategies for Hb-Microarchitectures				
Biconcave	(hHb/BSA)4/hHb capsules	7 ± 2 μm	–	–
	Ca(OH)2-Hb particles	6.5 μm[d]	68%[a]	–
Spherical	(Hb/DHP)5 capsules	3.4 μm[c]	55.3%[b]	–
	CaCO3/(Hb/PEG)5 microparticles	N5 μm[d]	–	–
	Hb-albumin microparticles	4–5 μm[d]	30–70%[a]	5–12

Table 1.2. Several examples of encapsulation approaches for the creation of hemoglobin-based oxygen carriers. Hb: hemoglobin, hHb: human Hb, p50: partial pressure with 50% oxygenated Hb, PLA: poly(lactic acid), PEG: poly(ethylene glycol), PLGA: poly(lactide-co-glycolide), PAGE(MPA): poly(allyl glycidyl ether) (functionalized with mercaptopropionic acid), MAP: mean arterial blood pressure, PCL: poly(ε-caprolactone), DPPC: dipalmitoylphosphatidylcholine, Chol: cholesterol, DHSG: 1,5-O-dihexadecyl-N-succinyl-l-glutamate, DSPE: 1, 2-distearoyl-sn-glycero-3-phosphatidyl-ethanolamine HDAS: hexadecylcarbamoylmethylhexadecanoate, VitE: vitamin E, BSA: bovine serum albumin, O2: oxygen, Ca(OH)2: calcium hydroxide, DHP: dialdehyde heparin, $CaCO_3$: calcium carbonate. ([a] Weight content. [b] Encapsulation efficiency: (Hbtotal − Hbfree) / Hbtotal *100%. [c] Hydrodynamic size. [d] Size by electron microscopy.) Adapted with permission from Jansman et al.[24] Copyright ©2018, Elsevier B.V.

1.3.3. Antioxidant properties.

Within natural RBCs, Hb is surrounded by several kinds of ROS which can be generated endogenously and exogenously. That is, in the natural RBC the autoxidation of Hb results in the production of metHb and endogenous ROS (such as superoxide radical anion ($O_2^{\bullet-}$) and H_2O_2 as by-products.[91,92] On the one hand, the resulting metHb is incapable of O_2 delivery, and further, a metHb content larger than 10% results in a significant decrease in O_2 supply to the tissues.[93] On the other hand, during the circulation in the microvasculature, the RBCs can take up exogenous ROS (e.g., $O_2^{\bullet-}$) produced by other cells such as the endothelial cells of the vascular wall.[94] In the meantime, when perfusing the ischemic tissue under pathological conditions (e.g., during hemorrhagic shock), the Hb's oxidative toxicity and oxidative injuries will be increased by the extra produced $O_2^{\bullet-}$ and H_2O_2. However, the Hb in native RBCs is protected by two kinds of biological antioxidant agents, including enzymatic entities such as SOD, CAT, and GPx, and the non-enzymatic entities such as GSH and ascorbic acid. Consequently, it is crucial to incorporate an effective antioxidant entity when designing the HBOCs.

Several approaches have been developed to fabricate HBOCs with antioxidant properties, including the incorporation of native antioxidants, the loading of nanozymes, and adding antioxidant material coatings. To enable HBOCs antioxidant properties, Chang et al. synthesized a complex by crosslinking Hb with SOD and CAT together.[95] Bian et al. further reported a soluble polyHb-SOD-CAT-CA nano-complex, where the authors crosslinked Hb, SOD, CAT, and carbonic anhydrase (CA) together, which displayed enhanced functionality of the three functions of RBC, that is, O_2 delivery, CO_2 transporting and the ROS scavenging capability.[96] Besides, Simoni et al. reported a HBOC system called HemoTech, which is fabricated by cross-linking purified bovine Hb together with ATP (intramolecularly) and adenosine (intermolecularly), followed by conjugating with reduced GSH, which can shield Hb from ROS.[97] However, serval limitations exist when incorporating native antioxidants. For example, the enzyme incorporation faces problems such as a short half-life of catalytic, restricted active sites, sensitivity to the environment, and high cost.[98,99] And the non-enzyme compounds such as the reduced GSH can not be reused on its own, since additional GSH reductase (i.e., nicotinamide adenine dinucleotide phosphate ($NADP^+$/NADPH) system) was needed to reuse the GSH.[22]

Nanozymes, which are inorganic NPs with multiple enzyme-like properties, attracted attention for HBOCs design in recent years. Hosaka et al. reported a system where a Pt-NP was incorporated into Hb-loaded protein nanocluster (Hb-HSA_3(PtNP)), where the PtNP embedded into the HSA unit enables this novel HBOC to have both CAT and SOD activities.[100] Furthermore, Jansman et al. incorporated Hb and cerium oxide NPs (CeO_2-NPs) into larger poly(lactide-coglycolide) (PLGA) NPs, where the CeO_2-NPs provided both $O_2^{\bullet-}$ and H_2O_2 scavenging properties, thereby obtaining a HBOC system with remarkable antioxidant and Hb protection abilities.[101]

Other than the native antioxidants and nanozymes, more novel biocompatible materials are further explored to increase the antioxidant properties of HBOCs. This included PDA, which is a self-polymerizing coating with antioxidant properties (which will be further discussed in Section 1.4.2).[61] Another example is metal phenolic networks (MPN), which are coordination complexes consisting of polyphenol and metal ions. Interestingly, the reported MPN displays multifunctional properties (e.g., antioxidant capacity), which means MPN also shows great potential in the application of HBOCs (which will be further discussed in Section 1.4.3).[102]

1.3.4. Stealth properties.

While the O_2 carrying capacity (by incorporation of Hb) and antioxidant properties (by incorporation of an antioxidant system) are important factors when designing novel HBOCs, the HBOCs do need to be long-circulating for them to have a sufficient therapeutical effect. Therefore, designing HBOCs with stealth properties is another important issue.

In the past few decades, considerable interest was devoted to improve the stealth properties of a nano-drug delivery system to get prolonged circulation in vivo, including PEG modification, “self” peptides modification, protein corona coating, RBC-membrane coating, and other kinds of biomimetic membrane coating (e.g., semi-artificial lipo-exosome membrane).[103] (Scheme 1.4)

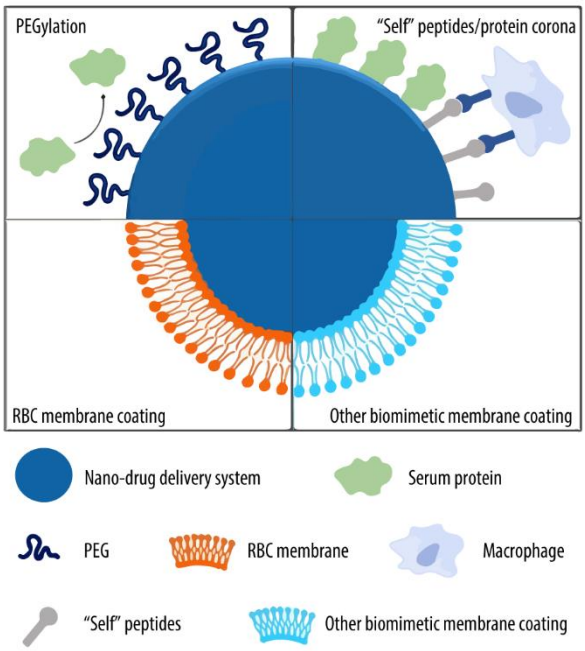

Scheme 1.4. Stealth strategies applied in drug delivery system. Adapted with permission from Fam et.al.[103] Copyright ©2020, MDPI

Due to the 120 days of survival time of native RBCs, and similar to the drug delivery system, the design of HBOCs which can reach a long circulation time is also very crucial. Great efforts have been put into the development of stealth properties in HBOCs so far. The main interest lays with PEG, which is a FDA-approved biomaterial with a wide application in the pharmaceutical field, where many marketed products benefit from PEGylation to reach prolonged in vivo circulation and lower systemic toxicity.[104,105] In the chemically modified HBOCs, the PEG has mainly been conjugated to the Hb molecule, resulting in a Hb-polymer complex with a larger size and longer vascular retention.[106] For the Hb-encapsulated HBOCs, the PEG modifications are commonly found on the surface of a carrier. Liu et al. reported a low-fouling PEG-decorated Hb NPs (Hb/PEG-NP) by conjugating poly-l-lysine-graft-PEG (PLL-g-PEG) and PDA coating layer by forming amine-catechol adducts between the amino groups of PLL and the catechol moieties of PDA. The PEG layer decreased the surface protein absorption of the Hb-NP, which could indicate prolonged circulation times.[90] Jansman et al. also employed the PLL-g-PEG to decorate their CeO_2-NPs containing HBOC system, where a decreased protein absorption and cell uptake was observed after the PEG modification.[101]

Regardless of the remarkable features of PEG, it also displayed some disadvantages such as non-biodegradability.[107] Furthermore, the usage of PEG could result in the particular antibodies produced by immune system which can specifically bind to PEG (anti-PEG Abs), these anti-PEG Abs were related to the extra side effects and decreased therapeutic efficacy.[108] Thus, researchers have tried to find other alternatives to PEG, including more biomimetic approaches, such as cell-derived membrane coatings. Zhuang et al. reported an RBC-membrane-coated biomimetic nanoemulsion, where it was suggested that by using the biocompatibility of natural RBC membranes, an enhanced circulation time could be expected.[109] Liu et al. fabricated a MOF followed by Hb loading and human RBC membrane coating, which enabled the novel HBOCs to decrease the uptake by endothelial cells and macrophages. Similarly, Jansman et al. reported a human RBC-membrane-coated multi-multifunctional Hb-loaded PLGA NPs to obtain low fouling properties.[110] Despite the good biocompatibility of cell-derived membrane coatings, the high cost of this pure cell membrane-related strategy and the challenge of upscale is an obvious bottleneck. Some easier and cheaper methods therefore display promising solutions. For example, Lin et al. fabricated a hybrid membrane consisting of liposomes and exosomes to be used for NPs coating, which may decrease the cost of using a 100% cell-derived membrane coating.[111] Finally, an alternative could lie in the usage of a specifically selected protein corona, where long circulating and low immune responsive proteins are crosslinked onto the NP's surface. Peng et al. reported an albumin corona coated poly (3-hydroxybutyrate-co-3-hydroxyhexanoate) (PHBHHx) nanoparticle (PHBHHx NP) by simply incubating the NPs with albumin, where the albumin corona could decrease the protein adsorption onto the PHBHHx NPs, resulting in a longer blood circulation time.[112] Thus, the protein corona decoration would prolong the circulation time of the particles, but with an expected easier protocol and lower associated costs, which can be a promising way to improve stealth properties in the future design of HBOCs.

1.4. Design of HBOCs

As mentioned in Section 1.3, to reach the important features of HBOCs, in this thesis, we make use of the desolvation technique to fabricate HBOCs with high Hb content. Besides, PDA coating and MPN coating were performed to stabilize the HBOCs and, at the same time, provide antioxidant properties.

1.4.1. Desolvation technique.

The desolvation technique is a widely used technique to fabricate protein-based particles, where the formation is thermodynamically driven and based on a self-assembly process.[113] Scheme 1.5 shows the protocol and principle of a protein particle prepared by the desolvation technique. The principle of desolvation is that, by adding an antisolvent (i.e., a solvent in which the protein is insoluble) to the protein solution, the water molecule in a water-soluble protein solution is replaced, and as a result, the protein becomes supersaturated. When a critical point of protein saturation is reached, nucleation happens and results in particle formation.[114] However, since the as-formed protein particles are not stable enough and can be redissolved in the water phase again, a crosslinking process is performed to stabilize the as-formed protein particles.[115–118] Thus, important parameters within the fabrication process, including the protein concentration, the type of organic solvent, the ratio of organic phase/aqueous phase, and the used crosslinker, need to be optimized to ensure protein particles with particular physicochemical properties.

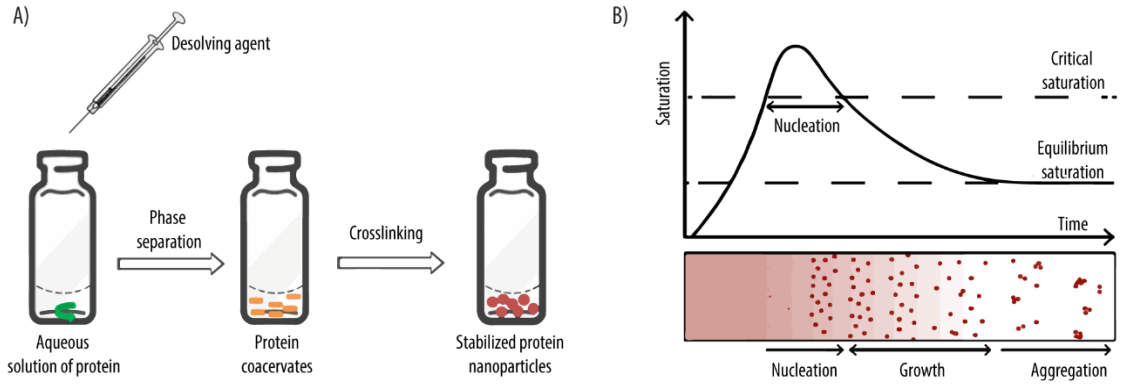

Scheme 1.5. A) protocol of desolvation and B) During desolvation, the addition of an antisolvent creates supersaturation of the protein in the solution. At a critical protein saturation point, nucleation occurs and particles are formed. Over time, protein particles will tend to continue to grow or aggregate if not stabilized. Adapted with permission from Mehta et. al. Copyright ©2019, Springer Nature; Hickey et. al.[114] Copyright ©2020, American Chemical Society.

1.4.1.1. Controllable parameters within the desolvation technique.

Characteristics of a protein particle such as the size, surface charge, stability, and yield determine the application field of protein particles. For example, the nano-sized protein particles are normally

used in drug delivery systems, while the miro-sized protein particles are more frequently applied in food industry. Thus, when using the desolvation technique to fabricate protein particles, other than the nature of the proteins themselves, the optimization of controllable parameters (e.g., protein concentration, type of organic solvent, the ratio of organic phase/water phase, and used crosslinker) is very important to fabricate protein particles with particular properties for a specific application.

The concentration of protein in the initial solution is one of the major factors that contribute to the size of protein particles for different applications. This means that the protein concentration should be high enough to enable nucleation during desolvation, but on the other hand, not too high so that it can result in uncontrollable particle aggregates, which can result in particles with irregular shapes and larger size (Scheme 1.5B).[114] Thus, the screening of protein concentration is crucial for using the desolvation technique. Langer et al. reported an available concentration of HSA ranging from 25 - 100 mg mL^{-1}, which resulted in HSA NPs of less than 250 nm, and when the HSA concentration researched 50 mg mL^{-1} and above, a higher HSA concentration resulting in larger nanoparticle sizes.[119] What is more, by using BSA at a similar concentration range (12 - 100 mg mL^{-1}), Galisteo-González et al. fabricated BSA NPs with a size from ~75 nm to ~140 nm, and interestingly, the increase in BSA concentration resulted in a larger particle size.[120] This was attributed to increased viscosity with an increased protein concentration, which resulted in a decreased transportation frequency of protein between water and ethanol . Then, followed by a reduced rate of nucleation, a larger diameter of the particles was obtained. Besides, higher protein concentration can also result in enhanced supersaturation during desolvation, causing accelerated agglomeration and resulting in larger particles.[120]

Other than the protein concentration, the type of organic solvent and the ratio of organic phase/water phase are two remarkable factors to control the properties of resulting particles. Von Storp et al. reported several factors in the desolvation technique that can promote a predictable size of albumin NPs such as the type of organic solvent agent. According to the authors, by using methanol only or a mixture of methanol and ethanol, NPs with a size smaller than 100 nm could be fabricated, while larger sizes of NPs (140-300 nm) could be reached by using either only ethanol or only acetone.[121] In addition, not only the type of organic solvent but also the ratio of organic phase/water phase can affect protein nanoparticle formation significantly. It was reported that an

increased ratio of organic phase/water phase (i.e., increasing the volume of organic phase) resulted in increased size of BSA NPs, pea proteins NPs, and whey protein NPs.[122–124]

After the protein NPs have been formed during the desolvation step, these particles are not stable enough to be purified and thus a crosslinker is needed to stabilize them. For example, by using a traditional crosslinker for protein crosslinking, that is, GA, Weber et al. found that after the desolvation step, at least a GA concentration of ~ 40% (v/v) is needed to produce stable HSA NPs.[115] However, the crosslinker has an effect on the properties of protein particles, such as surface charge which, in turn, can affect their biocompatibility. Specifically, the surface charge is related to the toxicity of NPs, specifically, due to a higher capacity to enter cells and stronger binding capacity to the negatively charged DNA, positively charged NPs shows higher toxicity compared to neutral and negatively charged NPs.[125] Furthermore, the crosslinker can be toxic by itself (i.e., GA), thus resulting in lower biocompatibility. Therefore, Lin et al. reported methyl-PEG decorated oxidized dextran (Dextranox-MPEG) as a novel alternative crosslinking agent used for HSA nanoparticle fabrication. As compared to GA, by making use of this novel crosslinker, the obtained nanoparticle displayed a reduced zeta potential (i.e., −19 mV of GA crosslinked HSA NPs, and −8 mV of Dextranox-MPEG crosslinked HSA NPs) and reduced plasma protein absorption, which indicated better biocompatibility for these HSA NPs.[126]

1.4.1.2. Bio-application of desolvation.

Based on the controllable fabrication process and tunable physicochemical properties of the products, protein particles fabricated by desolvation are widely explored for various bio-applications. For example, one of the most common applications is the albumin nanoparticle fabricated for usage as a drug delivery system. By using surface ethylenediamine cationized BSA (cBSA), Sumeyra Cigdem et al. synthesized cationic cBSA NPs via the desolvation method, and due to the modified surface charge, cBSA NPs displayed enhanced drug loading and cell uptake compared to the anionic BSA NPs.[127] Moreover, Li et al. prepared sodium ferulate-loaded BSA NPs (SF-BSA-NP) (100−200 nm) by using desolvation as well, and compare to the free drug (i.e., sodium ferulate), the obtained SF-BSA-NP displayed an enhanced distribution in liver than other tissues, which shows great potential for liver targeted drug delivery. Other than pharmaceutical applications, the protein particles made by desolvation techniques also displayed a potential

application in the food industry. Chi Diem et al. reported an ethanol-induced desolvation method for the fabrication of pea protein NPs, which displayed great potential as a stabilizing agent for Pickering oil-in-water emulsions or as a food additive for the delivery of bioactive agent (e.g., vitamin D3).[128,129]

Due to the aforementioned broad applications and the great potential in the upscaling of protein particles applied in pharmaceutical applications,[130,131] researchers tried to borrow the desolvation technique for HBOCs fabrication to solve two bottlenecks of encapsulation-based HBOCs (i.e., low Hb content and difficulties in upscaling). Richard et al. reported HBOCs fully made of Hb (Hb-dNPs) by using desolvation precipitation, followed by oxidized Dex crosslinking. After purification, the Hb-dNPs could be up-concentrated to 49.7 ± 4.3 mg mL^{-1} compared to the starting Hb concentration of 15 mg mL^{-1}, and this protocol displayed an easy transition from milliliter to liter scale,[114] which brings new possibilities to fabricate HBOCs in a clinical scale.

1.4.2. Polydopamine.

In 2007, Lee et al. reported a bio-inspired technique for surface functionalization based on PDA coating. By getting inspiration from the procedure of mussel adhesive proteins, the self-polymerization of DA was used to form a thin multifunctional film onto various substrates, such as noble metals, polymers, and oxides.[132] In spite of a lot of research being focused on PDA film formation, the detailed mechanism of DA polymerization into PDA is still unclear. However, there are three widely accepted pathways of PDA formation. Firstly, as shown in Scheme 1.6A (upper pathway in blue), under external stimulation such as O_2, UV, and heat, 3,4-dihydroxyindole (DHI) is produced from DA by multiple oxidation steps. Secondly, as shown in Scheme 1.6A (lower pathway in green), during the formation of DA–quinone, with the external stimulation as mentioned above, the DA molecule can lose only one electron, resulting in the DA –semiquinone radical, which can further trigger dimerization and result in the catechol-catechol dimer.[133] The catechol-catechol dimer can also be polymerized together with the DHI to form PDA. Thirdly, other than the chemical building blocks of PDA, the self-assembled physical trimer ($(dopamine)_2$/DHI), is important in the construction of the final PDA product, which is based on

strong noncovalent interactions (e.g., hydrogen bond, π–π stacking, and cation–π interactions) (Scheme 1.6B).[133]

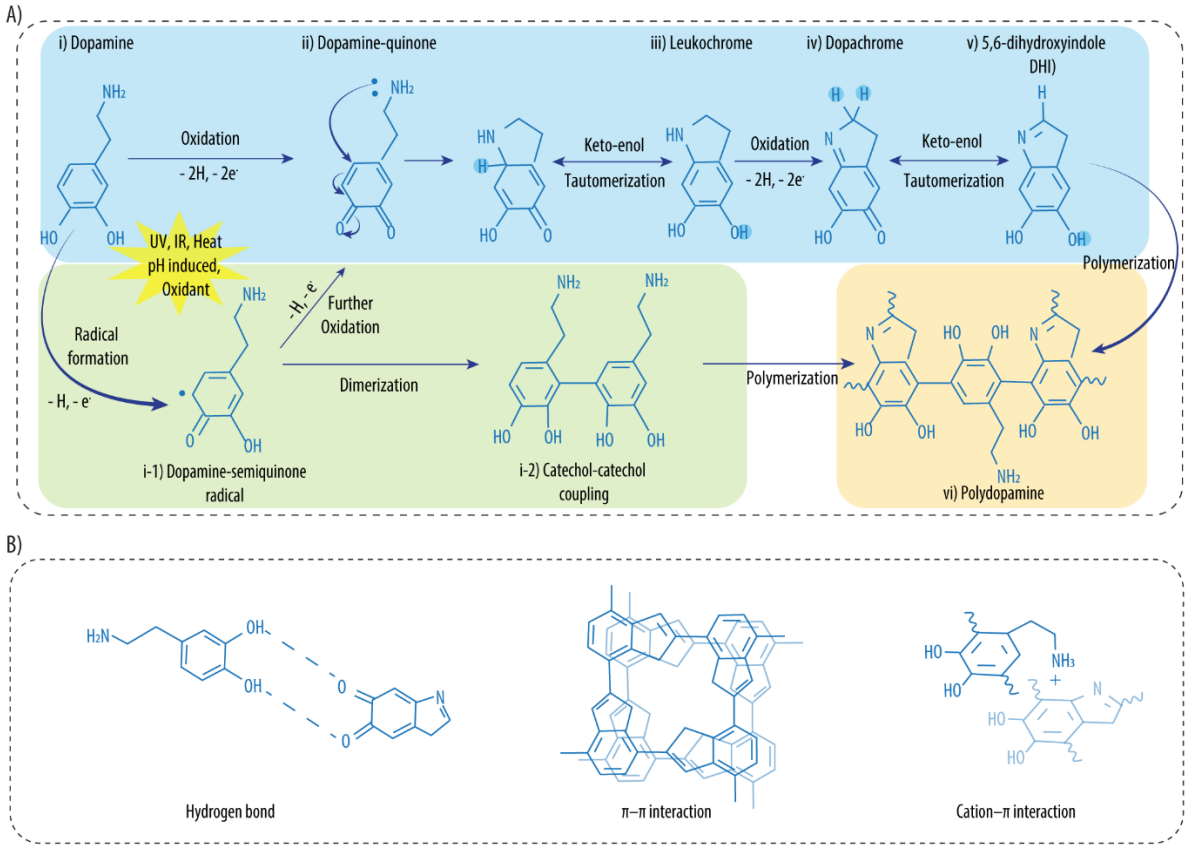

Scheme 1.6. A) Chemically polymerization mechanism of PDA, and B) Noncovalent interactions within PDA. Adapted with permission from Hu et. al.[141] Copyright ©2020, Royal Society of Chemistry.

Despite the complicated possible mechanisms of DA 's oxidative self-polymerization to PDA, the condition which needs to trigger the polymerization is quite simple, which includes phototriggered, chemical oxidants triggered, and basic pH triggered polymerization.[134] The basic pH triggered PDA coating is one of the most widely used methods. For example, Nicola et al. reported an O_2/air containing buffer system at a basic pH (Tris (Tris(hydroxymethyl) aminomethane) buffer (pH 8.5)), which is an efficient way for PDA buildup.[135]

1.4.2.1. Properties of PDA and its application in biomedicine.

Together with the fundamental feature of its strong adhesive feature on almost all kinds of surfaces (e.g., NPs' surface), the remarkable advantages of PDA also include good biocompatibility and biodegradability.[136] This resulted in a large growing interest in exploring the application of PDA in pharmaceutics and biomedicine. By using the cavities and the surface of PDA capsules for drug molecules loading, PDA capsules are the most common form of PDA-based drug delivery system. For example, Cui et al. reported a hydrophobic cargo (including iron oxide (Fe_3O_4) NPs, quantum dots, and thiocoraline) loaded into PDA capsules, where the hydrophobic cargo was preloaded in dimethyldiethoxysilane (DMDES) emulsion droplets, followed by PDA coating. After the PDA coating, the DMDES was removed, thereby obtaining the cargo-encapsulated PDA capsules.[137] Instead of encapsulating the drug inside the PDA capsule, by hydrogen bonding interaction and π–π stacking, Zhuang et al. reported that the anticancer drug doxorubicin (DOX) can be loaded on the surface of PDA capsule, and together with the photothermal property of PDA, this prepared DOX loaded PDA capsule was used as chemo-photothermal therapy.[138]

In addition to drug delivery applications, PDA also displayed great potential in biomedical applications such as cell/surface interaction and bioimaging. By decorating the surface of living yeast cells with PDA coating, Yang et al. found a biomimetic way to functionalize the cells. That is, not only the cell division became controllable because of the PDA coating, but also the as-obtained PDA-coated yeast cells could resist the external invasion from lyticase.[139] Moreover, it has been reported that under different wavelengths of UV excitation (360-500 nm), PDA displayed fluorescence with an emission peak at 400-550 nm, which makes PDA a promising material used for bioimaging.[136] For example, Zhang et al synthesized PDA fluorescent organic NPs (PDA-FONs) that can be used for cell imaging, specifically, the PDA particles were obtained via basic pH triggered strategy of PDA fabrication (at pH 10.5), and followed by the H_2O_2 oxidation of PDA particles, the PDA-FONs with photoluminescence were fabricated.[140]

Another important property of PDA is its antioxidant properties, which make PDA an excellent free radical scavenger. Based on this remarkable feature, PDA shows promise in a large amount of antioxidant-based biomedical applications, such as ischemic brain protection, acute inflammation-induced injury treatment, and wound healing.[141] However, more importantly, by

making use of the antioxidant properties of PDA, great promise also lays in the usage of PDA in the HBOC field.[69]

1.4.2.2. Antioxidant properties of PDA and its application in HBOCs.

The key component structure in PDA is the catechols, which play an important role in the mechanism of the PDA's antioxidant/radical scavenging properties. Specifically, as shown in Scheme 1.7, the phenolic hydroxyl groups in the catechol can donate hydrogen atoms which can easily react with radicals. However, by electron transfer, catechols can also be reducing agents, where the produced phenoxyl radicals can further react with another radical, which results in a stable quinone structure.[142]

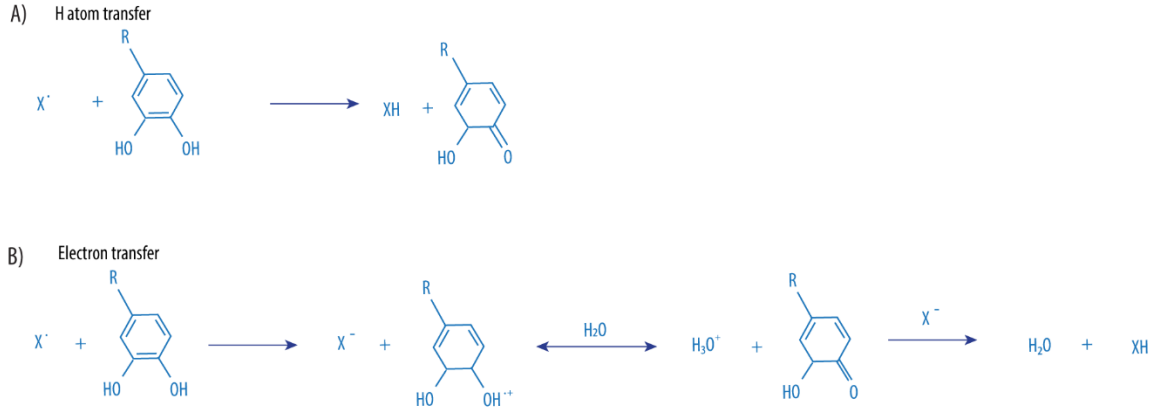

Scheme 1.7. free radical scavenging mechanism of PDA including A) H atom transfer and B) electron transfer. Adapted with permission from Zhang et. al.[142] Copyright ©2020, John Wiley and Sons.

As mentioned in Section 1.1.3, part of the design of HBOCs is the incorporation of an antioxidant system. Within the RBCs, this is mainly achieved by the enzymes SOD and CAT, which SOD can react with $O_2^{\bullet-}$ and CAT can react with H_2O_2. For PDA, as shown in Scheme 1.8A, the $O_2^{\bullet-}$ scavenging mechanism is similar to that of SOD, where the H_2O_2 and O_2 were produced due to the $O_2^{\bullet-}$ disproportionation reaction.[141] Moreover, PDA can also scavenge H_2O_2 (Scheme 1.8B), thereby mimicking the CAT activity. For the mechanism of H_2O_2 scavenging, the catechols in PDA

react with H_2O_2, resulting in PDA quinone subunits and H_2O and O_2 side products. Finally, PDA can chelate with metal irons (e.g., Fe^{2+}) to block the Fenton reaction (Scheme 1.8C), which results in the prevention of hydroxyl radical (•OH) production.[141]

Other than the antioxidant properties for ROS scavenging, PDA also displays remarkable reactive nitrogen species (RNS) scavenging. Despite the exact mechanism of the RNS scavenging is still unclear, Liu et al. reported that nitration and nitrosation of melanin by •NO and ONOO− could be the main mechanism for their scavenging.[143] In this context, melanin has a very similar structure compared to PDA (i.e., PDA was considered as a synthetic melanin).[144]

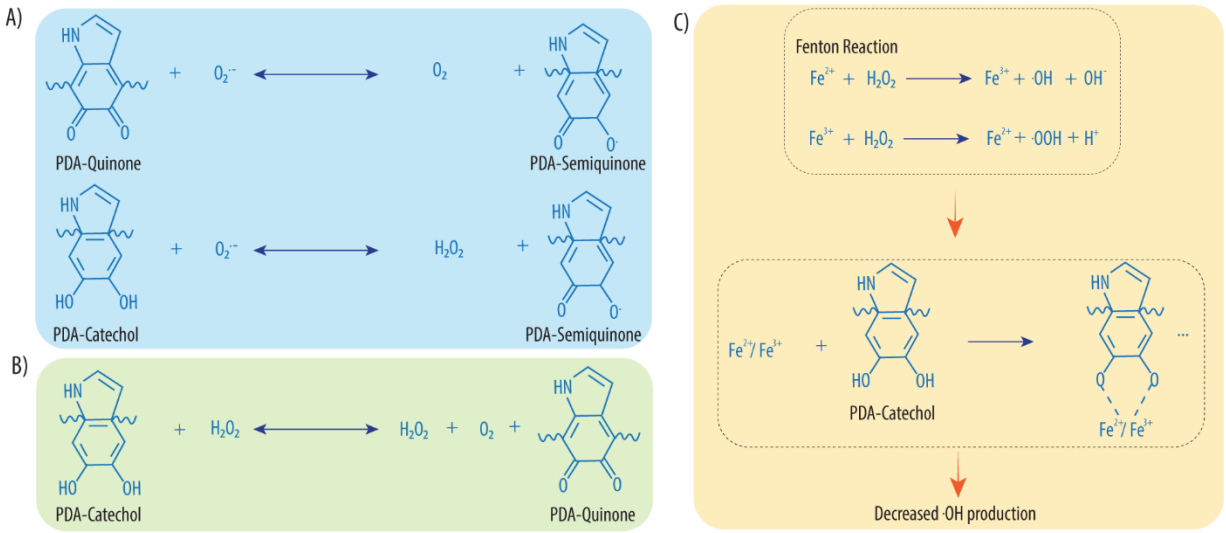

Scheme 1.8. The mechanisms of PDA scavenging the A) superoxide radical ($O_2^{\bullet-}$), B) H_2O_2, and C) the mechanism of preventing the hydroxyl radical (•OH) production. Based on structures discussed in Hong et. al.[133] Copyright ©2012, John Wiley and Sons; Hu et. al.[141] Copyright ©2020, Royal Society of Chemistry.

Due to the large interest in unraveling the mechanism of PDA's antioxidant properties, a wide range of antioxidant-based applications of PDA have been evaluated in the biomedical field. For example, by taking advantage of the ROS-scavenging properties of PDA, Bao et al. synthesized PDA nanoparticles (PDA-NPs) for the treatment of the ROS-triggered periodontal disease. Moreover, Zhang et al reported puerarin-loaded PDA nanoparticles (PDA/PUE) that were incorporated into PEG diacrylate hybrid hydrogels. The obtained composite hydrogel (PEG-DA/PDA/PUE) displayed good proliferation and antioxidant properties, which further sped up the

wound healing process.[145] Inspired by a broad range of applications in the biomedical field, together with one of the crucial requirements for successful HBOCs (i.e., antioxidant properties), research was also performed to evaluate the potential of PDA for the fabrication of RBC substitutes. As such, in 2017, Wang et al. reported PDA-coated Hb (Hb-PDA) with integrity preservation of the Hb structure which could be prepared in a single step. Notably, Hb-PDA shows remarkable antioxidant activity and inhibition activity on the ROS generation inside the cells.[61] Moreover, the PDA coating with antioxidant properties was used to protect Hb inside the HBOCs, such as the electrosprayed hemoglobin nanoparticles fully made of Hb (Hb-NPs) and PDA-coated Hb/ CeO_2-NPs co-loaded PLGA NPs.[90,101] Moreover, due to the remarkable antioxidant properties, the PDA coating can protect Hb from being oxidized into metHb.[61,90,101]

Rather than making use of the antioxidant properties of PDA, the PDA coating can also improve the stability of HBOCs and work as a biocompatible surface crosslinker. Similar to the PDA capsule fabrication mentioned in Section 1.4.2.1, Yu et al synthesized microparticles by pre-loading Hb in the $MnCO_3$ microparticles, followed by crosslinking the Hb by GA and removing the $MnCO_3$ template.[146] After the template removal, a PDA coating with good biocompatibility was deposited, which can further increase the stability of these microparticles.[146] Furthermore, Hu et al. reported that after using a similar template assemble technique to pre-load Hb, the post PDA coating could work as a surface crosslinker which helps to decrease the Hb leakage from the particle (without crosslinking between Hb molecules) under both static and flow conditions.[147] At the same time, the PDA coating could reduce oxidative injury toward human umbilical vein cells (HUVEC) by acting as a ROS scavenger.[147] In all, the research demonstrates that, as a multifunctional material, PDA has great potential to be applied in the design of HBOCs.

1.4.3. Metal phenolic networks.

MPN are supramolecular complexes coordinated by metal irons and phenolic ligands. (Scheme 1.9). First reported by Ejima and co-workers in 2013, the MPN consisting of natural polyphenol (tannic acid (TA)) and Fe^{3+} ions was fabricated by simply mixing TA and Fe^{3+} ions in a water solution.[148] This MPN was performed to coat various substrates including organic particles (e.g.,

polystyrene (PS) particles), inorganic particles (e.g., calcium carbonate ($CaCO_3$) particles and gold NPs), and biological particulate substrates (e.g., staphylococcus epidermidis).

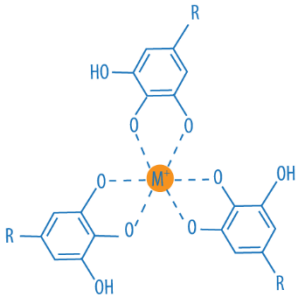

Scheme 1.9. The structure of MPN, R represents the remainder of the polyphenols. Adapted with permission from Ejima et. al.[102] Copyright ©2017, Elsevier.

1.4.3.1. Metal ions and polyphenols used for MPN fabrication.

As shown in Table 1.3 multiple kinds of metal ions and polyphenols can be used for MPN fabrication. The metal ions can be selected depending on the final application of the MPN. For example, noble metal ions such as Ag^+ were widely used for antibacterial applications since they displayed obvious antibacterial properties at relatively low concentrations.[149] Xie et al. reported an MPN nanoplatform incorporating Ag^+ and Cu^{2+} to form an alloyed nanostructure (Ag@Cu-MPN_{NC}) for wound disinfection, the metal ions in this platform enhanced the antibacterial properties in both Gram-positive and Gram-negative bacteria.[150] Other than noble metals, some trace elements of the human body such as Fe^{3+}, Cu^{2+}, and Zn^{2+} are also used in the fabrication of MPN. For example, iron plays an important role in physiological processes (e.g., act as the building material of Hb, ferritin, and hematopoiesis-related enzymes).[151] By using Fe^{3+} and PEG functionalized phenolic compounds (i.e., PEG-polyphenol) for $CaCO_3$ particle coating and followed by $CaCO_3$ core removal, Ju et al. prepared a low-fouling PEG-MPN capsule for promising drug delivery.[152]

Polyphenols, which have multiple phenolic hydroxyl groups that can coordinate with metal ions, are the other building materials for MPN fabrication. As shown in table 1.3, there are typical polyphenols that have been used in the fabrication of MPN, including natural polyphenols (e.g.,

inepigallocatechin gallate (EGCG) and TA) and artificial polyphenols (e.g., catechol-functionalized PEG and catechol-functionalized HA). Due to different final applications, a variety of polyphenols were used. For example, the remarkable medical features including anti-inflammation, anti-cancer, and antioxidant of natural polyphenols (e.g., TA, EGCG, and resveratrol (RESV)) can be used for the MPN-based therapeutics of diseases such as cancer and wound healing.[153] In contrast, the artificial polyphenols can render MPN coatings with particular properties. In this context, Ju et al. fabricated an MPN capsule by using the phenolic-functionalized hyaluronic acid (HA)/PEG-polyphenol and Fe^{3+} for the MPN coating on a $CaCO_3$ template, after the template was removed by EDTA, the $MPN_{HA\text{-}PEG}$ capsules were obtained. In this system, HA helps to enhance the binding with target tumor cells (e.g., CD44 overexpressing ($CD44^+$) cells) and PEG enables this system low fouling properties.[154]

Phenolic ligands	Metal ions	Bio-applications
TA	Fe^{3+}	pH-responsive capsules
TA	Gd^{3+}/Fe^{3+} Cr^{3+}/Fe^{3+}	Hybrid capsules
TA, GA, EGCG	Fe^{3+}	Catalysis
TA	Fe^{3+}, Mn^{3+}, Gd^{3+}	MRI imaging
TA	$^{64}Cu^{2+}$	PET imaging
TA	Fe^{3+}, Ti^{4+}	Enzyme-immobilized capsules
TA	Fe^{3+}	Magnetic and enzyme-loaded
TA	Al^{3+}	Drug delivery
TA	Fe^{3+}, Al^{3+}, Eu^{3+}	Drug delivery/Cell imaging
Catechol-functionalized PEG	Fe^{3+}	Low-fouling and pH-degradable capsules
Catechol-functionalized HA and PEG	Fe^{3+}	Cancer cell targeting
Catechol-functionalized HA	Fe^{3+}	Protein corona-coated MPN capsules
TA	Fe^{3+}	pH- and glutathione-responsive release of curcumin
TA	Fe^{3+}	Anticancer therapy
TA	Fe^{3+}	Cytoprotective coating
TA	Fe^{3+}	Cellular surface engineering
TA	Fe^{3+}	Enhanced stability of virus
TA/GA	Fe^{3+}	Dental hypersensitivity
TA	Ti^{4+}	Enzyme immobilization
Dopamine	Ti^{4+}	Enzyme immobilization
TA	Fe^{3+}	Micropatterned adhesion of proteins and cells
TA	Fe^{3+}	Anti-biofouling

Table 1.3. Summary of recent studies of MPN on bio-applications. Abbreviations in the table are: epigallocatechin gallate (EGCG); magnetic resonance imaging (MRI); positron emission tomography (PET); gallic acid (GA); polyethylene glycol (PEG); hyaluronic acid (HA). Adapted with permission from Ejima et. al.[102] Copyright ©2017, Elsevier.

1.4.3.2. TA-Fe^{3+} based MPN.

Despite a large range of metal ions and polyphenols that can be used for MPN fabrication, as shown in Table 1.3 TA and Fe^{3+} are the most widely used compounds for MPN synthesis in the biomedical field. This is because both compounds are inexpensive and both of them are generally recognized as safe by the FDA.[102,155] Moreover, TA has been approved by the FDA as a food additive.[156] The structure of TA (Scheme 1.10) includes a glucose core in the center and five digalloyl ester groups on the outside. Due to the abundant phenolic hydroxyl group, TA can easily chelate metal ions (e.g., Fe^{3+}) working as the polydentate ligand in the MPN fabrication.

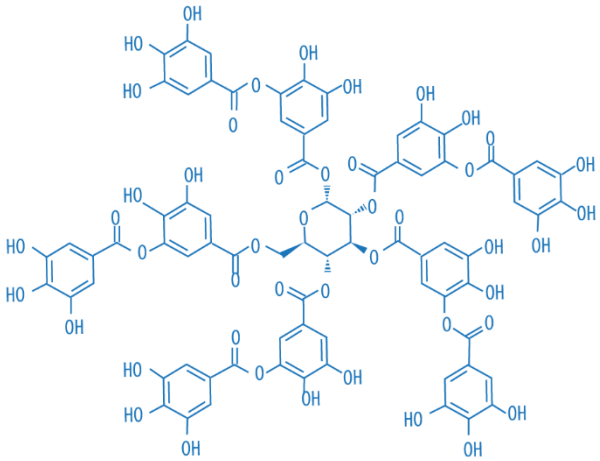

Scheme 1.10. Structure of TA. Adapted with permission from Ejima et. al.[102] Copyright ©2017, Elsevier.

The coordination between TA and Fe^{3+} is a spontaneous and pH-dependent process (Scheme 1.11).[148] Specifically, a stable tris-complex can be formed at a pH higher than 7, while the tris-complex can be transformed to bis-complex at a pH between 3 and 6, and further, when the pH is below 2, the mono-complex can be formed and can result in the disassembly of the MPN structure. The transition between these three complexes is reversible due to the pH, which makes the MPN fabrication and disassembling also a pH-dependent process.[148] Moreover, two methods can be used for TA-Fe^{3+}-based MPN coating fabrication. (Scheme 1.12). On the one hand, MPN coating can be formed in a couple of seconds by an easy one-pot mixing method, resulting in a thickness of ~ 10 nm. On the other hand, to obtain a thinner MPN coating (~2 nm) a multiple-step coating method can be performed, where a substrate is immersed into TA and Fe^{3+} separately for several rounds.[102]

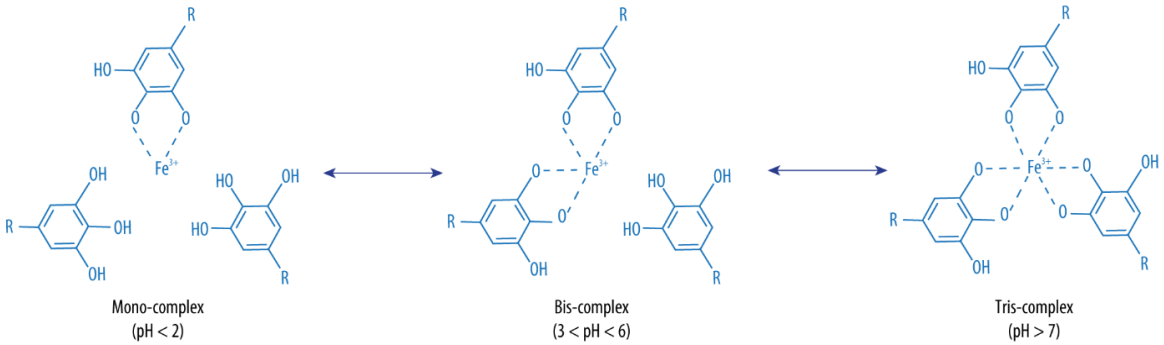

Scheme 1.11. pH dependent TA-Fe^{3+} coordination process, R represents the remainder of the TA molecule. Adapted with permission from Ejima et. al.[148] Copyright ©2013, Science.

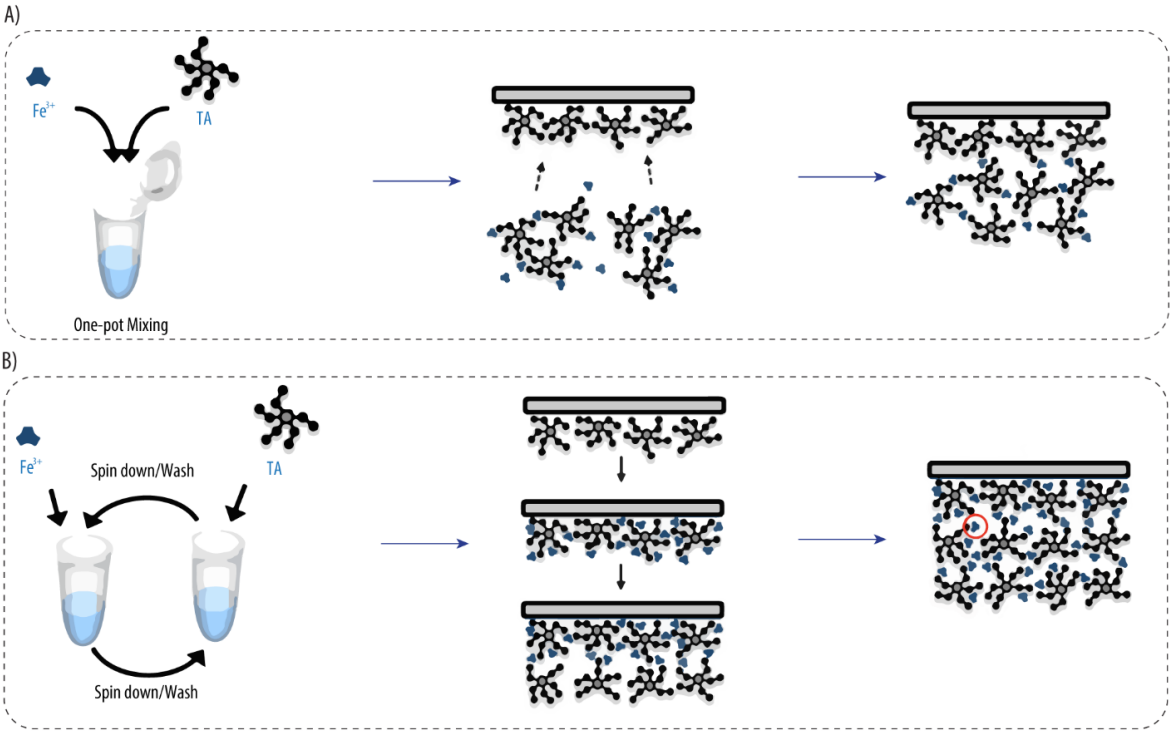

Scheme 1.12. One-step (a) and multistep (b) assembly of MPNs. Adapted with permission from Ejima et. al.[102] Copyright ©2017, Elsevier.

1.4.3.2.1. Self-assembled systems formed by TA-Fe^{3+} based MPN.

By a physical mix, the fabrication of TA-Fe^{3+} based MPN is very simple and efficient. Specifically, the metal ion (positively charged) can coordinate with the phenolic hydroxyl groups (electron-

dense) to form different self-assembly systems such as particles and surface coatings. Also, by combining the template assembly technique, MPN hollow capsules can be fabricated. Besides, the abundant phenolic hydroxyl groups and good water solubility of TA makes that it can act as a building block of the hydrogel, and at the same time, the TA-Fe^{3+} based MPN can improve the mechanical properties of the hydrogel. What's more, together with the antibacterial, anti-inflammation, and antioxidant properties of TA,[102] the self-assembly systems based on TA-Fe^{3+} MPN displayed great potential to be applied in biomedicine.

For example, by making use of hydroxypropyl chitin (HPCH), TA, and Fe^{3+}, Ma et al synthesized a pH-responsive and thermosensitive hydrogel. In this system, HPCH worked as a thermosensitive biomaterial, while TA acted as an antibacterial material for wound healing and as a crosslinker to increase the mechanical properties of the hydrogel.[157] Besides, the TA-Fe^{3+}-based MPN can also form solid NPs. Saowalak et al. prepared Fe^{3+}-TA NPs (Fe-TA NPs) by simply mixing ferric chloride and TA in PBS buffer (pH 7.4) at room temperature. The as-prepared Fe-TA NPs displayed a size of ~3 nm and showed enhanced uptake by hepatocellular carcinoma cells (HepG2.2.15). Followed by resulting in autophagic cell death on HepG2.2.15, together with the enhanced magnetic resonance imaging (MRI) signal (from the Fe^{3+}) in the liver, the Fe-TA NPs shows great potential for theranostic therapy of hepatocellular carcinoma.[158]

Other than the self-assembled hydrogel and NPs, by combining the template assembly technique, the MPN can also form hollow capsules. By using TA and 18 kinds of metal ions (e.g., radioactive $^{64}Cu^{II}$ for positron emission tomography (PET), and Fe^{3+}/Mn^{2+}/Gd^{3+} for MRI), Guo et al. fabricated robust MPN coatings on the surface of a template (e.g., polystyrene particles). Once the coatings were successfully deposited, the template was removed by tetrahydrofuran (THF), resulting in a large array of different MPN capsules. The chosen of particular metal ions, together with the hollow structure, enable these MPN capsules to display great potential for bio-applications in drug delivery, PET, and MRI.[159] Other than removing the template to form a hollow capsule, TA-Fe^{3+} based MPN coating itself can also work as a functional surface modification. Yang and co-workers fabricated DOX loaded mesoporous silica nanoparticles (MSN), which were coated by a surface of TA-Fe^{3+} based MPN (consisting of TA and Fe^{3+}/Al^{3+}). In this research, the MPN coating works not only as a photothermal agent for photothermal therapy (PTT), but also as a dual photothermal and pH-responsive shell for DOX release to enhance tumor therapies.[160] Moreover,

TA-based MPN can also be used for biointerfaces coating. Park et al. reported an artificial TA–Fe^{3+} shell on the surface of yeast, which can protect the yeast from external attacks such as lytic enzymes and UV-C irradiation. Meanwhile, this TA-Fe^{3+} shell can suppress in a controllable manner cell division which is quite crucial for cell-based devices that need long-term cell preservation and controlled cell exposure.[161]

1.4.3.2.2. Antioxidant properties of TA-Fe^{3+} based MPN.

Another important and widely applied feature of TA-Fe^{3+} based MPN is their antioxidant/radical scavenging properties, which is derived from TA. Interestingly, it was reported that TA is one of the polyphenol with the highest antioxidant capacity among eight representative polyphenols (e.g., quercetin, rutin, catechin, resveratrol, TA, gallic, caffeic, and ferulic).[162] The structures in TA that are responsible for the antioxidant properties are the five digalloyl ester groups (Scheme 1.10), which include the gallol structure (Scheme 1.13). Interestingly, the gallol structure of TA is very similar to the catechol structure, which is the building block of PDA. PDA was also recognized as one of the polyphenols,[163] and most polyphenols (including PDA and TA) share a similar antioxidant mechanism.[142] That is, as specifically discussed in Section 1.4.2.2, H atom transfer, electron transfer, and chelate transition metal ions are included in the potential antioxidant mechanism (i.e., ROS/RNS scavenging) of TA.[142]

Scheme 1.13. Key structure of PDA (i.e., catechol) and TA (i.e., gallol), which are responsible for antioxidant properties

Based on the remarkable antioxidant properties of TA, great interest in the antioxidant applications of TA-Fe^{3+} based MPN was aroused in the past few years. For example, by combining the antioxidant properties of Fe_3O_4 NPs and TA, Wei et al fabricated an MPN nanoplatform (Fe_3O_4 @

TA nanoflowers) with a broad-spectrum radical scavenging capacity. Herein, both the Fe_3O_4 and TA acted as antioxidant compounds that can scavenge multiple ROS (e.g., $O_2^{\cdot-}$, $HO^{\cdot}$, and H_2O_2). According to the in vivo experiments, by renewing the antioxidant level of cells, this system displayed an enhanced therapeutic capacity for wound healing and endotoxemia.[164] Moreover, Qin and co-workers synthesized multifunctional NPs by using MPN (TA–Fe^{3+}) coating for the surface modification of starch nanocrystals (SNCs) and debranched starch nanoparticles (DBS-NPs). Due to the excellent antioxidant capacity of TA, the obtained MPN@SNCs (MPN-coated SCNs) and MPN@DBS-NPs (MPN-coated DBS-NPs) displayed remarkable antioxidant bioactivities, which enabled this system to have great potential for food and biomedical applications.[165]

1.4.3.2.3. Coordination-driven crosslinking properties of TA-Fe^{3+} based MPN.

While TA is responsible for the antioxidant properties within the coating, the TA and Fe^{3+} together are responsible for the coordination-driven crosslinking process within the TA-Fe^{3+} based MPN. Specifically, at physiological condition (pH 7.4) a stable network is obtained which can improve the stability/mechanical properties of a drug delivery system. However, as shown in Scheme 1.11, when the pH drops to the pH below 6, the tris-complex disassembles into the bis- or the mono-complex, which results in the disassembly of the MPN, and this can be used for controlled release of a drug delivery system. For example, by using the solvent exchange technique, Yi et al. synthesized a dimeric paclitaxel (diPTX) prodrug nanoparticle, followed by a TA-Fe^{3+} based MPN coating to stabilize this nanocore. At pH 7.4, a negligible amount of diPTX was released due to the stability of the MPN shell, while a remarkable release of diPTX (~40%) could be obtained at pH 5.2, which was used for pH-responsive drug delivery for tumor therapy.[166]

In all, based on the remarkable features of TA-Fe^{3+} based MPN (i.e., antioxidant properties and property of coordination-driven crosslinking), together with the high safety, low cost, and easy fabrication, a great promise can be forseen in the usage of TA-Fe^{3+} based MPN in the HBOCs field.

1.5. References

(1) Liu, W.-L.; Liu, T.; Zou, M.-Z.; Yu, W.-Y.; Li, C.-X.; He, Z.-Y.; Zhang, M.-K.; Liu, M.-D.; Li, Z.-H.; Feng, J.; Zhang, X.-Z. Aggressive Man-Made Red Blood Cells for Hypoxia-Resistant Photodynamic Therapy. *Advanced Materials* **2018**, *30* (35), 1802006. https://doi.org/https://doi.org/10.1002/adma.201802006.

(2) sen Gupta, A.; Doctor, A. Oxygen Carriers. In *Damage Control Resuscitation: Identification and Treatment of Life-Threatening Hemorrhage*; Spinella, P. C., Ed.; Springer International Publishing: Cham, 2020; pp 197–222. https://doi.org/10.1007/978-3-030-20820-2_11.

(3) Bialas, C.; Moser, C.; Sims, C. A. Artificial Oxygen Carriers and Red Blood Cell Substitutes: A Historic Overview and Recent Developments toward Military and Clinical Relevance. *Journal of Trauma and Acute Care Surgery* **2019**, *87* (1S).

(4) Cap, A. P.; Pidcoke, H. F.; DePasquale, M.; Rappold, J. F.; Glassberg, E.; Eliassen, H. S.; Bjerkvig, C. K.; Fosse, T. K.; Kane, S.; Thompson, P.; Sikorski, R.; Miles, E.; Fisher, A.; Ward, K. R.; Spinella, P. C.; Strandenes, G. Blood Far Forward: Time to Get Moving! *Journal of Trauma and Acute Care Surgery* **2015**, *78* (6).

(5) Spinella, P. C.; Dunne, J.; Beilman, G. J.; O'Connell, R. J.; Borgman, M. A.; Cap, A. P.; Rentas, F. Constant Challenges and Evolution of US Military Transfusion Medicine and Blood Operations in Combat. *Transfusion (Paris)* **2012**, *52* (5), 1146–1153. https://doi.org/https://doi.org/10.1111/j.1537-2995.2012.03594.x.

(6) Chang, R.; Eastridge, B. J.; Holcomb, J. B. Remote Damage Control Resuscitation in Austere Environments. *Wilderness Environ Med* **2017**, *28* (2, Supplement), S124–S134. https://doi.org/https://doi.org/10.1016/j.wem.2017.02.002.

(7) D'Alessandro, A.; Kriebardis, A. G.; Rinalducci, S.; Antonelou, M. H.; Hansen, K. C.; Papassideri, I. S.; Zolla, L. An Update on Red Blood Cell Storage Lesions, as Gleaned through Biochemistry and Omics Technologies. *Transfusion (Paris)* **2015**, *55* (1), 205–219. https://doi.org/https://doi.org/10.1111/trf.12804.

(8) Devine, D. v; Serrano, K. The Platelet Storage Lesion. *Clin Lab Med* **2010**, *30* (2), 475–487. https://doi.org/10.1016/j.cll.2010.02.002.

(9) Njoku, M.; Peter, D. S.; Mackenzie, C. F. Haemoglobin-Based Oxygen Carriers: Indications and Future Applications. *Br J Hosp Med* **2015**, *76* (2), 78–83. https://doi.org/10.12968/hmed.2015.76.2.78.

(10) Acker, J. P.; Marks, D. C.; Sheffield, W. P. Quality Assessment of Established and Emerging Blood Components for Transfusion. *J Blood Transfus* **2016**, *2016*.

(11) Noorman, F.; van Dongen, T. T. C. F.; Plat, M.-C. J.; Badloe, J. F.; Hess, J. R.; Hoencamp, R. Transfusion: -80°C Frozen Blood Products Are Safe and Effective in Military Casualty Care. *PLoS One* **2016**, *11* (12), e0168401-.

(12) Kauvar, D. S.; Holcomb, J. B.; Norris, G. C.; Hess, J. R. Fresh Whole Blood Transfusion: A Controversial Military Practice. *Journal of Trauma and Acute Care Surgery* **2006**, *61* (1).

(13) Pidcoke, H. F.; McFaul, S. J.; Ramasubramanian, A. K.; Parida, B. K.; Mora, A. G.; Fedyk, C. G.; Valdez-Delgado, K. K.; Montgomery, R. K.; Reddoch, K. M.; Rodriguez, A. C.; Aden, J. K.; Jones, J. A.; Bryant, R. S.; Scherer, M. R.; Reddy, H. L.; Goodrich, R. P.; Cap, A. P. Primary Hemostatic Capacity of Whole Blood: A Comprehensive Analysis of Pathogen Reduction and Refrigeration

Effects over Time. *Transfusion (Paris)* **2013**, *53* (S1), 137S-149S. https://doi.org/https://doi.org/10.1111/trf.12048.

(14) Simoni, J. Artificial Oxygen Carriers: Exactly How Close Are We to an Ultimate Product? *Artif Organs* **2017**, *41* (4), 316–318. https://doi.org/https://doi.org/10.1111/aor.12939.

(15) Modery-Pawlowski, C. L.; Tian, L. L.; Pan, V.; McCrae, K. R.; Mitragotri, S.; sen Gupta, A. Approaches to Synthetic Platelet Analogs. *Biomaterials* **2013**, *34* (2), 526–541. https://doi.org/https://doi.org/10.1016/j.biomaterials.2012.09.074.

(16) Chang, T. M. S. Red Blood Cell Replacement, or Nanobiotherapeutics with Enhanced Red Blood Cell Functions? *Artif Cells Nanomed Biotechnol* **2015**, *43* (3), 145–147. https://doi.org/10.3109/21691401.2015.1047557.

(17) Imamura, T. [Human hemoglobin structure and respiratory transport]. *Nihon Rinsho* **1996**, *54* (9), 2320–2325.

(18) Mohanty, J.; Nagababu, E.; Rifkind, J. Red Blood Cell Oxidative Stress Impairs Oxygen Delivery and Induces Red Blood Cell Aging. *Front Physiol* **2014**, *5*.

(19) Patel, S.; Mohiuddin, S. S. Physiology, Oxygen Transport And Carbon Dioxide Dissociation Curve. *In StatPearls Publishing; Treasure Island, 2020*.

(20) Madan, A. Correlation between the Levels of SpO2and PaO2. *Lung India* **2017**, *34* (3). https://doi.org/https://doi.org/10.4103/lungindia.lungindia_106_17.

(21) Ferenz, K. B.; Steinbicker, A. U. Artificial Oxygen Carriers—Past, Present, and Future—a Review of the Most Innovative and Clinically Relevant Concepts. *Journal of Pharmacology and Experimental Therapeutics* **2019**, *369* (2), 300. https://doi.org/10.1124/jpet.118.254664.

(22) Cortese-Krott, M. M.; Shiva, S. The Redox Physiology of Red Blood Cells and Platelets: Implications for Their Interactions and Potential Use as Systemic Biomarkers. *Curr Opin Physiol* **2019**, *9*, 56–66. https://doi.org/https://doi.org/10.1016/j.cophys.2019.04.016.

(23) Kuhn, V.; Diederich, L.; Keller, T. C. S.; Kramer, C. M.; Lückstädt, W.; Panknin, C.; Suvorava, T.; Isakson, B. E.; Kelm, M.; Cortese-Krott, M. M. Red Blood Cell Function and Dysfunction: Redox Regulation, Nitric Oxide Metabolism, Anemia. *Antioxid Redox Signal* **2016**, *26* (13), 718–742. https://doi.org/10.1089/ars.2016.6954.

(24) Jansman, M. M. T.; Hosta-Rigau, L. Recent and Prominent Examples of Nano- and Microarchitectures as Hemoglobin-Based Oxygen Carriers. *Adv Colloid Interface Sci* **2018**, *260*, 65–84. https://doi.org/https://doi.org/10.1016/j.cis.2018.08.006.

(25) Allen, B. W.; Stamler, J. S.; Piantadosi, C. A. Hemoglobin, Nitric Oxide and Molecular Mechanisms of Hypoxic Vasodilation. *Trends Mol Med* **2009**, *15* (10), 452–460. https://doi.org/https://doi.org/10.1016/j.molmed.2009.08.002.

(26) Ludlow, J. T.; Wilkerson, R. G.; Nappe, T. M. *Methemoglobinemia*; StatPearls Publishing, Treasure Island (FL), 2022.

(27) Bunn, H. F.; Esham, W. T.; Bull, R. W. THE RENAL HANDLING OF HEMOGLOBIN : I. GLOMERULAR FILTRATION. *Journal of Experimental Medicine* **1969**, *129* (5), 909–924. https://doi.org/10.1084/jem.129.5.909.

(28) Buehler, P. W.; D'Agnillo, F.; Schaer, D. J. Hemoglobin-Based Oxygen Carriers: From Mechanisms of Toxicity and Clearance to Rational Drug Design. *Trends Mol Med* **2010**, *16* (10), 447–457. https://doi.org/https://doi.org/10.1016/j.molmed.2010.07.006.

(29) Kim-Shapiro, D. B.; Schechter, A. N.; Gladwin, M. T. Unraveling the Reactions of Nitric Oxide, Nitrite, and Hemoglobin in Physiology and Therapeutics. *Arterioscler Thromb Vasc Biol* **2006**, *26* (4), 697–705. https://doi.org/10.1161/01.ATV.0000204350.44226.9a.

(30) Ortiz, D.; Barros, M.; Yan, S.; Cabrales, P. Resuscitation from Hemorrhagic Shock Using Polymerized Hemoglobin Compared to Blood. *Am J Emerg Med* **2014**, *32* (3), 248–255. https://doi.org/https://doi.org/10.1016/j.ajem.2013.11.045.

(31) Mer, M.; Hodgson, E.; Wallis, L.; Jacobson, B.; Levien, L.; Snyman, J.; Sussman, M. J.; James, M.; van Gelder, A.; Allgaier, R.; Jahr, J. S. Hemoglobin Glutamer-250 (Bovine) in South Africa: Consensus Usage Guidelines from Clinician Experts Who Have Treated Patients. *Transfusion (Paris)* **2016**, *56* (10), 2631–2636. https://doi.org/https://doi.org/10.1111/trf.13726.

(32) Jahr, J. S.; Moallempour, M.; Lim, J. C. HBOC-201, Hemoglobin Glutamer-250 (Bovine), Hemopure® (Biopure Corporation). *Expert Opin Biol Ther* **2008**, *8* (9), 1425–1433. https://doi.org/10.1517/14712598.8.9.1425.

(33) Staub, A.; Rudaz, S.; Saugy, M.; Veuthey, J.-L.; Schappler, J. Analysis of Hemoglobin-Based Oxygen Carriers by CE-UV/Vis and CE-ESI-TOF/MS. *Electrophoresis* **2010**, *31* (7), 1241–1247. https://doi.org/https://doi.org/10.1002/elps.200900513.

(34) Cabrales, P.; Intaglietta, M. Blood Substitutes: Evolution from Noncarrying to Oxygen- and Gas-Carrying Fluids. *ASAIO Journal* **2013**, *59* (4).

(35) Moradi, S.; Jahanian-Najafabadi, A.; Roudkenar, M. H. Artificial Blood Substitutes: First Steps on the Long Route to Clinical Utility. *Clin Med Insights Blood Disord* **2016**, *9*, CMBD.S38461. https://doi.org/10.4137/CMBD.S38461.

(36) S Jahr, J.; Sadighi Akha, A.; J Holtby, R. Crosslinked, Polymerized, and PEG-Conjugated Hemoglobin-Based Oxygen Carriers: Clinical Safety and Efficacy of Recent and Current Products. *Curr Drug Discov Technol* **2012**, *9* (3), 158–165.

(37) Olofsson, C.; Ahl, T.; Johansson, T.; Larsson, S.; Nellgård, P.; Ponzer, S.; Fagrell, B.; Przybelski, R.; Keipert, P.; Winslow, N.; Winslow, R. M. A Multicenter Clinical Study of the Safety and Activity of Maleimide-Polyethylene Glycol–Modified Hemoglobin (Hemospan®) in Patients Undergoing Major Orthopedic Surgery. *Anesthesiology* **2006**, *105* (6), 1153–1163. https://doi.org/10.1097/00000542-200612000-00015.

(38) Winslow, R. M. MP4, a New Nonvasoactive Polyethylene Glycol–Hemoglobin Conjugate. *Artif Organs* **2004**, *28* (9), 800–806. https://doi.org/https://doi.org/10.1111/j.1525-1594.2004.07392.x.

(39) Sloan, E. P.; Koenigsberg, M. D.; Philbin, N. B.; Gao, W.; Investigators, for the Dclh. T. H. S. S. G. and the E. H. Diaspirin Cross-Linked Hemoglobin Infusion Did Not Influence Base Deficit and Lactic Acid Levels in Two Clinical Trials of Traumatic Hemorrhagic Shock Patient Resuscitation. *Journal of Trauma and Acute Care Surgery* **2010**, *68* (5).

(40) Chen, J.-Y.; Scerbo, M.; Kramer, G. A Review of Blood Substitutes: Examining The History, Clinical Trial Results, and Ethics of Hemoglobin-Based Oxygen Carriers. *Clinics* **2009**, *64* (8), 803–813. https://doi.org/https://doi.org/10.1590/S1807-59322009000800016.

(41) Cabrales, P.; Intaglietta, M. Blood Substitutes: Evolution from Noncarrying to Oxygen- and Gas-Carrying Fluids. *ASAIO Journal* **2013**, *59* (4).

(42) Simoni, J.; Simoni, G.; E Wesson, D.; Feola, M. ATP-Adenosine-Glutathione Cross-Linked Hemoglobin as Clinically Useful Oxygen Carrier. *Curr Drug Discov Technol* **2012**, *9* (3), 173–187.

(43) Simoni, J.; Simoni, G.; Moeller, J. F.; Feola, M.; Wesson, D. E. Artificial Oxygen Carrier With Pharmacologic Actions of Adenosine-5′-Triphosphate, Adenosine, and Reduced Glutathione

Formulated to Treat an Array of Medical Conditions. *Artif Organs* **2014**, *38* (8), 684–690. https://doi.org/https://doi.org/10.1111/aor.12337.

(44) D'agnillo, F.; Chang, T. M. S. Cross-Linked Hemoglobin-Superoxide Dismutase-Catalase Scavenges Oxygen-Derived Free Radicals and Prevents Methemoglobin Formation and Iron Release. *Biomaterials, Artificial Cells and Immobilization Biotechnology* **1993**, *21* (5), 609–621. https://doi.org/10.3109/10731199309117385.

(45) Haruki, R.; Kimura, T.; Iwasaki, H.; Yamada, K.; Kamiyama, I.; Kohno, M.; Taguchi, K.; Nagao, S.; Maruyama, T.; Otagiri, M.; Komatsu, T. Safety Evaluation of Hemoglobin-Albumin Cluster "HemoAct" as a Red Blood Cell Substitute. *Sci Rep* **2015**, *5* (1), 12778. https://doi.org/10.1038/srep12778.

(46) Chang, T. M. S. ARTIFICIAL CELL Evolves into Nanomedicine, Biotherapeutics, Blood Substitutes, Drug Delivery, Enzyme/Gene Therapy, Cancer Therapy, Cell/Stem Cell Therapy, Nanoparticles, Liposomes, Bioencapsulation, Replicating Synthetic Cells, Cell Encapsulation/Scaffold, Biosorbent/Immunosorbent Haemoperfusion/Plasmapheresis, Regenerative Medicine, Encapsulated Microbe, Nanobiotechnology, Nanotechnology. *Artif Cells Nanomed Biotechnol* **2019**, *47* (1), 997–1013.

(47) CHANG, T. M. S.; POZNANSKY, M. J. Semipermeable Microcapsules Containing Catalase for Enzyme Replacement in Acatalasaemic Mice. *Nature* **1968**, *218* (5138), 243–245. https://doi.org/10.1038/218243a0.

(48) Chang, T. M. S.; Powanda, D.; Yu, W. P. Analysis of Polyethylene-glycol-polylactide Nano-Dimension Artificial Red Blood Cells in Maintaining Systemic Hemoglobin Levels and Prevention of Methemoglobin Formation. *Artificial Cells, Blood Substitutes, and Biotechnology* **2003**, *31* (3), 231–247. https://doi.org/10.1081/BIO-120023155.

(49) Gao, W.; Bian, Y.; Chang, T. M. S. Novel Nanodimension Artificial Red Blood Cells That Act as O2 and CO2 Carrier with Enhanced Antioxidant Activity: PLA-PEG Nanoencapsulated PolySFHb-Superoxide Dismutase-Catalase-Carbonic Anhydrase. *Artif Cells Nanomed Biotechnol* **2013**, *41* (4), 232–239. https://doi.org/10.3109/21691401.2012.751180.

(50) Chang, T. M. S.; D'Agnillo, F.; Yu, W. P.; Razack, S. Two Future Generations of Blood Substitutes Based on Polyhemoglobin–SOD–Catalase and Nanoencapsulation. *Adv Drug Deliv Rev* **2000**, *40* (3), 213–218. https://doi.org/https://doi.org/10.1016/S0169-409X(99)00051-4.

(51) Kunert, M. P.; Liard, J. F.; Abraham, D. J. RSR-13, an Allosteric Effector of Hemoglobin, Increases Systemic and Iliac Vascular Resistance in Rats. *American Journal of Physiology-Heart and Circulatory Physiology* **1996**, *271* (2), H602–H613. https://doi.org/10.1152/ajpheart.1996.271.2.H602.

(52) Pan, D.; Rogers, S.; Misra, S.; Vulugundam, G.; Gazdzinski, L.; Tsui, A.; Mistry, N.; Said, A.; Spinella, P.; Hare, G.; Lanza, G.; Doctor, A. Erythromer (EM), a Nanoscale Bio-Synthetic Artificial Red Cell: Proof of Concept and In Vivo Efficacy Results. *Blood* **2016**, *128* (22), 1027. https://doi.org/https://doi.org/10.1182/blood.V128.22.1027.1027.

(53) Yadav, V. R.; Nag, O.; Awasthi, V. Biological Evaluation of Liposome-Encapsulated Hemoglobin Surface-Modified With a Novel PEGylated Nonphospholipid Amphiphile. *Artif Organs* **2014**, *38* (8), 625–633. https://doi.org/https://doi.org/10.1111/aor.12304.

(54) Tao, Z.; Ghoroghchian, P. P. Microparticle, Nanoparticle, and Stem Cell-Based Oxygen Carriers as Advanced Blood Substitutes. *Trends Biotechnol* **2014**, *32* (9), 466–473. https://doi.org/https://doi.org/10.1016/j.tibtech.2014.05.001.

(55) Sakai, H. Present Situation of the Development of Cellular-Type Hemoglobin-Based Oxygen Carrier (Hemoglobin-Vesicles). *Curr Drug Discov Technol* **2012**, *9* (3), 188–193.

(56) Yadav, V. R.; Rao, G.; Houson, H.; Hedrick, A.; Awasthi, S.; Roberts, P. R.; Awasthi, V. Nanovesicular Liposome-Encapsulated Hemoglobin (LEH) Prevents Multi-Organ Injuries in a Rat Model of Hemorrhagic Shock. *European Journal of Pharmaceutical Sciences* **2016**, *93*, 97–106. https://doi.org/https://doi.org/10.1016/j.ejps.2016.08.010.

(57) Sakai, H.; Sou, K.; Horinouchi, H.; Kobayashi, K.; Tsuchida, E. Review of Hemoglobin-Vesicles as Artificial Oxygen Carriers. *Artif Organs* **2009**, *33* (2), 139–145. https://doi.org/https://doi.org/10.1111/j.1525-1594.2008.00698.x.

(58) Rideau, E.; Dimova, R.; Schwille, P.; Wurm, F. R.; Landfester, K. Liposomes and Polymersomes: A Comparative Review towards Cell Mimicking. *Chem Soc Rev* **2018**, *47* (23), 8572–8610. https://doi.org/10.1039/C8CS00162F.

(59) Li, B.; Li, T.; Chen, G.; Li, X.; Yan, L.; Xie, Z.; Jing, X.; Huang, Y. Regulation of Conjugated Hemoglobin on Micelles through Copolymer Chain Sequences and the Protein's Isoelectric Aggregation. *Macromol Biosci* **2013**, *13* (7), 893–902. https://doi.org/https://doi.org/10.1002/mabi.201300012.

(60) Xiong, Y.; Liu, Z. Z.; Georgieva, R.; Smuda, K.; Steffen, A.; Sendeski, M.; Voigt, A.; Patzak, A.; Bäumler, H. Nonvasoconstrictive Hemoglobin Particles as Oxygen Carriers. *ACS Nano* **2013**, *7* (9), 7454–7461. https://doi.org/10.1021/nn402073n.

(61) Wang, Q.; Zhang, R.; Lu, M.; You, G.; Wang, Y.; Chen, G.; Zhao, C.; Wang, Z.; Song, X.; Wu, Y.; Zhao, L.; Zhou, H. Bioinspired Polydopamine-Coated Hemoglobin as Potential Oxygen Carrier with Antioxidant Properties. *Biomacromolecules* **2017**, *18* (4), 1333–1341. https://doi.org/10.1021/acs.biomac.7b00077.

(62) Baidukova, O.; Wang, Q.; Chaiwaree, S.; Freyer, D.; Prapan, A.; Georgieva, R.; Zhao, L.; Bäumler, H. Antioxidative Protection of Haemoglobin Microparticles (HbMPs) by PolyDopamine. *Artif Cells Nanomed Biotechnol* **2018**, *46* (sup3), S693–S701. https://doi.org/10.1080/21691401.2018.1505748.

(63) Yuan, S.; Feng, L.; Wang, K.; Pang, J.; Bosch, M.; Lollar, C.; Sun, Y.; Qin, J.; Yang, X.; Zhang, P.; Wang, Q.; Zou, L.; Zhang, Y.; Zhang, L.; Fang, Y.; Li, J.; Zhou, H.-C. Stable Metal–Organic Frameworks: Design, Synthesis, and Applications. *Advanced Materials* **2018**, *30* (37), 1704303. https://doi.org/https://doi.org/10.1002/adma.201704303.

(64) Qin, J.-S.; Yuan, S.; Lollar, C.; Pang, J.; Alsalme, A.; Zhou, H.-C. Stable Metal–Organic Frameworks as a Host Platform for Catalysis and Biomimetics. *Chemical Communications* **2018**, *54* (34), 4231–4249. https://doi.org/10.1039/C7CC09173G.

(65) Howarth, A. J.; Liu, Y.; Li, P.; Li, Z.; Wang, T. C.; Hupp, J. T.; Farha, O. K. Chemical, Thermal and Mechanical Stabilities of Metal–Organic Frameworks. *Nat Rev Mater* **2016**, *1* (3), 15018. https://doi.org/10.1038/natrevmats.2015.18.

(66) Peng, S.; Liu, J.; Qin, Y.; Wang, H.; Cao, B.; Lu, L.; Yu, X. Metal–Organic Framework Encapsulating Hemoglobin as a High-Stable and Long-Circulating Oxygen Carriers to Treat Hemorrhagic Shock. *ACS Appl Mater Interfaces* **2019**, *11* (39), 35604–35612. https://doi.org/10.1021/acsami.9b15037.

(67) Liu, X.; Jansman, M. M. T.; Hosta-Rigau, L. Haemoglobin-Loaded Metal Organic Framework-Based Nanoparticles Camouflaged with a Red Blood Cell Membrane as Potential Oxygen Delivery Systems. *Biomater Sci* **2020**, *8* (21), 5859–5873. https://doi.org/10.1039/D0BM01118E.

(68) Feng, D.; Liu, T.-F.; Su, J.; Bosch, M.; Wei, Z.; Wan, W.; Yuan, D.; Chen, Y.-P.; Wang, X.; Wang, K.; Lian, X.; Gu, Z.-Y.; Park, J.; Zou, X.; Zhou, H.-C. Stable Metal-Organic Frameworks Containing Single-Molecule Traps for Enzyme Encapsulation. *Nat Commun* **2015**, *6* (1), 5979. https://doi.org/10.1038/ncomms6979.

(69) Fang, R. H.; Jiang, Y.; Fang, J. C.; Zhang, L. Cell Membrane-Derived Nanomaterials for Biomedical Applications. *Biomaterials* **2017**, *128*, 69–83. https://doi.org/https://doi.org/10.1016/j.biomaterials.2017.02.041.

(70) Longmire, M.; Choyke, P. L.; Kobayashi, H. Clearance Properties of Nano-Sized Particles and Molecules as Imaging Agents: Considerations and Caveats. *Nanomedicine* **2008**, *3* (5), 703–717. https://doi.org/10.2217/17435889.3.5.703.

(71) Jasinski, D. L.; Li, H.; Guo, P. The Effect of Size and Shape of RNA Nanoparticles on Biodistribution. *Molecular Therapy* **2018**, *26* (3), 784–792. https://doi.org/https://doi.org/10.1016/j.ymthe.2017.12.018.

(72) Venturoli, D.; Rippe, B. Ficoll and Dextran vs. Globular Proteins as Probes for Testing Glomerular Permselectivity: Effects of Molecular Size, Shape, Charge, and Deformability. *American Journal of Physiology-Renal Physiology* **2005**, *288* (4), F605–F613. https://doi.org/10.1152/ajprenal.00171.2004.

(73) Hardonk, M. J.; Harms, G.; Koudstaal, J. Zonal Heterogeneity of Rat Hepatocytes in the in Vivo Uptake of 17 Nm Colloidal Gold Granules. *Histochemistry* **1985**, *83* (5), 473–477. https://doi.org/10.1007/BF00509211.

(74) Tabata, Y.; Ikada, Y. Effect of the Size and Surface Charge of Polymer Microspheres on Their Phagocytosis by Macrophage. *Biomaterials* **1988**, *9* (4), 356–362. https://doi.org/https://doi.org/10.1016/0142-9612(88)90033-6.

(75) Champion, J. A.; Walker, A.; Mitragotri, S. Role of Particle Size in Phagocytosis of Polymeric Microspheres. *Pharm Res* **2008**, *25* (8), 1815–1821. https://doi.org/10.1007/s11095-008-9562-y.

(76) Venturoli, D.; Rippe, B. Ficoll and Dextran vs. Globular Proteins as Probes for Testing Glomerular Permselectivity: Effects of Molecular Size, Shape, Charge, and Deformability. *American Journal of Physiology-Renal Physiology* **2005**, *288* (4), F605–F613. https://doi.org/10.1152/ajprenal.00171.2004.

(77) Jasinski, D. L.; Li, H.; Guo, P. The Effect of Size and Shape of RNA Nanoparticles on Biodistribution. *Molecular Therapy* **2018**, *26* (3), 784–792. https://doi.org/https://doi.org/10.1016/j.ymthe.2017.12.018.

(78) Cabrales, P. Examining and Mitigating Acellular Hemoglobin Vasoactivity. *Antioxid Redox Signal* **2012**, *18* (17), 2329–2341. https://doi.org/10.1089/ars.2012.4922.

(79) Paciello, A.; Amalfitano, G.; Garziano, A.; Urciuolo, F.; Netti, P. A. Hemoglobin-Conjugated Gelatin Microsphere as a Smart Oxygen Releasing Biomaterial. *Adv Healthc Mater* **2016**, *5* (20), 2655–2666. https://doi.org/https://doi.org/10.1002/adhm.201600559.

(80) Stadler, A. M.; Digel, I.; Artmann, G. M.; Embs, J. P.; Zaccai, G.; Büldt, G. Hemoglobin Dynamics in Red Blood Cells: Correlation to Body Temperature. *Biophys J* **2008**, *95* (11), 5449–5461. https://doi.org/https://doi.org/10.1529/biophysj.108.138040.

(81) McCarthy, M. R.; Vandegriff, K. D.; Winslow, R. M. The Role of Facilitated Diffusion in Oxygen Transport by Cell-Free Hemoglobins: Implications for the Design of Hemoglobin-Based Oxygen Carriers. *Biophys Chem* **2001**, *92* (1), 103–117. https://doi.org/https://doi.org/10.1016/S0301-4622(01)00194-6.

(82) Coll-Satue, C.; Bishnoi, S.; Chen, J.; Hosta-Rigau, L. Stepping Stones to the Future of Haemoglobin-Based Blood Products: Clinical, Preclinical and Innovative Examples. *Biomater Sci* **2021**, *9* (4), 1135–1152. https://doi.org/10.1039/D0BM01767A.

(83) Paciello, A.; Amalfitano, G.; Garziano, A.; Urciuolo, F.; Netti, P. A. Hemoglobin-Conjugated Gelatin Microsphere as a Smart Oxygen Releasing Biomaterial. *Adv Healthc Mater* **2016**, *5* (20), 2655–2666. https://doi.org/https://doi.org/10.1002/adhm.201600559.

(84) Bu, H.; Xu, X.; Chen, J.; Cui, Y.; Wang, L.-Q. Synthesis of a Hemoglobin-Conjugated Triblock Copolymer for Oxygen Carrying and Specific Recognition of Cancer Cells. *RSC Adv* **2017**, *7* (76), 48166–48175. https://doi.org/10.1039/C7RA09747F.

(85) Wei, X.; Xiong, H.; He, S.; Wang, Y.; Zhou, D.; Jing, X.; Huang, Y. A Facile Way to Prepare Functionalized Dextran Nanogels for Conjugation of Hemoglobin. *Colloids Surf B Biointerfaces* **2017**, *155*, 440–448. https://doi.org/https://doi.org/10.1016/j.colsurfb.2017.04.047.

(86) Li, B.; Qi, Y.; He, S.; Wang, Y.; Xie, Z.; Jing, X.; Huang, Y. Asymmetric Copolymer Vesicles to Serve as a Hemoglobin Vector for Ischemia Therapy. *Biomater Sci* **2014**, *2* (9), 1254–1261. https://doi.org/10.1039/C4BM00123K.

(87) Lai, Y.-T.; Sato, M.; Ohta, S.; Akamatsu, K.; Nakao, S.; Sakai, Y.; Ito, T. Preparation of Uniform-Sized Hemoglobin–Albumin Microspheres as Oxygen Carriers by Shirasu Porous Glass Membrane Emulsification Technique. *Colloids Surf B Biointerfaces* **2015**, *127*, 1–7. https://doi.org/https://doi.org/10.1016/j.colsurfb.2015.01.018.

(88) Lai, Y.-T.; Ohta, S.; Akamatsu, K.; Nakao, S.; Sakai, Y.; Ito, T. Size-Dependent Interaction of Cells and Hemoglobin–Albumin Based Oxygen Carriers Prepared Using the SPG Membrane Emulsification Technique. *Biotechnol Prog* **2015**, *31* (6), 1676–1684. https://doi.org/https://doi.org/10.1002/btpr.2170.

(89) Yu, C.; Qian, D.; Huang, X.; Han, F.; Bao, N.; Gu, H. Construction of Biconcave Hemoglobin-Based Microcapsules and Electrochemical Evaluation for Its Ability of Oxygen Carry. *Sens Actuators B Chem* **2018**, *256*, 217–225. https://doi.org/https://doi.org/10.1016/j.snb.2017.09.166.

(90) Liu, X.; Jansman, M. M. T.; Thulstrup, P. W.; Mendes, A. C.; Chronakis, I. S.; Hosta-Rigau, L. Low-Fouling Electrosprayed Hemoglobin Nanoparticles with Antioxidant Protection as Promising Oxygen Carriers. *Macromol Biosci* **2020**, *20* (2), 1900293. https://doi.org/https://doi.org/10.1002/mabi.201900293.

(91) Kuhn, V.; Diederich, L.; Keller, T. C. S.; Kramer, C. M.; Lückstädt, W.; Panknin, C.; Suvorava, T.; Isakson, B. E.; Kelm, M.; Cortese-Krott, M. M. Red Blood Cell Function and Dysfunction: Redox Regulation, Nitric Oxide Metabolism, Anemia. *Antioxid Redox Signal* **2016**, *26* (13), 718–742. https://doi.org/10.1089/ars.2016.6954.

(92) Nagababu, E.; Rifkind, J. M. Heme Degradation by Reactive Oxygen Species. *Antioxid Redox Signal* **2004**, *6* (6), 967–978. https://doi.org/10.1089/ars.2004.6.967.

(93) Nagababu, E.; Ramasamy, S.; Rifkind, J. M.; Jia, Y.; Alayash, A. I. Site-Specific Cross-Linking of Human and Bovine Hemoglobins Differentially Alters Oxygen Binding and Redox Side Reactions Producing Rhombic Heme and Heme Degradation. *Biochemistry* **2002**, *41* (23), 7407–7415. https://doi.org/10.1021/bi0121048.

(94) Staiculescu, M. C.; Foote, C.; Meininger, G. A.; Martinez-Lemus, L. A. The Role of Reactive Oxygen Species in Microvascular Remodeling. *Int J Mol Sci* **2014**, *15* (12), 23792–23835.

(95) Chang, T. M. S.; Powanda, D.; Yu, W. P. Analysis of Polyethylene-glycol-polylactide Nano-Dimension Artificial Red Blood Cells in Maintaining Systemic Hemoglobin Levels and Prevention

of Methemoglobin Formation. *Artificial Cells, Blood Substitutes, and Biotechnology* **2003**, *31* (3), 231–247. https://doi.org/10.1081/BIO-120023155.

(96) Bian, Y.; Chang, T. M. S. A Novel Nanobiotherapeutic Poly-[Hemoglobin-Superoxide Dismutase-Catalase-Carbonic Anhydrase] with No Cardiac Toxicity for the Resuscitation of a Rat Model with 90 Minutes of Sustained Severe Hemorrhagic Shock with Loss of 2/3 Blood Volume. *Artif Cells Nanomed Biotechnol* **2015**, *43* (1), 1–9. https://doi.org/10.3109/21691401.2014.964554.

(97) Simoni, J.; Simoni, G.; Moeller, J. F.; Feola, M.; Wesson, D. E. Artificial Oxygen Carrier With Pharmacologic Actions of Adenosine-5′-Triphosphate, Adenosine, and Reduced Glutathione Formulated to Treat an Array of Medical Conditions. *Artif Organs* **2014**, *38* (8), 684–690. https://doi.org/https://doi.org/10.1111/aor.12337.

(98) Kang, T.; Kim, Y. G.; Kim, D.; Hyeon, T. Inorganic Nanoparticles with Enzyme-Mimetic Activities for Biomedical Applications. *Coord Chem Rev* **2020**, *403*, 213092. https://doi.org/https://doi.org/10.1016/j.ccr.2019.213092.

(99) Liu, X.; Gao, Y.; Chandrawati, R.; Hosta-Rigau, L. Therapeutic Applications of Multifunctional Nanozymes. *Nanoscale* **2019**, *11* (44), 21046–21060. https://doi.org/10.1039/C9NR06596B.

(100) Hosaka, H.; Haruki, R.; Yamada, K.; Böttcher, C.; Komatsu, T. Hemoglobin–Albumin Cluster Incorporating a Pt Nanoparticle: Artificial O2 Carrier with Antioxidant Activities. *PLoS One* **2014**, *9* (10), e110541-.

(101) Jansman, M. M. T.; Liu, X.; Kempen, P.; Clergeaud, G.; Andresen, T. L.; Thulstrup, P. W.; Hosta-Rigau, L. Hemoglobin-Based Oxygen Carriers Incorporating Nanozymes for the Depletion of Reactive Oxygen Species. *ACS Appl Mater Interfaces* **2020**, *12* (45), 50275–50286. https://doi.org/10.1021/acsami.0c14822.

(102) Ejima, H.; Richardson, J. J.; Caruso, F. Metal-Phenolic Networks as a Versatile Platform to Engineer Nanomaterials and Biointerfaces. *Nano Today* **2017**, *12*, 136–148. https://doi.org/https://doi.org/10.1016/j.nantod.2016.12.012.

(103) Fam, S. Y.; Chee, C. F.; Yong, C. Y.; Ho, K. L.; Mariatulqabtiah, A. R.; Tan, W. S. Stealth Coating of Nanoparticles in Drug-Delivery Systems. *Nanomaterials* **2020**, *10* (4), 787.

(104) Knop, K.; Hoogenboom, R.; Fischer, D.; Schubert, U. S. Poly(Ethylene Glycol) in Drug Delivery: Pros and Cons as Well as Potential Alternatives. *Angewandte Chemie International Edition* **2010**, *49* (36), 6288–6308. https://doi.org/https://doi.org/10.1002/anie.200902672.

(105) Harris, J. M.; Chess, R. B. Effect of Pegylation on Pharmaceuticals. *Nat Rev Drug Discov* **2003**, *2* (3), 214–221. https://doi.org/10.1038/nrd1033.

(106) Winslow, R. M. Blood Substitutes. *Adv Drug Deliv Rev* **2000**, *40* (3), 131–142. https://doi.org/https://doi.org/10.1016/S0169-409X(99)00045-9.

(107) Knop, K.; Hoogenboom, R.; Fischer, D.; Schubert, U. S. Poly(Ethylene Glycol) in Drug Delivery: Pros and Cons as Well as Potential Alternatives. *Angewandte Chemie International Edition* **2010**, *49* (36), 6288–6308. https://doi.org/https://doi.org/10.1002/anie.200902672.

(108) Zhang, P.; Sun, F.; Liu, S.; Jiang, S. Anti-PEG Antibodies in the Clinic: Current Issues and beyond PEGylation. *Journal of Controlled Release* **2016**, *244*, 184–193. https://doi.org/https://doi.org/10.1016/j.jconrel.2016.06.040.

(109) Zhuang, J.; Ying, M.; Spiekermann, K.; Holay, M.; Zhang, Y.; Chen, F.; Gong, H.; Lee, J. H.; Gao, W.; Fang, R. H.; Zhang, L. Biomimetic Nanoemulsions for Oxygen Delivery In Vivo. *Advanced Materials* **2018**, *30* (49), 1804693. https://doi.org/https://doi.org/10.1002/adma.201804693.

(110) Jansman, M. M. T.; Coll-Satue, C.; Liu, X.; Kempen, P. J.; Andresen, T. L.; Thulstrup, P. W.; Hosta-Rigau, L. Hemoglobin-Based Oxygen Carriers Camouflaged with Membranes Extracted from Red Blood Cells: Optimization and Assessment of Functionality. *Biomaterials Advances* **2022**, *134*, 112691. https://doi.org/https://doi.org/10.1016/j.msec.2022.112691.

(111) Lin, Y.; Wu, J.; Gu, W.; Huang, Y.; Tong, Z.; Huang, L.; Tan, J. Exosome–Liposome Hybrid Nanoparticles Deliver CRISPR/Cas9 System in MSCs. *Advanced Science* **2018**, *5* (4), 1700611. https://doi.org/https://doi.org/10.1002/advs.201700611.

(112) Peng, Q.; Wei, X.-Q.; Yang, Q.; Zhang, S.; Zhang, T.; Shao, X.-R.; Cai, X.-X.; Zhang, Z.-R.; Lin, Y.-F. Enhanced Biostability of Nanoparticle-Based Drug Delivery Systems by Albumin Corona. *Nanomedicine* **2015**, *10* (2), 205–214. https://doi.org/10.2217/nnm.14.86.

(113) Giri, T. K. 20 - Alginate Containing Nanoarchitectonics for Improved Cancer Therapy. In *Nanoarchitectonics for Smart Delivery and Drug Targeting*; Holban, A. M., Grumezescu, A. M., Eds.; William Andrew Publishing, 2016; pp 565–588. https://doi.org/https://doi.org/10.1016/B978-0-323-47347-7.00020-3.

(114) Hickey, R.; Palmer, A. F. Synthesis of Hemoglobin-Based Oxygen Carrier Nanoparticles By Desolvation Precipitation. *Langmuir* **2020**, *36* (47), 14166–14172. https://doi.org/10.1021/acs.langmuir.0c01698.

(115) Weber, C.; Coester, C.; Kreuter, J.; Langer, K. Desolvation Process and Surface Characterisation of Protein Nanoparticles. *Int J Pharm* **2000**, *194* (1), 91–102. https://doi.org/https://doi.org/10.1016/S0378-5173(99)00370-1.

(116) Q. Li B. Lu H. Yao W. G. Zhang F., J. H. H. Ciprofloxacin-Loaded Bovine Serum Albumin Microspheres: Preparation and Drug-Release in Vitro. *J Microencapsul* **2001**, *18* (6), 825–829. https://doi.org/10.1080/02652040110055298.

(117) Meziani, M. J.; Sun, Y.-P. Protein-Conjugated Nanoparticles from Rapid Expansion of Supercritical Fluid Solution into Aqueous Solution. *J Am Chem Soc* **2003**, *125* (26), 8015–8018. https://doi.org/10.1021/ja030104k.

(118) Merodio, M.; Arnedo, A.; Renedo, M. J.; Irache, J. M. Ganciclovir-Loaded Albumin Nanoparticles: Characterization and in Vitro Release Properties. *European Journal of Pharmaceutical Sciences* **2001**, *12* (3), 251–259. https://doi.org/https://doi.org/10.1016/S0928-0987(00)00169-X.

(119) Langer, K.; Balthasar, S.; Vogel, V.; Dinauer, N.; von Briesen, H.; Schubert, D. Optimization of the Preparation Process for Human Serum Albumin (HSA) Nanoparticles. *Int J Pharm* **2003**, *257* (1), 169–180. https://doi.org/https://doi.org/10.1016/S0378-5173(03)00134-0.

(120) Galisteo-González, F.; Molina-Bolívar, J. A. Systematic Study on the Preparation of BSA Nanoparticles. *Colloids Surf B Biointerfaces* **2014**, *123*, 286–292. https://doi.org/https://doi.org/10.1016/j.colsurfb.2014.09.028.

(121) von Storp, B.; Engel, A.; Boeker, A.; Ploeger, M.; Langer, K. Albumin Nanoparticles with Predictable Size by Desolvation Procedure. *J Microencapsul* **2012**, *29* (2), 138–146. https://doi.org/10.3109/02652048.2011.635218.

(122) Sadeghi, R.; Moosavi-Movahedi, A. A.; Emam-jomeh, Z.; Kalbasi, A.; Razavi, S. H.; Karimi, M.; Kokini, J. The Effect of Different Desolvating Agents on BSA Nanoparticle Properties and Encapsulation of Curcumin. *Journal of Nanoparticle Research* **2014**, *16* (9), 2565. https://doi.org/10.1007/s11051-014-2565-1.

(123) Doan, C. D.; Ghosh, S. Formation and Stability of Pea Proteins Nanoparticles Using Ethanol-Induced Desolvation. *Nanomaterials* **2019**, *9* (7), 949.

(124) Gülseren, İ.; Fang, Y.; Corredig, M. Whey Protein Nanoparticles Prepared with Desolvation with Ethanol: Characterization, Thermal Stability and Interfacial Behavior. *Food Hydrocoll* **2012**, *29* (2), 258–264. https://doi.org/https://doi.org/10.1016/j.foodhyd.2012.03.015.

(125) Sukhanova, A.; Bozrova, S.; Sokolov, P.; Berestovoy, M.; Karaulov, A.; Nabiev, I. Dependence of Nanoparticle Toxicity on Their Physical and Chemical Properties. *Nanoscale Res Lett* **2018**, *13* (1), 1–21.

(126) Lin, W.; Coombes, A. G. A.; Garnett, M. C.; Davies, M. C.; Schacht, E.; Davis, S. S.; Illum, L. Preparation of Sterically Stabilized Human Serum Albumin Nanospheres Using a Novel Dextranox-MPEG Crosslinking Agent. *Pharm Res* **1994**, *11* (11), 1588–1592. https://doi.org/10.1023/A:1018957704209.

(127) Sozer, S. C.; Egesoy, T. O.; Basol, M.; Cakan-Akdogan, G.; Akdogan, Y. A Simple Desolvation Method for Production of Cationic Albumin Nanoparticles with Improved Drug Loading and Cell Uptake. *J Drug Deliv Sci Technol* **2020**, *60*, 101931. https://doi.org/https://doi.org/10.1016/j.jddst.2020.101931.

(128) Doan, C. D.; Ghosh, S. Formation and Stability of Pea Proteins Nanoparticles Using Ethanol-Induced Desolvation. *Nanomaterials* **2019**, *9* (7), 949.

(129) Teng, Z.; Luo, Y.; Wang, Q. Carboxymethyl Chitosan–Soy Protein Complex Nanoparticles for the Encapsulation and Controlled Release of Vitamin D3. *Food Chem* **2013**, *141* (1), 524–532. https://doi.org/https://doi.org/10.1016/j.foodchem.2013.03.043.

(130) Yedomon, B.; Fessi, H.; Charcosset, C. Preparation of Bovine Serum Albumin (BSA) Nanoparticles by Desolvation Using a Membrane Contactor: A New Tool for Large Scale Production. *European Journal of Pharmaceutics and Biopharmaceutics* **2013**, *85* (3, Part A), 398–405. https://doi.org/https://doi.org/10.1016/j.ejpb.2013.06.014.

(131) Wacker, M.; Zensi, A.; Kufleitner, J.; Ruff, A.; Schütz, J.; Stockburger, T.; Marstaller, T.; Vogel, V. A Toolbox for the Upscaling of Ethanolic Human Serum Albumin (HSA) Desolvation. *Int J Pharm* **2011**, *414* (1), 225–232. https://doi.org/https://doi.org/10.1016/j.ijpharm.2011.04.046.

(132) Lee, H.; Dellatore, S. M.; Miller, W. M.; Messersmith, P. B. Mussel-Inspired Surface Chemistry for Multifunctional Coatings. *Science (1979)* **2007**, *318* (5849), 426–430. https://doi.org/10.1126/science.1147241.

(133) Hong, S.; Na, Y. S.; Choi, S.; Song, I. T.; Kim, W. Y.; Lee, H. Non-Covalent Self-Assembly and Covalent Polymerization Co-Contribute to Polydopamine Formation. *Adv Funct Mater* **2012**, *22* (22), 4711–4717. https://doi.org/https://doi.org/10.1002/adfm.201201156.

(134) Lee, H. A.; Ma, Y.; Zhou, F.; Hong, S.; Lee, H. Material-Independent Surface Chemistry beyond Polydopamine Coating. *Acc Chem Res* **2019**, *52* (3), 704–713. https://doi.org/10.1021/acs.accounts.8b00583.

(135) della Vecchia, N. F.; Luchini, A.; Napolitano, A.; D'Errico, G.; Vitiello, G.; Szekely, N.; d'Ischia, M.; Paduano, L. Tris Buffer Modulates Polydopamine Growth, Aggregation, and Paramagnetic Properties. *Langmuir* **2014**, *30* (32), 9811–9818. https://doi.org/10.1021/la501560z.

(136) Liu, Y.; Ai, K.; Lu, L. Polydopamine and Its Derivative Materials: Synthesis and Promising Applications in Energy, Environmental, and Biomedical Fields. *Chem Rev* **2014**, *114* (9), 5057–5115. https://doi.org/10.1021/cr400407a.

(137) Cui, J.; Wang, Y.; Postma, A.; Hao, J.; Hosta-Rigau, L.; Caruso, F. Monodisperse Polymer Capsules: Tailoring Size, Shell Thickness, and Hydrophobic Cargo Loading via Emulsion Templating. *Adv Funct Mater* **2010**, *20* (10), 1625–1631. https://doi.org/https://doi.org/10.1002/adfm.201000209.

(138) Zhuang, H.; Su, H.; Bi, X.; Bai, Y.; Chen, L.; Ge, D.; Shi, W.; Sun, Y. Polydopamine Nanocapsule: A Theranostic Agent for Photoacoustic Imaging and Chemo-Photothermal Synergistic Therapy. *ACS Biomater Sci Eng* **2017**, *3* (8), 1799–1808. https://doi.org/10.1021/acsbiomaterials.7b00260.

(139) Yang, S. H.; Kang, S. M.; Lee, K.-B.; Chung, T. D.; Lee, H.; Choi, I. S. Mussel-Inspired Encapsulation and Functionalization of Individual Yeast Cells. *J Am Chem Soc* **2011**, *133* (9), 2795–2797. https://doi.org/10.1021/ja1100189.

(140) Zhang, X.; Wang, S.; Xu, L.; Feng, L.; Ji, Y.; Tao, L.; Li, S.; Wei, Y. Biocompatible Polydopamine Fluorescent Organic Nanoparticles: Facile Preparation and Cell Imaging. *Nanoscale* **2012**, *4* (18), 5581–5584. https://doi.org/10.1039/C2NR31281F.

(141) Hu, J.; Yang, L.; Yang, P.; Jiang, S.; Liu, X.; Li, Y. Polydopamine Free Radical Scavengers. *Biomater Sci* **2020**, *8* (18), 4940–4950. https://doi.org/10.1039/D0BM01070G.

(142) Zhang, J.; Fu, Y.; Yang, P.; Liu, X.; Li, Y.; Gu, Z. ROS Scavenging Biopolymers for Anti-Inflammatory Diseases: Classification and Formulation. *Adv Mater Interfaces* **2020**, *7* (16), 2000632. https://doi.org/https://doi.org/10.1002/admi.202000632.

(143) Liu, Y.; Ai, K.; Ji, X.; Askhatova, D.; Du, R.; Lu, L.; Shi, J. Comprehensive Insights into the Multi-Antioxidative Mechanisms of Melanin Nanoparticles and Their Application To Protect Brain from Injury in Ischemic Stroke. *J Am Chem Soc* **2017**, *139* (2), 856–862. https://doi.org/10.1021/jacs.6b11013.

(144) Zou, Y.; Wang, Z.; Chen, Z.; Zhang, Q.-P.; Zhang, Q.; Tian, Y.; Ren, S.; Li, Y. Synthetic Melanin Hybrid Patchy Nanoparticle Photocatalysts. *The Journal of Physical Chemistry C* **2019**, *123* (9), 5345–5352. https://doi.org/10.1021/acs.jpcc.8b10469.

(145) Zhang, S.; Ou, Q.; Xin, P.; Yuan, Q.; Wang, Y.; Wu, J. Polydopamine/Puerarin Nanoparticle-Incorporated Hybrid Hydrogels for Enhanced Wound Healing. *Biomater Sci* **2019**, *7* (10), 4230–4236. https://doi.org/10.1039/C9BM00991D.

(146) Yu, C.; Huang, X.; Qian, D.; Han, F.; Xu, L.; Tang, Y.; Bao, N.; Gu, H. Fabrication and Evaluation of Hemoglobin-Based Polydopamine Microcapsules as Oxygen Carriers. *Chemical Communications* **2018**, *54* (33), 4136–4139. https://doi.org/10.1039/C8CC00095F.

(147) Hu, J.; Wang, Q.; Wang, Y.; You, G.; Li, P.; Zhao, L.; Zhou, H. Polydopamine-Based Surface Modification of Hemoglobin Particles for Stability Enhancement of Oxygen Carriers. *J Colloid Interface Sci* **2020**, *571*, 326–336. https://doi.org/https://doi.org/10.1016/j.jcis.2020.03.046.

(148) Ejima, H.; Richardson, J. J.; Liang, K.; Best, J. P.; van Koeverden, M. P.; Such, G. K.; Cui, J.; Caruso, F. One-Step Assembly of Coordination Complexes for Versatile Film and Particle Engineering. *Science (1979)* **2013**, *341* (6142), 154–157. https://doi.org/10.1126/science.1237265.

(149) Li, Y.; Miao, Y.; Yang, L.; Zhao, Y.; Wu, K.; Lu, Z.; Hu, Z.; Guo, J. Recent Advances in the Development and Antimicrobial Applications of Metal–Phenolic Networks. *Advanced Science* **2022**, *9* (27), 2202684. https://doi.org/https://doi.org/10.1002/advs.202202684.

(150) Xie, Y.; Chen, S.; Peng, X.; Wang, X.; Wei, Z.; Richardson, J. J.; Liang, K.; Ejima, H.; Guo, J.; Zhao, C. Alloyed Nanostructures Integrated Metal-Phenolic Nanoplatform for Synergistic Wound Disinfection and Revascularization. *Bioact Mater* **2022**, *16*, 95–106. https://doi.org/https://doi.org/10.1016/j.bioactmat.2022.03.004.

(151) Zeidan, R. S.; Han, S. M.; Leeuwenburgh, C.; Xiao, R. Iron Homeostasis and Organismal Aging. *Ageing Res Rev* **2021**, *72*, 101510. https://doi.org/https://doi.org/10.1016/j.arr.2021.101510.

(152) Ju, Y.; Cui, J.; Müllner, M.; Suma, T.; Hu, M.; Caruso, F. Engineering Low-Fouling and PH-Degradable Capsules through the Assembly of Metal-Phenolic Networks. *Biomacromolecules* **2015**, *16* (3), 807–814. https://doi.org/10.1021/bm5017139.

(153) Zhang, Z.; Xie, L.; Ju, Y.; Dai, Y. Recent Advances in Metal-Phenolic Networks for Cancer Theranostics. *Small* **2021**, *17* (43), 2100314. https://doi.org/https://doi.org/10.1002/smll.202100314.

(154) Ju, Y.; Cui, J.; Sun, H.; Müllner, M.; Dai, Y.; Guo, J.; Bertleff-Zieschang, N.; Suma, T.; Richardson, J. J.; Caruso, F. Engineered Metal-Phenolic Capsules Show Tunable Targeted Delivery to Cancer Cells. *Biomacromolecules* **2016**, *17* (6), 2268–2276. https://doi.org/10.1021/acs.biomac.6b00537.

(155) Whittaker, P. Iron and Zinc Interactions in Humans. *Am J Clin Nutr* **1998**, *68* (2), 442S-446S. https://doi.org/10.1093/ajcn/68.2.442S.

(156) Guo, Z.; Xie, W.; Lu, J.; Guo, X.; Xu, J.; Xu, W.; Chi, Y.; Takuya, N.; Wu, H.; Zhao, L. Tannic Acid-Based Metal Phenolic Networks for Bio-Applications: A Review. *J Mater Chem B* **2021**, *9* (20), 4098–4110. https://doi.org/10.1039/D1TB00383F.

(157) Ma, M.; Zhong, Y.; Jiang, X. Thermosensitive and PH-Responsive Tannin-Containing Hydroxypropyl Chitin Hydrogel with Long-Lasting Antibacterial Activity for Wound Healing. *Carbohydr Polym* **2020**, *236*, 116096. https://doi.org/https://doi.org/10.1016/j.carbpol.2020.116096.

(158) Saowalak, K.; Titipun, T.; Somchai, T.; Chalermchai, P. Iron(III)-Tannic Molecular Nanoparticles Enhance Autophagy Effect and T1 MRI Contrast in Liver Cell Lines. *Sci Rep* **2018**, *8* (1), 6647. https://doi.org/10.1038/s41598-018-25108-1.

(159) Guo, J.; Ping, Y.; Ejima, H.; Alt, K.; Meissner, M.; Richardson, J. J.; Yan, Y.; Peter, K.; von Elverfeldt, D.; Hagemeyer, C. E.; Caruso, F. Engineering Multifunctional Capsules through the Assembly of Metal–Phenolic Networks. *Angewandte Chemie International Edition* **2014**, *53* (22), 5546–5551. https://doi.org/https://doi.org/10.1002/anie.201311136.

(160) Yang, B.; Zhou, S.; Zeng, J.; Zhang, L.; Zhang, R.; Liang, K.; Xie, L.; Shao, B.; Song, S.; Huang, G.; Zhao, D.; Chen, P.; Kong, B. Super-Assembled Core-Shell Mesoporous Silica-Metal-Phenolic Network Nanoparticles for Combinatorial Photothermal Therapy and Chemotherapy. *Nano Res* **2020**, *13* (4), 1013–1019. https://doi.org/10.1007/s12274-020-2736-6.

(161) Park, J. H.; Kim, K.; Lee, J.; Choi, J. Y.; Hong, D.; Yang, S. H.; Caruso, F.; Lee, Y.; Choi, I. S. A Cytoprotective and Degradable Metal–Polyphenol Nanoshell for Single-cell Encapsulation. *Angewandte Chemie* **2014**, *126* (46), 12628–12633.

(162) Pulido, R.; Bravo, L.; Saura-Calixto, F. Antioxidant Activity of Dietary Polyphenols As Determined by a Modified Ferric Reducing/Antioxidant Power Assay. *J Agric Food Chem* **2000**, *48* (8), 3396–3402. https://doi.org/10.1021/jf9913458.

(163) Dai, Q.; Geng, H.; Yu, Q.; Hao, J.; Cui, J. Polyphenol-Based Particles for Theranostics. *Theranostics* **2019**, *9* (11), 3170–3190. https://doi.org/10.7150/thno.31847.

(164) Wei, Z.; Wang, L.; Tang, C.; Chen, S.; Wang, Z.; Wang, Y.; Bao, J.; Xie, Y.; Zhao, W.; Su, B.; Zhao, C. Metal-Phenolic Networks Nanoplatform to Mimic Antioxidant Defense System for Broad-Spectrum Radical Eliminating and Endotoxemia Treatment. *Adv Funct Mater* **2020**, *30* (49), 2002234. https://doi.org/https://doi.org/10.1002/adfm.202002234.

(165) Qin, Y.; Wang, J.; Qiu, C.; Hu, Y.; Xu, X.; Jin, Z. Self-Assembly of Metal–Phenolic Networks as Functional Coatings for Preparation of Antioxidant, Antimicrobial, and PH-Sensitive-Modified Starch Nanoparticles. *ACS Sustain Chem Eng* **2019**, *7* (20), 17379–17389. https://doi.org/10.1021/acssuschemeng.9b04332.

(166) Yi, X.; Zeng, W.; Wang, C.; Chen, Y.; Zheng, L.; Zhu, X.; Ke, Y.; He, X.; Kuang, Y.; Huang, Q. A Step-by-Step Multiple Stimuli-Responsive Metal-Phenolic Network Prodrug Nanoparticles for Chemotherapy. *Nano Res* **2022**, *15* (2), 1205–1212. https://doi.org/10.1007/s12274-021-3626-2.

Chapter 2

Thesis Objectives and Outline

2.1. Objectives

In this PhD thesis, I am focusing on the fabrication and characterization of multifunctional HBOCs. Specifically, the Hb loading content needs to be improved to enable the HBOCs to have a remarkable O_2 delivery capacity, and the Hb in the HBOCs needs to be protected to display the natural O_2 binding and releasing features. By employing the desolvation technique and antioxidant surface coating, we expect the results of this PhD thesis to bring promising strategies to develop an HBOCs with high Hb content and antioxidant properties. Four main objectives of this PhD thesis are as follows:

1) The fabrication of Hb-NPs by desolvation technique, including the screening of parameters of desolvation to get a satisfied Hb-NPs.
2) The development of antioxidant surface coating for Hb-NPs.
3) The investigation of the antioxidant properties of the surface coated Hb-NPs which can protect the Hb.
4) The assessment of the HBOCs' O_2 binding and releasing properties.
5) The assessment of the HBOCs' biocompatibility.

2.2. Thesis outline

Chapter 3 consists of paper 1**:** Synthesis of Nanoparticles Fully Made of Hemoglobin with Antioxidant Properties: A Step toward the Creation of Successful Oxygen Carriers

This paper was published in 2021 in **Langmuir**. The fabrication and characterization of the NPs fully made of Hb and the subsequent PDA coated particles were included in this paper.

Chapter 4 consists of paper 2**:** Metal-Phenolic Networks as Broad-Spectrum Antioxidant Coatings for Hemoglobin Nanoparticles Working as Oxygen Carriers

This paper was published in 2022 in **Chemistry of Materials**. The fabrication of the Hb NPs were optimized, and the usage of an antioxidant MPN coating to stabilize the NPs was assessed.

Chapter 5 consists of the summary of all the work in this thesis and the outlook of the future design of HBOCs

Chapter 3

Synthesis of Nanoparticles Fully Made of Hemoglobin with Antioxidant Properties: A Step toward the Creation of Successful Oxygen Carriers

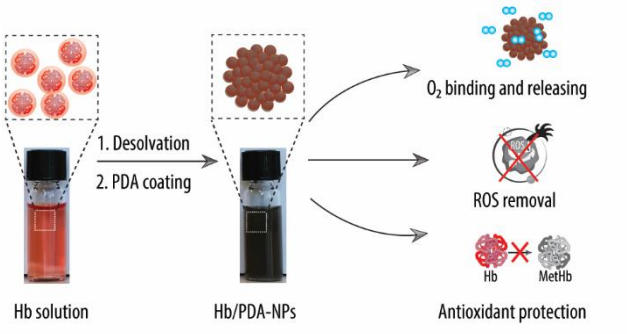

Chen, J.; Jansman, M. M. T.; Liu, X.; Hosta-Rigau, L. Synthesis of Nanoparticles Fully Made of Hemoglobin with Antioxidant Properties: A Step toward the Creation of Successful Oxygen Carriers. *Langmuir* **2021**, *37* (39), 11561–11572. https://doi.org/10.1021/acs.langmuir.1c01855

Abstract

Transfusion of donor RBCs is a crucial and widely employed clinical procedure. However, important constraints of blood transfusions include the limited availability of blood, the need for typing and cross-matching due to the RBC membrane antigens, the limited storage lifetime or the risk for disease transmission. Hence, a lot of effort has been devoted to develop RBC substitutes which are free from the limitations of donor blood. Despite the potential, the creation of HBOCs is still facing important challenges. To allow for proper tissue oxygenation, it is essential to develop carriers with high Hb loading since Hb comprises about 96% of the RBCs dry weight. In this work, NPs fully made of Hb are prepared by the desolvation precipitation method. Several parameters are screened (i.e., Hb concentration, desolvation ratio, time and sonication intensity) to finally obtain Hb-NPs with a diameter of ~568 nm and a PDI of 0.2. A polydopamine (PDA) coating is adsorbed to prevent the disintegration of the resulting Hb/PDA-NPs. Due to the antioxidant character of PDA, the Hb/PDA-NPs are able to deplete two harmful ROS, namely, $O_2^{\bullet -}$ and H_2O_2. Such antioxidant protection also translates into minimizing the oxidation of the entrapped Hb into non-functional metHb. This is a crucial aspect since metHb conversion also results in inflammatory reactions and dysregulated vascular tone. Finally, yet importantly, the reported Hb/PDA-NPs are also both hemo- and biocompatible and preserve the reversible O_2-binding and releasing properties of Hb.

3.1. Introduction

Blood transfusions, which usually involve the administration of packed RBCs, are a mainstream procedure used to treat acute blood loss (e.g., due to trauma), severe blood disorders (e.g., anemia or hemophilia) or for patients receiving tumor chemotherapy.[1,2] However, unfortunately, using blood from donors has also important limitations: blood is a scarce resource and the declining donor rate together with an increasing demand due to population growth and aging, will eventually result in a critical shortage of blood.[3–6] Additionally, other important drawbacks of blood are the risks of virus transmission or its short shelf-life; the later making impossible to create large blood stockpiles to be used when acute disasters occur (e.g., earthquakes, terrorist attacks).[3–6]

Thus, a robust volume of research is currently being devoted to the development of HBOCs which are free from the aforementioned limitations. HBOCs make use of the Hb protein, which is the main constituent and the O_2 carrying component of RBCs. HBOCs are free of certain restrictions of donor blood since they can be prepared in large quantities and in sterile conditions. There is no need for blood group typing and matching due to their universal compatibility and they also have long-term storage potential even at ambient temperature.[7] However, since the administration of cell-free Hb elicits important side effects, the challenge to create successful HBOCs is to preserve Hb's excellent O_2-binding and releasing properties while minimizing its toxicity. Cell-free Hb has an extremely short circulatory residence time since it is rapidly cleared from circulation by the kidneys and by the MPS in the spleen and liver. This results in Hb-induced toxicity in these organs.[3,8,9] Furthermore, once in the vasculature, cell-free Hb can extravasate into the sub-endothelial layer where it rapidly acts as a NO scavenger leading to the oxidation of Hb into metHb. Additionally, since NO is an important vasodilator, its sequestration generates vasoconstriction and the subsequent cardiovascular complications which, paradoxically, diminish the delivery of O_2 into the tissues.[3]

Approaches to overcome the limitations of native Hb involve its encapsulation within a protective shell in order to increase the molecular diameter of Hb and to shield it from permeating through the blood vessels. As such, Hb has already been entrapped within several systems including liposomes,[10,11] polymeric NPs[12] or MOFs.[13,14] Nonetheless, despite the progress, attaining a high Hb loading within a well-defined biocompatible and biodegradable structure still remains as a significant challenge. To achieve an O_2-carrying capacity similar to that of blood, carriers with high Hb loading are required since, within native RBCs, Hb comprises about 96% of their dry weight.[15] A promising approach to create HBOCs with a high Hb content, is to fabricate solid Hb NPs. We have recently reported the fabrication of small, solid Hb-NPs using the electrospraying technique, resulting in Hb-NPs with a diameter ranging from 370 to 480 nm.[15] However, an important drawback of these Hb-NPs is the low throughput of the electrospraying technique which creates challenges for their production at clinically relevant scales.[16] Using a different approach, the Palmer group was able to synthetize Hb-NPs by borrowing the techniques currently used for the fabrication of protein NPs. Specifically, by using the desolvation precipitation method, the authors reported Hb-NPs with a diameter of ~250 nm which were able to bind and release O_2.[17] However, to stabilize the resulting NPs, either GA or oxidized Dex were used as crosslinkers. GA

has been shown to exhibit toxicity due to the hydrolytic degradation of its Schiff base bond.[18–20] Since oxidized Dex also binds to Hb through aldehyde-based chemistry, it is also envisioned that the same hydrolytic degradation will take place. Furthermore, both crosslinkers covalently bind to the lysine residues present in Hb.21 Covalent modification of Hb is not desirable since this will impair its ability to undergo the quaternary change in conformation between the relaxed and tense states which will, in turn, affect its ability to bind and release O_2.[22] Thus, the development of new approaches to stabilize the Hb molecules without covalently modifying their structure is a central aspect that needs to be addressed. To this end, surface modification employing polydopamine (PDA) coatings has emerged as a promising strategy.[23] The self-polymerization of DA into PDA in alkaline aqueous media is an efficient, quick and controllable process that renders a continuous coating layer on a wide variety of surfaces ranging from planar substrates to nanoparticulate systems.[24–26] PDA coatings display excellent biocompatibility, hydrophilicity and offer the possibility of a straightforward post-functionalization.[27] As a result of these properties, PDA has been employed for the construction of HBOCs. Specifically, PDA has been mainly used to coat Hb-based particles prepared by the coprecipitation, cross-linking and dissolution method.[18,28,29] However, a limitation of this process is the relatively large diameter of the resulting Hb particles (which are typically in the range from 0.7 to 3.3 μm) and the general usage of a crosslinker during the synthesis step.

To address the aforementioned challenges, herein we report the assembly of a novel type of Hb-NPs by combining the desolvation precipitation method, which allows the production of protein-based NPs both at a small- and large-scale production, with a PDA surface modification approach. We start by studying the effect of several processing parameters (i.e., the concentration of Hb, amount of desolvating agent and sonication time and amplitude) on the size, PDI and yield of the Hb-NPs (Scheme 3.1). To stabilize the optimized Hb-NPs, we move away from covalent crosslinking by employing a PDA coating. We assess the O_2-carrying capacity of the resulting PDA-coated Hb-NPs, which is the most important aspect when developing HBOCs. The antioxidant properties due to the PDA layer are also evaluated. Specifically in the context of scavenging harmful ROS as well as by their ability to prevent the oxidation of Hb into non-functional metHb. Finally, biocompatibility in terms of hemolytic rate and cell viability of the Hb-NPs are also examined. With this work, we hope to provide a new type of NPs fully made of Hb with potential as an O_2 delivery solution to be used in situations where donor blood is not available.

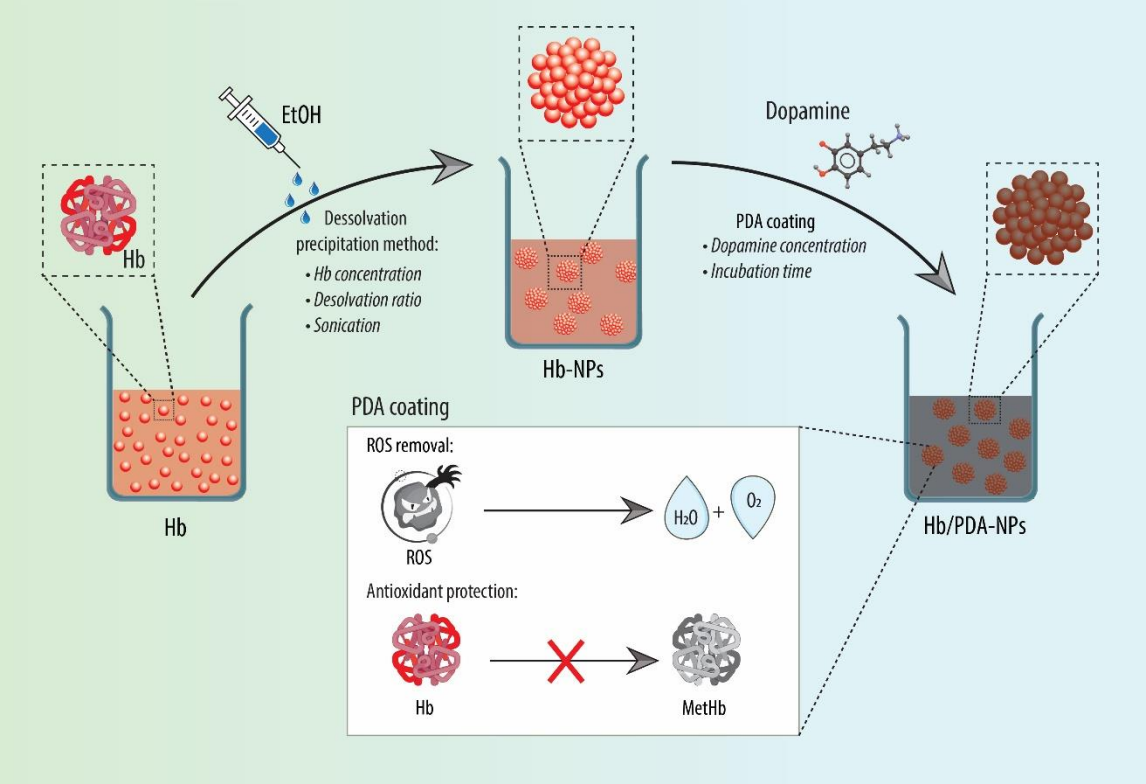

Schematic 3.1. Schematic illustration of the assembly process. Hb-NPs are prepared by the desolvation precipitation method. Several parameters are evaluated, namely, the concentration of Hb, the desolvation ratio and the sonication time an amplitude. The Hb-NPs are subsequently coated by the self-polymerization of DA into polydopamine (PDA). DA concentration and incubation time are screened. The resulting PDA-coated Hb/PDA-NPs are able to scavenge harmful reactive oxygen species (ROS) and, as a result, Hb oxidation into non-functional methemoglobin (metHb) is prevented.

3.2. Materials and methods

3.2.1. Materials.

Dopamine (DA), tris(hydroxymethyl)aminomethane (TRIS), sodium dithionite (SDT), H_2O_2, phosphate buffer saline (PBS), hydrochloric acid (HCl), cell proliferation reagent WST-1, horseradish peroxidase (HRP), xanthine oxidase (XO) from bovine milk, xanthine, ethylenediaminetetraacetic acid (EDTA) solution, potassium dioxide (KO2), trypsin, penicillin/streptomycin, HUVEC, Dulbecco's modified Eagle's medium-high glucose (DMEM D5796), and fetal bovine serum (FBS), ethanol absolute (EtOH) were bought from Merck Life Science A/S (Søborg, DK). Pierce Bicinchoninic Acid (BCA) Protein Assay Kit (Thermo Fisher

Scientific (Waltham, MA)). PrestoBlue cell viability reagent and Amplex Red reagent were purchased from Thermo Fisher Scientific (Waltham, MA, USA). Bovine blood was bought from SSI Diagnostica A/S (Hillerød, Denmark). The Hb used was extracted from the bovine blood. The RAW 264.7 cell line was obtained from the European Collection of Authenticated Culture Collections (ECACC, Wiltshire, UK). Endothelial cell medium (ECM), and related 1% penicillin/streptomycin solution, 5% FBS, and 1% endothelial cell growth supplement was obtained from Innoprot (Derio-Biskaia, Spain).

TRIS 1 buffer is composed of 10 mM TRIS (pH 8.5); TRIS 2 buffer is composed of 10 mM TRIS and 150 mM Sodium chloride (NaCl) (pH 7.4). Both of TRIS 1 and TRIS 2 were prepared with ultrapure water (Milli-Q (MQ), gradient A 10 system, TOC< 4 ppb, resistance 18 MV cm, EMD Millipore, USA).

3.2.2. Hb extraction.

Hb was extracted from bovine blood following our previous protocol.[14] Specifically, same volumes of 0.9% NaCl and bovine blood were mildly mixed and the resulting mixture was spun down (1500 *g*, 20 min) using a high speed centrifuge (SL16R centrifuge, ThermoScientific). The supernatant was removed and the pellet (which contained the RBCs) was washed in 0.9% NaCl (2×, 1500 *g*, 20 min). A solution of MQ and toluene at a volume ratio of 1:1:0.4 was added to the pellet and, following thorough mixing, the suspension was transferred to a separatory funnel (overnight, 4 ℃) to allow for the separation of the phases. Next, the organic part was removed and the Hb solution was collected from the bottom of the flask and placed into a centrifuge tube. The Hb solution was spun down (8000 *g*, 20 min) and filtered through using dust-free paper. The resulting Hb solution was stored in the freezer (-80 ℃). A BCA assay was used to assess the concentration of Hb.

3.2.3. Fabrication and characterization of Hb-NPs.

3.2.3.1. Fabrication of Hb-NPs.

Hb-NPs were fabricated by modifications of a reported protocol.[30,31] Specifically, Hb solutions in MQ (5 mL, 2.2, 4.4, 8.8, 17.5 and 35.0 mg mL^{-1}) were continuously stirred at 420 rpm using a magnetic stirring apparatus. Next, EtOH at different volume ratios with respect to the water phase (i.e., 0.6×, 0.9×, 1.2×, 1.5× and 1.8×) was added dropwise to the Hb solutions under continuous stirring. The obtained turbid suspensions were spun down (3011 *g*, 5 min) using a bench top centrifuge (MiniSpin, Hamburg, Germany) and washed in MQ (3×, 3011 *g*, 5 min). Next, the Hb-NPs were resuspended in MQ (2 mL) with or without the aid of sonication. When sonication was employed, different times (i.e., 5, 10, 20, 40 and 80 sec) and amplitudes (i.e., 5, 10, 30, 50 and 70) were considered.

3.2.3.2. Size, polydispersity index (PDI), zeta (ζ)-potentials and yield.

The size and PDI of the Hb-NPs fabricated using different conditions (i.e., concentration of Hb, desolvation ratio and sonication time and amplitude) were evaluated by dynamic light scattering (DLS) using a Zetasizer nano ZS instrument (Malvern Instruments Ltd, UK). The ζ-potentials were also assessed using the same instrument.

The yield of the resulting Hb-NPs was calculated by: yield (%) = $(m_{Hb\ in\ total} - m_{Hb\ in\ supernatant})/m_{Hb\ in\ total} \times 100$. Where m_{Hb} is the mass of Hb evaluated by a BCA assay.

3.2.3.3. Morphological characterization.

The suspensions of Hb-NPs were imaged by differential interference contrast (DIC) microscopy using an Olympus Inverted IX83 microscope equipped with a 60 × oil-immersion objective. For the scanning electron microscopy (SEM) images, droplets of suspensions of Hb-NPs were added onto a glass slide, left to dry overnight and mounted on a metal stub using double-sided adhesive tape. Next, gold was sputtered onto the surface of the sample under vacuum and, the resulting coated samples, were imaged using a FEI Quanta FEG 250 ESEM (FEI Company, USA) at an operating voltage of 20 kV.

3.2.3.4. Oxygen-binding and releasing assay.

The functionality of Hb within the Hb-NPs was evaluated conducting an O_2-binding and releasing assay. For that, suspensions of free Hb (3 mL, 0.413 mg mL^{-1} in MQ) and Hb-NPs (3 mL, 0.413 mg mL^{-1} in MQ) were purged with compressed air or nitrogen (N_2) gas for 10 min in a closed system. The spectra of the suspensions were recorded using a UV-2600 UV-vis Spectrophotometer (Shimadzu, Japan) in the wavelength range of 350–650 nm. When purging with N_2, a pinch of STD was added to the solution in order to remove any residual O_2 prior recording the spectrum.

3.2.4 Fabrication and characterization of PDA-coated Hb-NPs (Hb/PDA-NPs).

3.2.4.1. Fabrication of Hb/PDA-NPs.

The harvested Hb-NPs were coated by PDA following a reported protocol with slight modifications.[32] In brief, the Hb-NPs were incubated with DA solutions at different concentrations (0.1 to 5 mg mL^{-1} in TRIS 1) for either 30 or 60 min. The resulting Hb/PDA-NPs were collected after washing in MQ (3×, 3011 *g*, 5 min) using a benchtop centrifuge (MiniSpin, Hamburg, Germany).

3.2.4.2. Physicochemical characterization of the Hb/PDA-NPs.

The size and PDI of the Hb/PDA-NPs were evaluated by DLS using the Zetasizer nano ZS instrument (Malvern Instruments Ltd, UK). The ζ-potentials were also assessed using the same instrument. The DIC and SEM images of the Hb/PDA-NPs were obtained as previously described in Section 2.3.3.

3.2.5. Functionality of Hb/PDA-NPs.

3.2.5.1. Fourier-transform infrared (FTIR) spectroscopy.

FTIR analysis was conducted using a PerkinElmer Spectrum 100 FT-IR spectrometer (PerkinElmer Inc., Wellesley, MA). Free Hb, PDA and Hb-NPs were set as control groups.

3.2.5.2. O_2-binding and releasing assay.

The functionality of the coated Hb/PDA-NPs was evaluated as described in Section 3.2.3.4.

3.2.6. Antioxidant protection by the PDA coating.

3.2.6.1. ROS scavenging.

The ROS scavenging properties of the Hb-NPs and the PDA-coated Hb/PDA-NPs towards the $O_2^{\bullet-}$ and H_2O_2 were evaluated by the WST-1 and the Amplex Red assay, respectively. For the WST-1 assay, the Hb-NPs and Hb/PDA-NPs (200 µL at ~8×10^4 events μL^{-1} as assessed by flow cytometry using a BD Accuri C6 flow cytometer (BD Biosciences, Sparks, MD, USA) were added to 200 µL of a solution containing EDTA (0.1 mM), WST-1 (2.5% v/v), xanthine (0.1 mM) and 10 µL of XO (0.05 U mL^{-1}), all in TRIS 2 buffer and incubated using a thermoshaker (1400 rpm, 37 °C) for 10, 30 or 60 min. The samples were then spun down (6705 *g*, 5 min) and 180 µL of the obtained supernatants were transferred to a 96-well plate. The absorbance (Abs) readings at 438 nm due to the oxidized WST-1 reagent were recorded using a TECAN Spark multimode plate reader (Tecan Group Ltd., Maennendorf, Switzerland). A mixture of TRIS 2 (200 µL) and 200 µL of a solution of EDTA (0.1 mM), WST-1 (2.5% v/v) and xanthine (0.1 mM) with or without the addition of XO (10 µL, 0.05 U mL^{-1}) were used as positive and negative controls, respectively. The normalized Abs (nAbs) was calculated with this formula: nAbs (%) = ((Abs of sample - Abs of negative control)/(Abs of positive control - Abs of negative control)) × 100.

For the Amplex Red assay, H_2O_2 (10 µL, 0.2 mM) was added to a suspension of Hb-NPs or Hb/PDA-NPs (200 µL at ~5×10^3 events μL^{-1} as assessed by flow cytometry) all in TRIS 2 buffer. The samples were incubated using a thermoshaker (1400 rpm, 37 °C) for 10, 30 or 60 min, spun down (6705 *g*, 5 min) and 180 µL of the obtained supernatants were transferred to a new test tube and incubated for 5 min at 37 °C with HRP (10 µL, 2 U mL^{-1}) and Amplex Red (10 µL, 0.1 mM), all in TRIS 2 buffer. The mixtures (180 µL) were transferred to a black 96-well plate and the fluorescence intensity (FI) ($\lambda_{ex}/\lambda_{em}$ = 530/586 nm) was measured using the plate reader. A mixture of TRIS 2 (180 µL) and HRP (10 µL, 2 U mL^{-1}) and Amplex Red (10 µL, 0.1 mM) with and without the addition of H_2O_2 (10 µL, 0.2 mM) were used as positive and negative controls, respectively. The normalized fluorescence intensity (nFI) was calculated with this formula:

nFI (%) = ((FI of sample - FI of negative control)/(FI of positive control - FI of negative control)) × 100.

3.2.6.2. MetHb conversion.

30 µL of H_2O_2 (1 M) were added to a suspension of Hb-NPs and Hb/PDA-NPs (3 mL at ~1.07×10^5 events μL^{-1} as assessed by flow cytometry). The Soret peak height over time was recorded using the UV-vis spectrometer. The Soret peak was normalized to the starting Hb-NPs without the addition of H_2O_2 in order to calculate the percentage of decreased Soret peak height.

3.2.7. Biocompatibility.

3.2.7.1. Cell viability.

HUVECs were cultured in ECM enriched with streptomycin/penicillin (10 µg mL^{-1} and 1% v/v, 10 000 mL^{-1}, respectively), endothelial cell growth supplements (1% v/v) and FBS (5% v/v). RAW 264.7 cells were cultured in DMEM enriched with streptomycin/penicillin (10 µg mL^{-1} and 1% v/v, 10 000 mL^{-1}, respectively) and FBS (10% v/v). Both cell lines were cultured in T75 culture flasks using a humidified incubator (5% CO_2, 37 °C). The cell media were exchanged 2 to 3 times per week and the cells were sub-cultured upon reaching ~80% confluence. While the RAW 264.7 cells were detached from the flasks using a cell scraper, the HUVEC cells were detached by using trypsin. Both cell lines were re-suspended in fresh cell media and added into new T75 flasks at sub-cultivation ratios of 1:5 and 1:3 for RAW 264.7 and HUVEC cells, respectively. Only cells with passages between 5-18 (for RAW 264.7) and 3-14 (for HUVEC) were used in all experiments.

The cell viability was evaluated as follows: 15 000 HUVEC or 30 000 RAW 464.7 cells per well were seeded in a 96-well plate. After 24 h of incubation, the attached cells were washed with PBS (2×, 150 µL) and incubated for 4 h with increasing amounts of Hb-NPs and Hb/PDA-NPs (i.e., 240, 1200, 6000 and 30 000 NPs μL^{-1}). Next, the cells were washed with PBS (3×, 150 µL) and a PrestoBlue solution (10% v/v in cell media, 100 µL) was added to the wells and incubated for 1 h. The supernatants were transferred to a 96-well plate to measure the FI ($\lambda_{ex}/\lambda_{em}$: 535/615 nm). Media and cells only were set as a negative and positive control, respectively, for the normalized cell viability (nCV) calculation. The nCV was calculated as follows: nCV (%) = (experimental

value − negative control value)/(positive control value − negative control value) × 100. Each condition was evaluated in triplicate in, at least, two independent experiments.

3.2.7.2. Hemocompatibility.

The hemolysis rate was evaluated as follows: whole blood from healthy donors, which was collected in heparin-coated tubes, was washed in PBS (3×, 1000 *g*, 15 min, 4 °C) and 1 mL of RBCs was re-suspended in 50 mL of PBS. This diluted blood (200 μL) was transferred to a new Eppendorf and suspensions of Hb-NPs or Hb/PDA-NPs (300 μL at 240, 1200, 6000 and 30 000 NPs μL^{-1} in PBS) were added. PBS and MQ water (300 μL) were also added to the diluted blood and set as negative and positive controls, respectively. The obtained mixtures were incubated in a thermoshaker (37 °C, gently shaking) for 60 min. Then, they were spun down (1000 *g*, 10 min), the supernatants collected and further centrifuged (13 000 *g*, 10 min). The new supernatants were collected and transferred to a 96-well plate and the Abs was recorded at 540 nm. The hemolysis rate was calculated as hemolysis rate (%) = (experimental value − negative control value)/(positive control value − negative control value) × 100. Each condition was evaluated in triplicate in, at least, two independent experiments. The pellets collected during the first centrifugation step were re-suspended in PBS and the blood cell morphology was assessed by bright field microscopy using the Olympus Inverted IX83 microscope equipped with a 60 × oil-immersion objective.

3.2.8. Statistical Analysis.

To evaluate the statistical differences among different groups, a one-way ANOVA (confidence level of 95%, $\alpha = 0.05$) using Tukey's multiple comparisons test (*$p \leq 0.05$; **$p \leq 0.01$; ***$p \leq 0.001$; ****$p \leq 0.0001$) was employed using GraphPad Prism (9.1.2 (226)) software.

3.3. Results and discussion

3.3.1. Hb-NPs synthesis and characterization.

During desolvation, the water of the protein solution is replaced by an antisolvent that promotes the precipitation of the protein. The addition of the antisolvent promotes the protein−protein

interactions over the protein−solvent ones, which results in the formation of precipitates in agreement with the nucleation theory.[17,33] Polar solvents such as acetone or EtOH are usually employed, being the later the most common one since EtOH is currently used as a protein excipient.[17] In this study, the aim was to fabricate Hb-NPs to be used as HBOCs and, in order to achieve this goal, we evaluated the effect of several parameters affecting the desolvation process onto the size, PDI and yield of the resulting Hb-NPs.

3.3.1.1. The effect of the Hb concentration.

As a first step, different concentrations of Hb were considered since protein concentration has shown to have an effect on the size of the resulting NPs. While the initial concentration of protein in the solution should be high enough to allow for nucleation, very high protein concentrations result in unchecked particle growth.[17] The diameter of the NPs is one of the most important features when developing HBOCs. HBOCs should be large enough to avoid vasoconstriction, hypertension and short circulation times but, when too small, they can permeate through the gaps in between the endothelial cells lining our blood vessels. Once in the underlying smooth muscle tissue, the HBOCs can act as NO scavengers and, due to its vasodilatory properties, NO scavenging results in adverse cardiovascular events.[3] However, when too large (i.e., in the range of 1-3 μm), the HBOCs are strongly phagocytosed by the macrophages of the MPS.[34,35] Thus, the size of HBOCs should preferably be in the range from 100 nm to 1 μm.

In this work, bovine Hb was employed. As opposed to human Hb, which makes use of 2,3-diphosphoglycerate as an allosteric effector, bovine Hb only requires chloride ions for native operation. **Figure 3.1A** shows how, for an EtOH to water phase ratio of 0.9×, increasing the concentration of Hb results in increased size and PDI with the smallest values obtained for Hb-NPs fabricated using 4.4 mg mL^{-1} Hb. Doubling the concentration of Hb (to 8.8 mg mL^{-1}) resulted in an increase of both the size (from ~550 to ~900 nm) and the PDI (from 0.157 to 0.24). Further increases in Hb concentration resulted in increased diameter and, with the highest studied Hb concentration (i.e., 35.0 mg mL^{-1}), Hb-NPs as big as ~1300 nm were obtained. However, such a large size increase was also accompanied by a very large PDI (of ~0.5). Thus, an Hb concentration of 4.4 mg mL^{-1} was chosen for the following experiments. Such a concentration rendered Hb-NPs of ~550 nm in diameter and a PDI of 0.157. It is worth noticing that PDI values below 0.2 are

regarded as suitable for pharmaceutical applications.[36] Due to Hb's isoelectric point (pI) of 6.8, all the studied concentrations rendered Hb-NPs with positive ζ-potentials of ~35-40 mV.

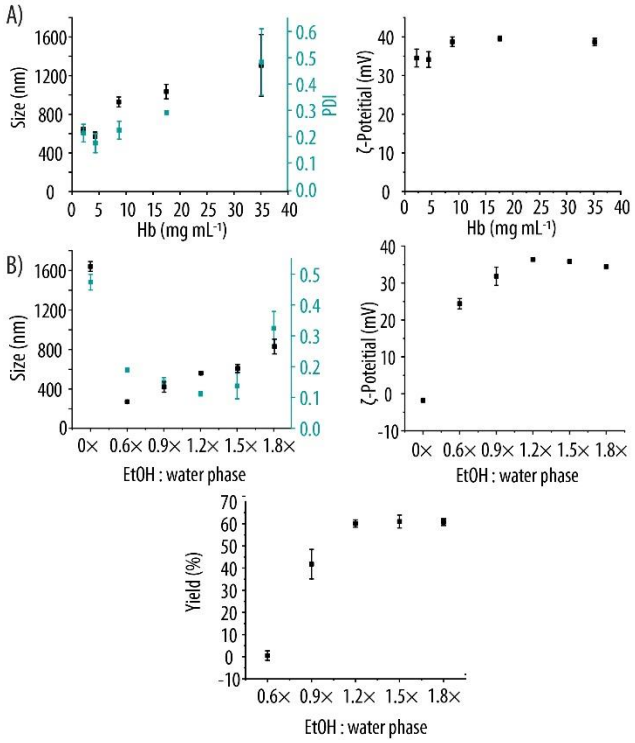

Figure 3.1. Size, polydispersity index (PDI), zeta (ζ)-potential and yield of Hb-NPs fabricated using different Hb concentrations (A) or EtOH to water phase ratios (B). 40 sec of sonication at an amplitude of 50 were used. A desolvation ratio of 0.9× was employed when screening the Hb concentration. An Hb concentration of 4.4 mg mL^{-1} was employed when screening the EtOH to water phase ratio.

3.3.1.2. The effect of the EtOH to water phase ratio.

Since the amount of desolvation agent has also an effect on the size of the resulting NPs, we next investigated the influence of the EtOH to water phase ratio on the size, PDI and ζ-potential of the Hb-NPs. Figure 3.1B shows how the non-desolvating Hb solution (i.e., 0×) displays a large size (~1600 nm) accompanied by a very large PDI (~0.5) suggesting that the free Hb solution contained aggregates which could be a result of the acidic pH (pH 6.35) of the solution or the sonication step required to re-disperse the sample.[37] Upon addition of EtOH at a 0.6× EtOH to water phase ratio, a decrease in size (to ~250 nm) accompanied by a reduction in PDI (~0.2) was observed. Further increases in the desolvation ratio promoted an increase in the size of the Hb-NPs, reaching ~750

nm in size for the highest studied ratio (i.e., of 1.8×). In contrast, the PDI values kept decreasing slightly upon increasing the EtOH to water phase ratios, with the lowest values obtained for a desolvation ratio of 1.5× (PDI ~0.1). This is in agreement with previous studies of protein NPs fabricated by the desolvation method.[38–40] For example, Doan *et al.* prepared pea protein-based NPs that experienced an increase in size from 0.2 to 2 μm upon increasing the EtOH to water phase ratio from 1× to 5×.[40] The pH of the suspension, which was also evaluated by the authors, had a dramatic effect on the size of the resulting NPs. Upon decreasing the pH from 10 to 3; the size of the NPs increased from 0.2 μm (for a 0.1× ratio) to ~12 μm (for a 5× ratio). Sadeghi *et al.* also showed an increase in the size of bovine serum albumin (BSA)-NPs upon increasing the desolvation ratios from zero to 4×.[39] Since Hb has a pI of 6.8, the surface charge of the Hb solution showed a ζ-potential close to neutral (Figure 3.1B). Interestingly, following the addition of EtOH, the Hb-NPs displayed positive ζ-potentials. We attribute this charge reversal to the protonation of amino groups of Hb since the pH of the solution was 5.98 and, below the pI, the amino groups of the proteins are protonated, making them positively charged. The ζ-potentials kept increasing upon increasing the EtOH to water phase ratios until a maximum ζ-potential of ~36.4 ± 0.14 was obtained for a ratio of 1.2×. This is quite surprising, since previous studies have shown a decrease in the charge of the protein NPs following an increase of the desolvation ratio.[40,41] Such a behavior is attributed to a reduction of the dielectric constant of the solution due to the presence of EtOH. This, in turn, hinders the ionization of the charged groups of the proteins thus lowering the ζ-potential. We next calculated the yield of the resulting Hb-NPs for the different desolvation ratios by quantifying the amount of Hb in the supernatant using a BCA assay (Figure 3.1B). Very low yields were obtained for the lowest studied desolvation ratio (i.e., ~5% yield for a ratio of 0.6×). However, a steep increase to ~40% was observed when the desolvation ratio was further increased to 0.9×. A maximum yield of ~60% was achieved for a 1.2× desolvation ratio and no further increase was observed upon increasing the amount of EtOH. Yields of ~40-60% of NPs fully made of Hb will result in much less waste of Hb than other reported systems. For example, Duan et al. prepared Hb loaded within $CaCO_3$ NPs displaying a drug loading of only 6.6%-28%.[42] Our own efforts include the fabrication of Hb-loaded MOFs with only ~50% of protein loading.[14] NPs fully made of Hb were also reported by our group, however, the electrospray technique used for their fabrication is a low through-put method resulting in very low yields.[15] Next, taking into account the size, PDI and yield, a desolvation ratio of 0.9× was selected for the following experiments.

Such a desolvation ratio rendered Hb-NPs with a size (~400 nm) and PDI (<0.2) that are regarded as suitable for pharmaceutical applications.

3.3.1.3. The effect of sonication.

We next aimed to assess whether the application of sonication (for 40 sec and at an amplitude of 50) had an effect onto the size and PDI of the resulting Hb-NPs. As a first investigation and, to demonstrate the importance of sonication, we repeated the experiments of the effect of the desolvation ratio on the size, PDI and ζ-potential of the resulting Hb-NPs but without the sonication step. **Figure 3.2A** shows how the absence of sonication results in a large increase in both the size and the PDI of the Hb-NPs. Interestingly, while for the non-desolvating Hb solution in the absence of sonication the expected size of ~7 nm was detected, for the sonicated one a size ~1.500 nm was observed, indicating aggregation of the individual Hb molecules. Upon addition of EtOH, Hb-NPs are formed, and a large increase in both size and PDI was detected for the non-sonicated samples as compared to the sonicated ones for all the studied desolvation ratios. For the non-sonicated Hb-NPs the largest increase in size was detected for the lowest EtOH to water phase ratio (i.e., ~2.100 nm for a 0.6× desolvation ratio). In contrast, the highest desolvation ratios resulted in the highest PDI values (i.e., ~0.6 and ~0.5 for desolvation ratios of 1.2× and 1.8×, respectively). Interestingly, for the non-desolvating Hb solution, sonication had also an effect on the charge of the Hb molecules. A ζ-potential of -11 ± 0.14 mV was detected for the non-sonicated Hb molecules which is in agreement with the previous reported values. However, following sonication a decrease in charge towards an almost neutral ζ-potential is detected. This is an observation that, at this point of time, we cannot explain.

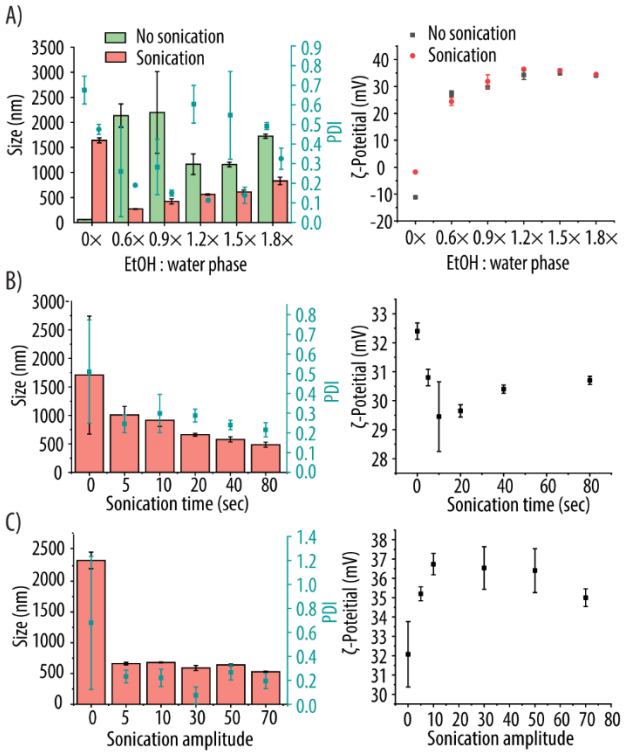

Figure 3.2. A) Size, polydispersity index (PDI) and zeta (ζ)-Potential measurements of Hb-NPs fabricated using different EtOH to water phase ratios with or without sonication. The Hb-NPs were fabricated using an Hb concentration of 4.4 mg mL^{-1}, 40 sec of sonication at an amplitude of 50. Size, PDI and ζ-Potential measurements of Hb-NPs prepared using different sonication times (B) or amplitudes (C). The Hb-NPs were fabricated using an Hb concentration of 4.4 mg mL-1 and a desolvation ratio of 0.9×.

After observing the positive effects of sonication, we evaluated whether by varying sonication time and intensity, it was possible to further reduce both the diameter and PDI of the Hb-NPs. Figure 3.2B shows how the duration of the sonication has a marked effect on reducing both the NPs diameter and the PDI, and the lowest values were obtained for the longest studied sonication times. Importantly, the application of sonication itself greatly reduced the size of the Hb-NPs (i.e., from ~1.700 nm in the absence of sonication to ~1.000 nm after sonicating only for 5 sec). This is not surprising since sonication fragments individual particles into smaller ones. When the sonication time is increased, the Hb-NPs are exposed to the high-power ultrasound waves for a longer period resulting on a further decrease in both size and PDI of the Hb-NPs. For longer sonication times, the reduction in size is not that pronounced (e.g., a decrease of only ~90 nm upon increasing the sonication time from 40 to 80 sec), which suggests a general milling of the formed Hb-NPs to a threshold size. Thus, a sonication time of 40 sec was used in the following experiments. Next, the

effect of the sonication intensity was evaluated (Figure 3.2C). Since the cavitation intensity is related to the amplitude, which can be defined as the distance covered by the probe tip when moving vertically from its resting position, an amplitude range from 0 to 70 was screened.[43] While the application of sonication had a profound effect decreasing the size and PDI of the Hb-NPs, only a very small decrease in size (from ~700 nm to ~500 nm) could be detected upon increasing the amplitude from 5 to 70. These results are in agreement with the observations of the Palmer group.[43] Specifically, McDonel *et al.* reported slight decreases in the size of Hb-NPs for the higher sonication values in terms of time and amplitude. However, in their study, the Hb-NPs were prepared by the coprecipitation, crosslinking and dissolution method.[43]

3.3.1.4. Characterization of the Hb-NPs.

The optimized Hb-NP formulation (assembled using a 4.4 mg mL^{-1} Hb concentration, a 0.9× desolvation ratio and 40 sec of sonication with an amplitude of 30) had an average hydrodynamic diameter of 568nm and a PDI of 0.2. DIC imaging showed a monodisperse and uniform suspension of Hb-NPs while visualization with SEM revealed a spherical shape (**Figure 3.3A**).

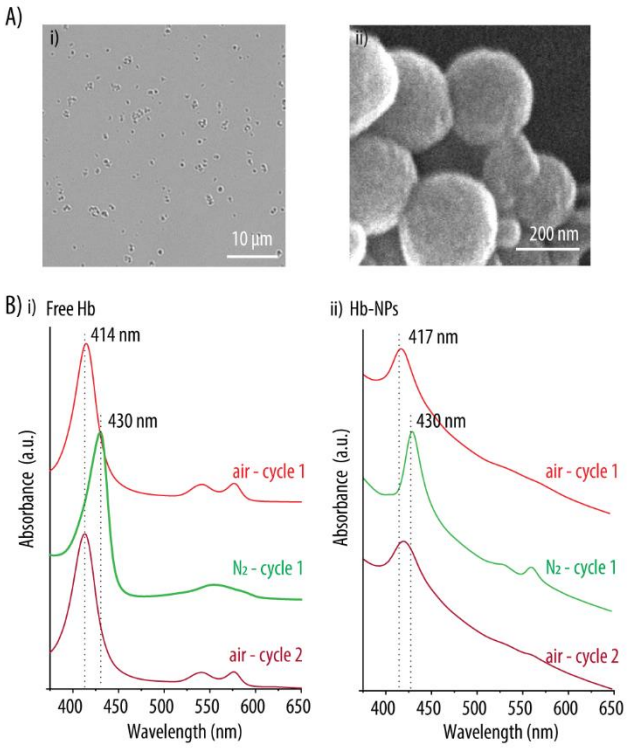

Figure 3.3. Characterization of the Hb-NPs. A) Differential interference contrast (DIC) (i) and scanning electron microscopy (ii) images of the Hb-NPs. B) UV-vis absorption spectra of free Hb (i) and Hb-NPs (ii) following purging with compressed air or nitrogen (N_2) gas. The wavelengths of the Soret peak are indicated.

The O_2-transporting ability is the most important aspect to consider when developing HBOCs. Thus, the ability of the as-prepared Hb-NPs to reversibly bind and release O_2 was evaluated by UV-vis spectroscopy (Figure 3.3B). As expected, the free Hb suspension which was used as a control, exhibited the three characteristic absorption peaks of oxygenated Hb (oxy-Hb) namely, a maxima peak at 414 nm (also known as the Soret peak) and two other maxima peaks at 542 and 576 nm (known as the Q band). Following purging with N_2, the Soret peak experienced a red shift to 430 nm while a single Q band could be detected at 554 nm. These peaks are characteristic of deoxygenated-Hb (deoxy-Hb) and confirm the ability of free Hb to reversibly bind and release O_2.[44] The free Hb solution was purged with compressed air again and a shift towards the characteristic peaks of oxy-Hb was again detected. The same procedure was repeated with the suspension of Hb-NPs by purging it with N_2 and compressed air for three subsequent rounds. As shown in other reports of Hb-loaded NPs, the Hb-NPs spectra display a background slope due to

the light scattering of the NPs themselves.[12,28] However, while some of Q band peaks disappear due to this scattering, the characteristic Soret peak can still be clearly distinguished allowing us to assess the functionality of Hb. Similar shifts of the maxima peaks towards the characteristic peaks of oxy-Hb or deoxy-Hb depicted in Figure 3.3Bii are a proof of the O_2-carrying capacity of the as-prepared Hb-NPs.

3.3.2. Fabrication and characterization of Hb/PDA-NPs.

To prevent the disintegration of the Hb-NPs we made use of a PDA surface coating. While many groups have made use of GA as a crosslinker to stabilize a wide range of Hb-based NPs, covalent modification of proteins results on the unpredictable alteration of their conformation and subsequent activity.[45,46] Furthermore, aldehyde-based crosslinkers have been shown to exhibit toxicity.[18–20] What is more, such an approach also leaves unprotected the Hb molecules located onto the NPs surface. This means that once administered in vivo, the Hb tetramer will get into direct contact with the surrounding tissues and blood components promoting its autoxidation and the subsequent heme-mediated oxidative reactions.[5] PDA coatings, which are obtained by the self-polymerization of DA at slightly basic conditions, can be deposited in a single step, onto virtually any type of surface independently of composition or shape.[24,25,47] Additionally, as a result of its free radical character, PDA displays excellent antioxidant properties.[48] While several groups have reported the ability of PDA-coated HBOCs to scavenge ROS, only our group and the Zhou group have been able to demonstrate that the antioxidant character of PDA can minimize the oxidation of Hb into metHb.[15,18,29,49,50] This is an important aspect since, apart of not being able to deliver O_2, the oxidation of Hb into metHb results in dysregulated vascular tone and inflammatory reactions.[4] The PDA coating was fabricated by incubating the Hb-NPs in DA solutions for 30 min and 60 min. Figure 4.4A shows how, increasing DA concentrations, result on a decrease in ζ-potential with the lowest value (~24.5 ± 0.4 mV) obtained for a DA concentration of 1.0 mg mL^{-1}. This decrease in ζ-potential following PDA coating has been shown in previous reports[49] and could be due to the covering of surface chemical groups of Hb (e.g., amino groups from the lysine residues) by PDA.

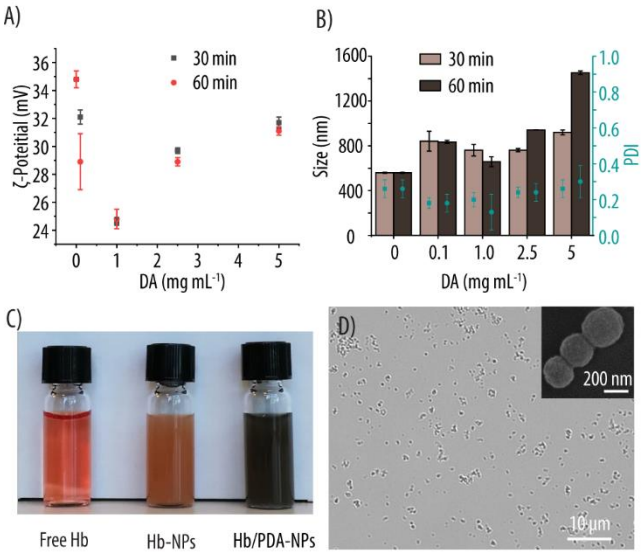

Figure 3.4. Zeta (ζ)-potential (A), size and polydispersity index (PDI) (B) measurements of Hb/PDA-NPs fabricated with increasing amounts of dopamine (DA). C) Photographic images of free Hb and the Hb-NPs before and after being coated with polydopamine (PDA) (Hb/PDA-NPs). D) Differential interference contrast (DIC) and scanning electron microscopy (insert) images of the Hb/PDA-NPs.

Interestingly, both studied reaction times gave rise to the similar ζ-potential values suggesting that 30 min already promoted the highest PDA deposition. Higher DA concentrations resulted in an increase of the ζ-potentials for the two studied time intervals. Specifically, a ζ-potential of ~32 mV was detected for the highest studied DA concentration (i.e., 5 mg mL^{-1}). We attribute this behavior to a potential aggregation of the Hb/PDA-NPs. Figure 3.4B shows the size and PDI of the Hb/PDA-NPs depending on the DA concentration. We would like to point out that the quantitative change in diameter depending on the DA concentration could be misleading since the resulting black PDA coating is expected to adsorb the laser light and affect the outcome of the measurement. However, the size measurements could still give us information regarding potential aggregation of the Hb/PDA-NPs. A size increase from 560 nm to 835 nm is observed upon incubation in the lowest DA solution. Further increases in the concentration of DA only results in a slight increase to ~942 nm for a DA concentration of 2.5 mg mL^{-1} and the longest time interval. The highest DA concentration promoted a size increase up to ~1450 nm for the 60 min incubation period. This, together with a PDI increase from ~0.2 for a 0.1 mg mL-1 DA concentration to ~0.3 for a 5 mg mL^{-1} DA concentration points again towards potential aggregation of the samples and it is also in agreement with the ζ-potential results. Thus, a DA concentration of 1 mg mL^{-1} for 30 min was

used for the next experiments. Figure 3.4C shows the change in color of the Hb-NPs following coating by PDA. The change from red to the characteristic dark grey color confirms the successful coating by PDA. The optimized Hb/PDA-NPs displayed an average diameter of 580 nm and a PDI of 0.2. DIC imaging showed a uniform and monodisperse suspension of Hb/PDA-NPs while SEM revealed a spherical shape with no apparent change with respect to the uncoated Hb-NPs (Figure 3.4D).

We next assessed whether the PDA coating had an effect on the functionality of the Hb/PDA-NPs. Since the structure of proteins is closely linked to their functionality, as a first step the potential effect of the PDA coating onto Hb's chemical structure was evaluated by FTIR spectroscopy. Figure 3.5A shows the FTIR spectra of PDA, free Hb, Hb-NPs and Hb/PDA-NPs. The three Hb-containing samples showed the characteristic bands of Amide I (at 1648 cm^{-1}) and Amide II (at 1533 cm^{-1}), indicating that Hb's chemical structure was preserved within Hb-NPs and also following PDA coating to render Hb/PDA-NPs. In proteins, the Amide I band (between 1600–1700 cm^{-1}) originates from the stretching vibrations of the C=O group and gives information about the conformation of the backbone and the hydrogen bonding while. In contrast, the Amide II band (between 1510 and 1580 cm^{-1}) results from the in-plane N-H bending and C-N stretching vibrations. Interestingly, in this work, the Hb/PDA-NPs did not display any characteristic bands that could be directly related to the PDA coating. The PDA has vibrational peaks in a similar region than Hb. Since there is a much higher amount of Hb than PDA within the Hb/PDA-NPs, the vibrational peaks of Hb hinder the contribution of PDA. For example, while the PDA spectrum shows a clear peak at 1506 cm^{-1} (N-H bending vibration), in the Hb/PDA-NPs spectrum this falls under the large Amide II peak originating from the Hb-NPs. Nonetheless, although the FTIR data did not show the contribution of the PDA coating in the Hb/PDA-NP spectrum, these data did confirm preservation of Hb's chemical structure within the Hb/PDA-NPs.

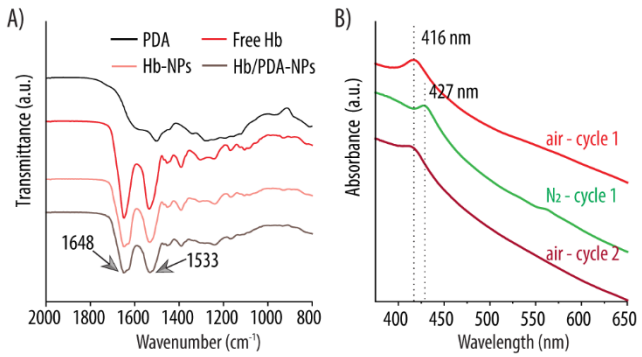

Figure 3.5. A) Fourier-transform infrared spectra of free Hb and the Hb-NPs before and after being coated with polydopamine (PDA) (Hb/PDA-NPs). B) UV–vis absorption spectra of the Hb/PDA-NPs following purging with compressed air or nitrogen (N_2) gas.

To assess whether the Hb entrapped within the NPs following coating by PDA preserved its functionality, compressed air and N_2 gas were flowed over the Hb/PDA-NPs and the resulting oxygenated and deoxygenated Hb/PDA-NPs were evaluated by UV-vis (Figure 3.5B). Following the initial purging with compressed air, the UV-vis spectrum shows the characteristic Soret peak for oxy-Hb at ~416 nm (red line). However, in this case, the two other characteristic peaks of oxy-Hb at 542 and 576 nm (known as the Q band) are not observed. We attribute this fact to the broad absorption peak resulting from the scattering of the NPs, which is probably hindering the two maxima peaks. Following purging with N_2, a red shift to 427 nm is observed revealing the characteristic Soret peak of deoxy-Hb (green line). In this case, the characteristic Q band of deoxy-Hb can be observed at 559 nm. Next, following a second flowing with compressed air, the characteristic deoxy-Hb Soret peak shifted back to 416 nm (dark red line), which means that the Hb in the Hb/PDA-NPs changed from the deoxy-Hb to oxy-Hb conformation. The Q-band was not detected also in this case, which we again attribute to the scattering of the NPs. This reversible shift on the Soret peak following purging with the two gases confirms that the PDA coating did not compromise the O_2-carrying properties of Hb, which is the one of the most important properties of the O_2 carriers.

3.3.3. Antioxidant protection.

3.3.3.1. ROS scavenging.

Overtime Hb autoxidizes into non-functional metHb. Within RBCs, metHb is reduced back to Hb by both enzymatic and non-enzymatic antioxidant systems.[51] In this work, we evaluate the antioxidant protection rendered by the PDA coating in terms of its ability to minimize Hb's autoxidation. Although, due to the complexity of the structure of PDA, the exact antioxidant mechanism has not been fully elucidated yet, PDA's antioxidant properties are believed to be a result of its ability to scavenge free radicals by means of its hydroquinone – quinone subunits.[52] Hence, as a first step, the ability of the PDA-coated Hb/PDA-NPs to scavenge two important ROS (i.e., $O_2^{\bullet-}$ and H_2O_2) was evaluated. While the kinetics of the depletion of $O_2^{\bullet-}$ and H_2O_2 by Hb-NPs and Hb/PDA-NPs was monitored by the WST-1 and Amplex Red assays, respectively. Figure 3.6A shows the principle of the WST-1 assay, were $O_2^{\bullet-}$ is generated from O_2 and xanthine in the presence of the enzyme XO. $O_2^{\bullet-}$ is then able to oxidize the WST-1 into the yellow formazan product which can be monitored by Abs measurements. Hence, the scavenging of $O_2^{\bullet-}$ results in reduced WST-1 oxidation and decreased Abs readings. The uncoated Hb-NPs displayed a ~20% decrease in nAbs after 10 min of incubation and an additional decrease of ~40% of nAbs after 30 min of reaction. No further decrease was detected for the longest incubation time. This result is not surprising and confirms Hb's scavenging properties due to its oxidation into metHb.[53] Upon coating with PDA, the resulting Hb/PDA-NPs promoted a ~70% decrease after only 10 min of incubation. No further decrease in nAbs could be detected for the longer incubation periods indicating saturation of the system. Therefore, in agreement with previous reports, the as-prepared Hb/PDA-NPs display important scavenging properties towards $O_2^{\bullet-}$ as a result of the PDA coating.[15,18,29,32,50] Since the depletion of $O_2^{\bullet-}$ generates H_2O_2 which is another harmful ROS, the ability of the Hb/PDA-NPs to decompose it into O_2 and H_2O was also evaluated. The Amplex Red assay relies in the oxidation of Amplex Red by H_2O_2 in the presence of the HRP enzyme to generate the fluorescent resorufin product (Figure 3.6B). Depletion of H_2O_2 will result in less Amplex Red oxidation and the resulting decrease in nFI. Both Hb-NPs and Hb/PDA-NPs promoted a slight increase in nFI after only 10 min of incubation. However, longer incubation times promoted the expected decrease in nFI. Specifically, both Hb-NPs and Hb/PDA-NPs promoted a time-dependent decrease of the nFI and such a decrease was more pronounced for the

PDA-coated Hb/PDA-NPs. While the Hb-NPs promoted a ~20% and a ~40% decrease in nFI after 30 and 60 min of reaction, respectively, the Hb/PDA-NPs resulted on a ~40% and 80% decrease in nFI after 30 and 60 min of reaction, respectively. These results highlight again the ability of PDA coating to scavenge ROS. Once confirmed the ability of the Hb/PDA-NPs to deplete $O_2^{\bullet-}$ and H_2O_2, we next evaluated if these ROS scavenging properties translated into antioxidant protection towards metHb conversion.

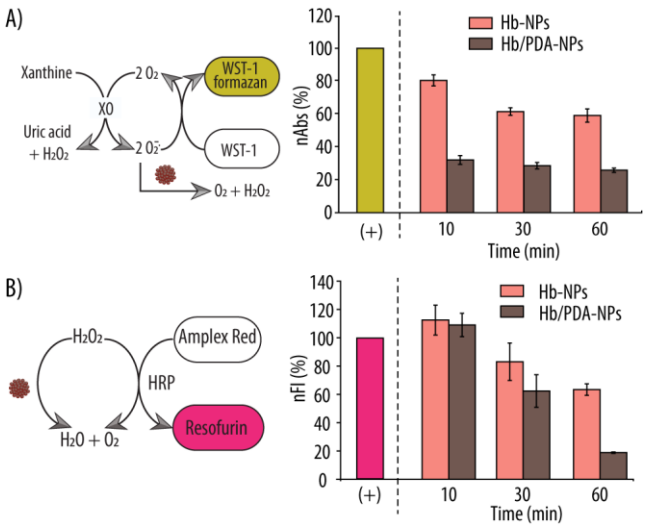

Figure 3.6. Scavenging properties. A) The xanthine/xanthine oxidase (XO) system is used to produce the superoxide radical anion ($O_2^{\bullet-}$) from O_2. The as-produced $O_2^{\bullet-}$ is then able to convert the WST-1 reagent into the yellow formazan product. Hb-NPs and polydopamine (PDA)-coated Hb/PDA-NPs are able to deplete $O_2^{\bullet-}$ by converting it into O_2 and hydrogen peroxide (H_2O_2) which will result in a decrease in the normalized absorbance (nAbs) of the WST-1 formazan. The nAbs readings of both Hb-NPs and Hb/PDA-NPs incubated with the $O_2^{\bullet-}$ solution for different time intervals are shown. B) The Amplex Red reagent, in the presence of the enzyme horseradish peroxidase (HRP), gets oxidized by H_2O_2 into red fluorescent resorufin. Hb-NPs and PDA-coated Hb/PDA-NPs are able to deplete H_2O_2 by converting it into O_2 and H_2O, which will result in a decrease in the normalized fluorescence intensity (nFI) of resorufin. The nFI readings of both Hb-NPs and Hb/PDA-NPs incubated with the H_2O_2 solution for different time intervals are shown.

3.3.3.2. MetHb conversion.

The Fe^{2+} iron within Hb has the ability to easily bind and release O_2. However, upon oxidation into Fe^{3+}, the resulting metHb has no O_2-carrying capacity. Thus, we next evaluated the ability of the PDA coating to protect Hb from oxidation into metHb. To accelerate the oxidation process, both Hb-NPs and Hb/PDA-NPs were incubated in a H_2O_2 solution and the height of the

characteristic oxy-Hb Soret peak was monitored over time. Figure 3.7 shows how the highest decrease in Soret peak height takes place for the uncoated Hb-NPs. Specifically, a ~20% decrease is observed after only 1 min of incubation followed by a further ~15% decrease after 10 min of incubation which gives a total of ~35% metHb conversion. In contrast, for the PDA-coated Hb/PDA-NPs barely any decrease in normalized Soret peak height could be detected after the 10 min incubation period, indicating that the PDA coating was able to prevent Hb's oxidation.

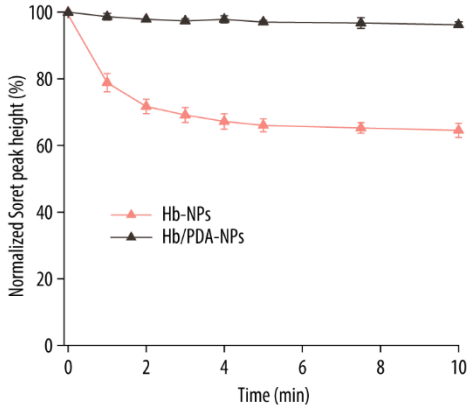

Figure 3.7. MetHb conversion. Normalized Soret peak height over time for Hb-NPs and Hb/PDA-NPs in the presence of 10 mM H_2O_2.

3.3.4. Biocompatibility.

3.3.4.1. Cell viability.

Good biocompatibility is a central aspect when developing HBOCs in order to preserve the normal physiological functions of the body. Thus, the biocompatibility of the Hb/PDA-NPs was evaluated by assessing the in vitro cell viability of HUVEC and RAW 264.7 cells. These two cell lines were chosen because of their relevance as the cells lining our blood vessels (for HUVECs) or as a defense mechanism for intruding pathogens (for the macrophage cell line RAW 264.7). **Figure 3.8** shows how neither the Hb-NPs nor the Hb/PDA-NPs produced a significant decrease in nCV for the studied concentration range. For RAW 264.7 cells, incubation with both Hb-NPs and Hb/PDA-NPs the nCV remained at ~100% for all the studied concentrations (Figure 3.8A). For

HUVEC cells, the results were slightly different an increase in nCV to ~110% for the concentrations of 240, 1200 and 6000 NPs μL^{-1} (Figure 3.8B). Although, in this study, such an increase in nCV was non-significant, it is in agreement with other reports that have shown enhanced nCV readings which have been attributed to an additional supply of O_2 by the HBOCs which could facilitate the viability of the cells.[15,53] Although non-significant when compared to the cells only group, a decrease of ~15% in nCV was observed for the highest concentration suggesting that 30 000 NPs μL^{-1} would be the highest tolerable concentration.

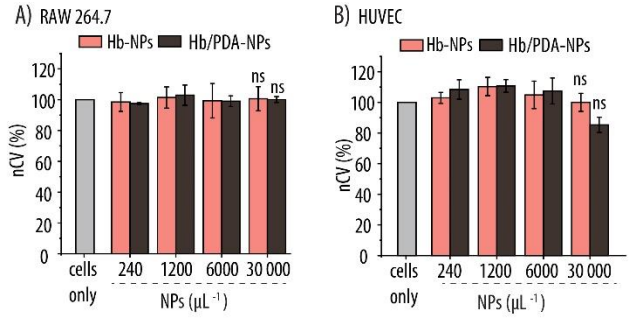

Figure 3.8. Normalized cell viability readings (nCV) of RAW 264.7 (A) and HUVEC (B) cells after incubating for 4 h with increasing concentrations of Hb-NPs and Hb/PDA-NPs. ns: non-significant, NPs vs cells only, $p \leq 0.05$.

3.3.4.2. Hemocompatibility.

Hemocompatibility is an essential property for any intravenously administered carrier. The impact of both the Hb-NPs and the Hb/PDA-NPs on RBCs was evaluated by a hemolysis assay. Figure 3.9A shows how, following incubation of increasing concentrations of both NPs (from 240 to 30 000 NPs μL^{-1}), the hemolysis rate was always below 1%. Since, it is stipulated that a carrier induces hemolysis when it displays hemolysis ratios larger than 5%, the developed Hb/PDA-NPs could be considered non hemolytic even at the highest studied concentration.[54] Figure 3.9B shows photographic images of the test tubes containing the negative (0% lysis) and the positive (100% lysis) controls and both Hb-NPs and Hb/PDA-NPs at the different studied concentrations. In agreement with the hemolysis rate results, free Hb with its distinctive red color can only be observed for the positive control. Additionally, the blood cells also retained their shape following incubation with both Hb-NPs and Hb/PDA-NPs (Figure 3.9C).

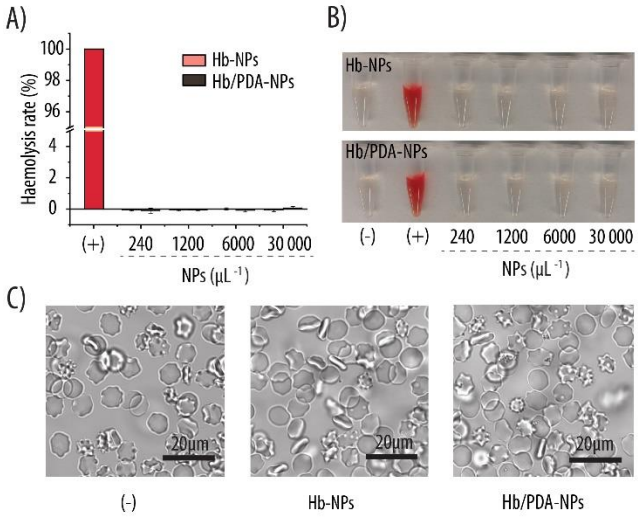

Figure 3.9. A) Hemolysis rate of Hb-NPs and Hb/PDA-NPs at different concentrations. B) Photographic images of the supernatants of the blood samples incubated with different concentrations of Hb-NPs and Hb/PDA-NPs and the corresponding controls. C) Bright field images of blood cells incubated with Hb-NPs and Hb/PDA-NPs at a concentration of ~3×10^4 NPs μL^{-1}. PBS and MQ have been used as negative (-) and positive (+) controls, respectively.

3.4. Conlusions

To sum up, we have prepared a new type of NPs fully made of Hb by the desolvation method. By screening several process parameters (i.e., Hb concentration, EtOH to water phase ratio and sonication time and amplitude) Hb-NPs with a size of 568 nm and a PDI of 0.2 have been obtained. These values are regarded as suitable for pharmaceutical applications. To stabilize the Hb-NPs, an antioxidant PDA coating has been deposited. Due to the redox character of PDA, the resulting Hb/PDA-NPs are able to scavenge two of the most important ROS of our body, i.e., $O_2^{\bullet -}$ and H_2O_2. Importantly, as a result of the PDA coating, the Hb/PDA-NPs were prevented from oxidation into non-functional metHb when exposed to a H_2O_2 solution for 10 min. The Hb/PDA-NPs did not promote a significant decrease in viability at the studied concentrations for two relevant cell lines namely, macrophages and endothelial cells. Finally, the Hb/PDA-NPs were also able to bind and release O_2 over several rounds, which is the most important feature when developing HBOCs.

3.5. Author information

Corresponding Author

*E-mail: leri@dtu.dk

Funding Sources

This work has been supported by the Danish Council for Independent Research (Grant No. 6111-00298B).

3.6. References

(1) Indications and hemoglobin thresholds for red blood cell transfusion in the adult - UpToDate https://www.uptodate.com/contents/indications-and-hemoglobin-thresholds-for-red-blood-cell-transfusion-in-the-adult (accessed Apr 21, 2021).

(2) Watkins, T.; Surowiecka, M. K.; McCullough, J. Transfusion Indications for Patients With Cancer. *Cancer Control* **2015**, *22* (1), 38–46. https://doi.org/10.1177/107327481502200106.

(3) Sen Gupta, A.; Doctor, A. Oxygen Carriers. *Damage Control Resusc.* **2020**, 197–222. https://doi.org/10.1007/978-3-030-20820-2.

(4) Sen Gupta, A. Bio-Inspired Nanomedicine Strategies for Artificial Blood Components. *WIREs Nanomed. Nanobiotechnol.* **2017**, *9* (6), e1464. https://doi.org/10.1002/wnan.1464.

(5) Jansman, M. M. T.; Hosta-Rigau, L. Recent and Prominent Examples of Nano- and Microarchitectures as Hemoglobin-Based Oxygen Carriers. *Adv. Colloid Interface Sci.* **2018**, *260*, 65–84. https://doi.org/10.1016/j.cis.2018.08.006.

(6) Coll-Satue, C.; Bishnoi, S.; Chen, J.; Hosta-Rigau, L. Stepping Stones to the Future of Haemoglobin-Based Blood Products: Clinical, Preclinical and Innovative Examples. *Biomater. Sci.* **2021**, *9* (4), 1135–1152. https://doi.org/10.1039/d0bm01767a.

(7) Dessy, A.; Piras, A. M.; Schir, G.; Levantino, M.; Cupane, A.; Chiellini, F. Hemoglobin Loaded Polymeric Nanoparticles: Preparation and Characterizations. *Eur. J. Pharm. Sci.* **2011**, *43* (1–2), 57–64. https://doi.org/10.1016/j.ejps.2011.03.010.

(8) Buehler, P. W.; D'Agnillo, F.; Schaer, D. J. Hemoglobin-Based Oxygen Carriers: From Mechanisms of Toxicity and Clearance to Rational Drug Design. *Trends Mol. Med.* **2010**, *16* (10), 447–457. https://doi.org/10.1016/j.molmed.2010.07.006.

(9) Bunn, H. F.; Esham, W. T.; Bull, R. W. The Renal Handling of Hemoglobin. I. Glomerular Filtration. *J. Exp. Med.* **1969**, *129* (5), 909–924. https://doi.org/10.1084/jem.129.5.909.

(10) Kaneda, S.; Ishizuka, T.; Goto, H.; Kasukawa, H. Liposome-Encapsulated Hemoglobin as an Artificial Oxygen Carrier: Technological Features, Manufacturing and Issues for Practical Application. In *Hemoglobin-Based Oxygen Carriers as Red Cell Substitutes and Oxygen Therapeutics*; Springer Berlin Heidelberg: Berlin, Heidelberg, 2014; Vol. 9783642407, pp 273–282. https://doi.org/10.1007/978-3-642-40717-8_14.

(11) Kaneda, S.; Ishizuka, T.; Goto, H.; Kimura, T.; Inaba, K.; Kasukawa, H. Liposome-encapsulated Hemoglobin, TRM-645: Current Status of the Development and Important Issues for Clinical Application. *Artif. Organs* **2009**, *33* (2), 146–152.

(12) Jia, Y.; Cui, Y.; Fei, J.; Du, M.; Dai, L.; Li, J.; Yang, Y. Construction and Evaluation of Hemoglobin-Based Capsules as Blood Substitutes. *Adv. Funct. Mater.* **2012**, *22* (7), 1446–1453. https://doi.org/10.1002/adfm.201102737.

(13) Peng, S.; Liu, J.; Qin, Y.; Wang, H.; Cao, B.; Lu, L.; Yu, X. Metal-Organic Framework Encapsulating Hemoglobin as a High-Stable and Long-Circulating Oxygen Carriers to Treat Hemorrhagic Shock. *ACS Appl. Mater. Interfaces* **2019**, *11* (39), 35604–35612. https://doi.org/10.1021/acsami.9b15037.

(14) Liu, X.; Jansman, M. M. T.; Hosta-Rigau, L. Haemoglobin-Loaded Metal Organic Framework-Based Nanoparticles Camouflaged with a Red Blood Cell Membrane as Potential Oxygen Delivery Systems. *Biomater. Sci.* **2020**, *8* (21), 5859–5873. https://doi.org/10.1039/d0bm01118e.

(15) Liu, X.; Jansman, M. M. T.; Thulstrup, P. W.; Mendes, A. C.; Chronakis, I. S.; Hosta-Rigau, L.

Low-Fouling Electrosprayed Hemoglobin Nanoparticles with Antioxidant Protection as Promising Oxygen Carriers. *Macromol. Biosci.* **2020**, *20* (2), 1900293. https://doi.org/10.1002/mabi.201900293.

(16) McDonel, E. M.; Hickey, R.; Palmer, A. F. Sonication Effectively Reduces Nanoparticle Size in Hemoglobin-Based Oxygen Carriers (HBOCs) Produced through Coprecipitation: Implications for Red Blood Cell Substitutes. *ACS Appl. Nano Mater.* **2020**, *3* (12), 11736–11742. https://doi.org/10.1021/acsanm.0c02176.

(17) Hickey, R.; Palmer, A. F. Synthesis of Hemoglobin-Based Oxygen Carrier Nanoparticles by Desolvation Precipitation. *Langmuir* **2020**, *36* (47), 14166–14172. https://doi.org/10.1021/acs.langmuir.0c01698.

(18) Hu, J.; Wang, Q.; Wang, Y.; You, G.; Li, P.; Zhao, L.; Zhou, H. Polydopamine-Based Surface Modification of Hemoglobin Particles for Stability Enhancement of Oxygen Carriers. *J. Colloid Interface Sci.* **2020**, *571*, 326–336. https://doi.org/10.1016/j.jcis.2020.03.046.

(19) Jia, Y.; Duan, L.; Li, J. Hemoglobin-Based Nanoarchitectonic Assemblies as Oxygen Carriers. *Adv. Mater.* **2016**, *28* (6), 1312–1318. https://doi.org/10.1002/adma.201502581.

(20) Xiong, Y.; Steffen, A.; Andreas, K.; Müller, S.; Sternberg, N.; Georgieva, R.; Bäumler, H. Hemoglobin-Based Oxygen Carrier Microparticles: Synthesis, Properties, and In Vitro and In Vivo Investigations. *Biomacromolecules* **2012**, *13* (10), 3292–3300. https://doi.org/10.1021/bm301085x.

(21) Galisteo-González, F.; Molina-Bolívar, J. A. Systematic Study on the Preparation of BSA Nanoparticles. *Colloids Surf., B* **2014**, *123*, 286–292. https://doi.org/10.1016/j.colsurfb.2014.09.028.

(22) Eaton, W. A.; Henry, E. R.; Hofrichter, J.; Mozzarelli, A. Is Cooperative Oxygen Binding by Hemoglobin Really Understood? *Nature Structural Biology*. Nature Publishing Group 1999, pp 351–358. https://doi.org/10.1038/7586.

(23) Lynge, M. E.; Schattling, P.; Städler, B. Recent Developments in Poly(Dopamine)-Based Coatings for Biomedical Applications. *Nanomedicine* **2015**, *10* (17), 2725–2742. https://doi.org/10.2217/nnm.15.89.

(24) Godoy-Gallardo, M.; Portolés-Gil, N.; López-Periago, A. M.; Domingo, C.; Hosta-Rigau, L. Multi-Layered Polydopamine Coatings for the Immobilization of Growth Factors onto Highly-Interconnected and Bimodal PCL/HA-Based Scaffolds. *Mater. Sci. Eng. C* **2020**, *117*, 111245. https://doi.org/10.1016/j.msec.2020.111245.

(25) Godoy-Gallardo, M.; Portolés-Gil, N.; López-Periago, A. M.; Domingo, C.; Hosta-Rigau, L. Immobilization of BMP-2 and VEGF within Multilayered Polydopamine-Coated Scaffolds and the Resulting Osteogenic and Angiogenic Synergy of Co-Cultured Human Mesenchymal Stem Cells and Human Endothelial Progenitor Cells. *Int. J. Mol. Sci.* **2020**, *21* (17), 1–25. https://doi.org/10.3390/ijms21176418.

(26) Hosta-Rigau, L.; York-Duran, M. J.; Zhang, Y.; Goldie, K. N.; Städler, B. Confined Multiple Enzymatic (Cascade) Reactions within Poly(Dopamine)-Based Capsosomes. *ACS Appl. Mater. Interfaces* **2014**, *6* (15), 12771–12779. https://doi.org/10.1021/am502743z.

(27) Ryu, J. H.; Messersmith, P. B.; Lee, H. Polydopamine Surface Chemistry: A Decade of Discovery. *ACS Appl. Mater. Interfaces* **2018**, *10* (9), 7523–7540. https://doi.org/10.1021/acsami.7b19865.

(28) Yu, C.; Huang, X.; Qian, D.; Han, F.; Xu, L.; Tang, Y.; Bao, N.; Gu, H. Fabrication and Evaluation of Hemoglobin-Based Polydopamine Microcapsules as Oxygen Carriers. *Chem. Commun.* **2018**, *54* (33), 4136–4139. https://doi.org/10.1039/c8cc00095f.

(29) Baidukova, O.; Wang, Q.; Chaiwaree, S.; Freyer, D.; Prapan, A.; Georgieva, R.; Zhao, L.; Bäumler, H. Antioxidative Protection of Haemoglobin Microparticles (HbMPs) by PolyDopamine. *Artif. Cells, Nanomedicine, Biotechnol.* **2018**, *46* (3), 693–701. https://doi.org/10.1080/21691401.2018.1505748.

(30) Weber, C.; Coester, C.; Kreuter, J.; Langer, K. Desolvation Process and Surface Characterisation of Protein Nanoparticles. *Int. J. Pharm.* **2000**, *194* (1), 91–102. https://doi.org/10.1016/S0378-5173(99)00370-1.

(31) Langer, K.; Balthasar, S.; Vogel, V.; Dinauer, N.; Von Briesen, H.; Schubert, D. Optimization of the Preparation Process for Human Serum Albumin (HSA) Nanoparticles. *Int. J. Pharm.* **2003**, *257* (1–2), 169–180. https://doi.org/10.1016/S0378-5173(03)00134-0.

(32) York-Duran, M. J.; Godoy-Gallardo, M.; Jansman, M. M. T.; Hosta-Rigau, L. A Dual-Component Carrier with Both Non-Enzymatic and Enzymatic Antioxidant Activity towards ROS Depletion. *Biomater. Sci.* **2019**, *7* (11), 4813–4826. https://doi.org/10.1039/C9BM00913B.

(33) Kalikmanov, V. I. Classical Nucleation Theory; Springer, Dordrecht, 2013; pp 17–41. https://doi.org/10.1007/978-90-481-3643-8_3.

(34) Champion, J. A.; Walker, A.; Mitragotri, S. Role of Particle Size in Phagocytosis of Polymeric Microspheres. *Pharm. Res.* **2008**, *25* (8), 1815–1821. https://doi.org/10.1007/s11095-008-9562-y.

(35) Xiong, Y.; Liu, Z. Z.; Georgieva, R.; Smuda, K.; Steffen, A.; Sendeski, M.; Voigt, A.; Patzak, A.; Bäumler, H. Nonvasoconstrictive Hemoglobin Particles as Oxygen Carriers. *ACS Nano* **2013**, *7* (9), 7454–7461. https://doi.org/10.1021/nn402073n.

(36) Danaei, M.; Dehghankhold, M.; Ataei, S.; Hasanzadeh Davarani, F.; Javanmard, R.; Dokhani, A.; Khorasani, S.; Mozafari, M. R. Impact of Particle Size and Polydispersity Index on the Clinical Applications of Lipidic Nanocarrier Systems. *Pharmaceutics* **2018**, *10* (2), 57. https://doi.org/10.3390/pharmaceutics10020057.

(37) Stathopulos, P. B.; Scholz, G. A.; Hwang, Y.-M.; Rumfeldt, J. A. O.; Lepock, J. R.; Meiering, E. M. Sonication of Proteins Causes Formation of Aggregates That Resemble Amyloid. *Protein Sci.* **2008**, *13* (11), 3017–3027. https://doi.org/10.1110/ps.04831804.

(38) Gülseren, I.; Fang, Y.; Corredig, M. Whey Protein Nanoparticles Prepared with Desolvation with Ethanol: Characterization, Thermal Stability and Interfacial Behavior. *Food Hydrocoll.* **2012**, *29* (2), 258–264. https://doi.org/10.1016/j.foodhyd.2012.03.015.

(39) Sadeghi, R.; Moosavi-Movahedi, A. A.; Emam-Jomeh, Z.; Kalbasi, A.; Razavi, S. H.; Karimi, M.; Kokini, J. The Effect of Different Desolvating Agents on BSA Nanoparticle Properties and Encapsulation of Curcumin. *J. Nanoparticle Res.* **2014**, *16* (9), 1–14. https://doi.org/10.1007/s11051-014-2565-1.

(40) Doan, C. D.; Ghosh, S. Formation and Stability of Pea Proteins Nanoparticles Using Ethanol-Induced Desolvation. *Nanomaterials* **2019**, *9* (7), 949. https://doi.org/10.3390/nano9070949.

(41) Teng, Z.; Luo, Y.; Wang, Q. Nanoparticles Synthesized from Soy Protein: Preparation, Characterization, and Application for Nutraceutical Encapsulation. *J. Agric. Food Chem.* **2012**, *60* (10), 2712–2720. https://doi.org/10.1021/jf205238x.

(42) Duan, L.; Yan, X.; Wang, A.; Jia, Y.; Li, J. Highly Loaded Hemoglobin Spheres as Promising Arti Fi Cial Oxygen Carriers. *ACS Nano* **2012**, *6* (8), 6897–6904. https://doi.org/10.1021/nn301735u.

(43) McDonel, E.; Hickey, R.; Palmer, A. Sonication Effectively Reduces Nanoparticle Size in Hemoglobin Based Oxygen Carriers (HBOCs) Produced Through Co-Precipitation. *ACS Appl. Nano Mater.* **2020**.

(44) Dybas, J.; Bokamper, M. J.; Marzec, K. M.; Mak, P. J. Probing the Structure-Function Relationship of Hemoglobin in Living Human Red Blood Cells. *Spectrochim. Acta - Part A Mol. Biomol. Spectrosc.* **2020**, *239*, 118530. https://doi.org/10.1016/j.saa.2020.118530.

(45) Berg, J. M.; Tymoczko, J. L.; Stryer, L. Covalent Modification Is a Means of Regulating Enzyme Activity. In *Biochemistry*; Freeman, W. H., Ed.; New York, USA, 2002.

(46) Spicer, C. D.; Davis, B. G. Selective Chemical Protein Modification. *Nat. Commun.* **2014**, *5* (1), 1–14. https://doi.org/10.1038/ncomms5740.

(47) York-Duran, M. J.; Ek, P. K.; Godoy-Gallardo, M.; Hosta-Rigau, L. Shear Stress Regulated Uptake of Liposome-Decorated Microgels Coated with a Poly(Dopamine) Shell. *Colloids Surf., B* **2018**, *171*, 427–436. https://doi.org/10.1016/J.COLSURFB.2018.07.031.

(48) Ju, K.-Y.; Lee, Y.; Lee, S.; Park, S. B.; Lee, J.-K. Bioinspired Polymerization of Dopamine to Generate Melanin-Like Nanoparticles Having an Excellent Free-Radical-Scavenging Property. *Biomacromolecules* **2011**, *12* (3), 625–632. https://doi.org/10.1021/bm101281b.

(49) Wang, Q.; Zhang, R.; You, G.; Hu, J.; Li, P.; Wang, Y.; Zhang, J.; Wu, Y.; Zhao, L.; Zhou, H. Influence of Polydopamine-Mediated Surface Modification on Oxygen-Release Capacity of Haemoglobin-Based Oxygen Carriers. *Artif. Cells, Nanomedicine, Biotechnol.* **2018**, *46* (sup2), 484–492. https://doi.org/10.1080/21691401.2018.1459636.

(50) Wang, Q.; Zhang, R.; Lu, M.; You, G.; Wang, Y.; Chen, G.; Zhao, C.; Wang, Z.; Song, X.; Wu, Y.; et al. Bioinspired Polydopamine-Coated Hemoglobin as Potential Oxygen Carrier with Antioxidant Properties. *Biomacromolecules* **2017**, *18* (4), 1333–1341. https://doi.org/10.1021/acs.biomac.7b00077.

(51) Kuhn, V.; Diederich, L.; Keller, T. C. S.; Kramer, C. M.; Lückstädt, W.; Panknin, C.; Suvorava, T.; Isakson, B. E.; Kelm, M.; Cortese-Krott, M. M. Red Blood Cell Function and Dysfunction: Redox Regulation, Nitric Oxide Metabolism, Anemia. *Antioxid. Redox Signaling* **2017**, *26* (13), 718–742. https://doi.org/10.1089/ars.2016.6954.

(52) Hu, J.; Yang, L.; Yang, P.; Jiang, S.; Liu, X.; Li, Y. Polydopamine Free Radical Scavengers. *Biomater. Sci.* **2020**, *8* (18), 4940–4950. https://doi.org/10.1039/d0bm01070g.

(53) Jansman, M. M. T.; Liu, X.; Kempen, P.; Clergeaud, G.; Andresen, T. L.; Thulstrup, P. W.; Hosta-Rigau, L. Hemoglobin-Based Oxygen Carriers Incorporating Nanozymes for the Depletion of Reactive Oxygen Species. *ACS Appl. Mater. Interfaces* **2020**, *12* (45), 50275–50286. https://doi.org/10.1021/acsami.0c14822.

(54) Lu, M.; Zhao, C.; Wang, Q.; You, G.; Wang, Y.; Deng, H.; Chen, G.; Xia, S.; Zhao, J.; Wang, B.; et al. Preparation, Characterization and in Vivo Investigation of Blood-Compatible Hemoglobin-Loaded Nanoparticles as Oxygen Carriers. *Colloids Surf., B* **2016**, *139*, 171–179. https://doi.org/10.1016/j.colsurfb.2015.12.012.

Chapter 4

Metal-Phenolic Networks as Broad-Spectrum Antioxidant Coatings for Hemoglobin Nanoparticles Working as Oxygen Carriers

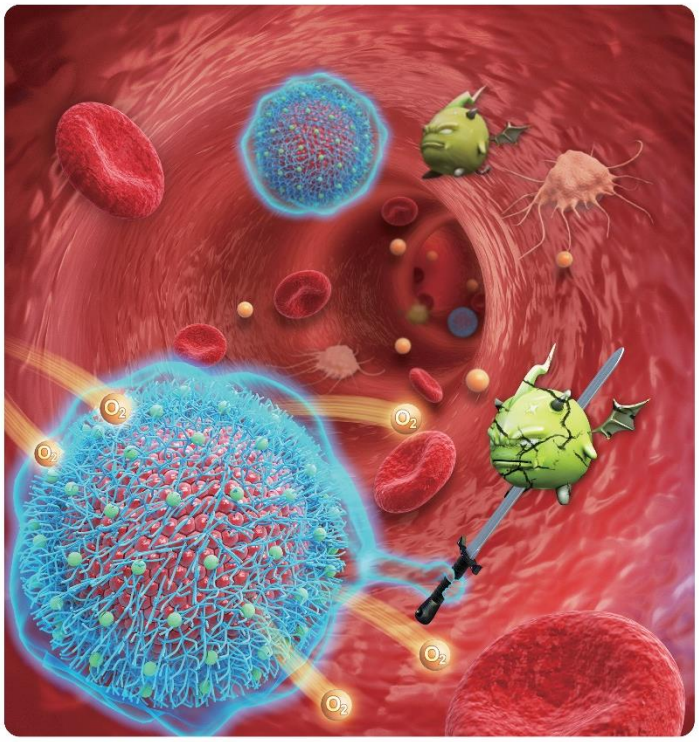

Chen, J.; Liu, X.; Jansman, M. M. T.; Thulstrup, P. W.; Hosta-Rigau, L. Metal-Phenolic Networks as Broad-Spectrum Antioxidant Coatings for Hemoglobin Nanoparticles Working as Oxygen Carriers. *Chemistry of Materials* **2022**, *34* (20), 9200–9211. https://doi.org/10.1021/acs.chemmater.2c02190.

Abstract

The timely administration of donor RBCs is a crucial and life-saving procedure to restore tissue oxygenation in patients suffering from acute blood loss. However, important drawbacks of using allogenic RBCs are their limited availability and portability, specific storage requirements, short shelf-life or the need for blood type matching. These limitations result in serious logistical challenges which make the transfusion of donor RBCs difficult in extreme life-threatening situations prior to hospital admission.

Thus, the engineering of Hb nanoparticles (Hb-NPs), which are free from the aforementioned limitations, has emerged as a promising strategy to create RBCs substitutes to be used when donor blood is not available. Despite the tremendous progress achieved in recent years many challenges still need to be overcome. For example, it is still difficult to create Hb-NPs with a high Hb content while also preventing the autoxidation of Hb into non-functional metHb. Herein, the fabrication of small, solid Hb-NPs with an antioxidant coating is reported. By desolvation precipitation, Hb-NPs with an average hydrodynamic diameter of ~250 nm and a PDI of ~0.1 are fabricated. A MPN layer consisting of a phenolic ligand (i.e., tannic acid) crosslinked through iron (III) ions is deposited onto the Hb-NPs surface to render antioxidant protection. The resulting MPN-coated Hb-NPs (MPN@Hb-NPs) maintain the ability of the encapsulated Hb to reversible bind and release O_2. The antioxidant properties are demonstrated, showing that MPN@Hb-NPs can effectively scavenge multiple reactive oxygen and nitrogen species, both in solution and in the presence of human RBCs and two relevant cell lines, namely macrophages and endothelial cells. Importantly, these outstanding antioxidant properties resulting from the MPN translate into decreased metHb conversion. Finally, the newly reported MPN@Hb-NPs are also biocompatible as shown by hemolysis rate and cell viability studies and can be used to protect the cells from oxidative damage. All in all, we have identified a novel strategy to minimize hem-mediated oxidative reactions which could potentially bring this new generation of HBOCs a step closer to the clinic.

4.1. Introduction

Despite being a lifesaving procedure, blood transfusions have important limitations which include the limited availability and portability, their short shelf life and special storage requirements, the need to check for blood type compatibility and the risk for disease transmission.[1]

Due to their ability to transport O_2, RBCs are the most essential component of transfused donor blood. Therefore, to overcome the limitations associated with donor blood, a lot of effort is currently being devoted to the fabrication of artificial RBCs[2–6]. An important class of RBCs substitutes are the so-called HBOCs. As indicated by their name, HBOCs make use of Hb which is the main functional component of RBCs and the responsible protein for binding and releasing O_2. Specifically, the current focus of HBOCs, rather than aiming to create a product that is either equivalent or superior to allogeneic RBCs, is to create an O_2 carrier to be used as a "bridging" solution in emergency situations.[4] In this context, the administration of HBOCs at the point-of-injury is envisioned to be a life-saving procedure for patients that have lost a significant volume of blood.[4] In contrast to donor RBCs, HBOCs are currently being engineered to display prolonged storage stability at ambient temperature, thus allowing for easy storage and portability. HBOCs are also universally employable due to the lack of blood antigens, which will allow for on-the-spot transfusion without the need for blood type testing. Additionally, HBOCs are expected to be free from disease transmission since they can potentially be prepared under sterile conditions. What is more, new research is indicating that HBOCs may find applications in other biomedical areas, such as organ preservation for transplant surgery, sickle cell crisis or brain oxygenation during circulatory arrest.[1,7–9]

Despite intense research efforts, no HBOC is currently approved for human use in USA or Europe which is a result of persistent safety concerns.[2,3] The first generation of HBOCs relied on the chemical modification of Hb to form complexes (i.e., the crosslinking or polymerization of Hb or its conjugation to polymers).[2] However, due to their small size, the resulting HBOCs, were able to extravasate in between the endothelial cells lining of the blood vessels.[10] Once extravasated, this first generation of HBOCs acted as NO scavengers leading to vasoconstriction and the subsequent cardiovascular complications, including the increased risk of myocardial infarction.[4] Additionally, these small-sized HBOCs had short circulation times since they were rapidly cleared by the kidneys and by the MPS in the spleen and liver, which also promoted toxicity in these organs.[4,11,12]

Thus, currently, a new generation of HBOCs aiming at increasing the overall size to the submicron range is being developed. For that, Hb is being encapsulated within a range of different carriers including liposomes, polymersomes, polymeric particles or MOFs-based particles.[13–17] Furthermore, the use of an encapsulating platform avoids the need to covalently modify Hb by polymerization or surface conjugation, which impairs Hb's cooperativity and modifies its O_2 transporting properties. However, despite the tremendous progress achieved in recent years, it is still challenging to develop encapsulating platforms with high loading content and encapsulation efficiency. This is an important aspect since, within RBCs, Hb constitutes about 96% of their dry weight and such a high amount of Hb is needed to supply the required amount of O_2 to our body.[13]

Another important limitation of HBOCs in general is that hem-mediated oxidative side reactions take place within the encapsulation platforms.[18,19] As such, without the reductase system present within native RBCs, Hb gets oxidized into metHb which is a process that results in the loss of O_2-transporting capability and in the generation of harmful ROS, which subsequently promotes cell and tissue damage.[18,20,21] In this context, the inclusion of antioxidants and anti-inflammatory molecules has emerged as a powerful strategy to protect Hb against oxidation.[18,22,23]

We recently reported a promising approach to create antioxidant HBOCs with a high Hb content by the fabrication of Hb-NPs.[24] We employed the desolvation precipitation method and screened several process parameters (i.e., the Hb concentration, ethanol (EtOH) to water phase ratio, sonication time and amplitude) to obtain Hb-NPs with a size of ~570 nm and a PDI of 0.2. Additionally, to stabilize the as-prepared Hb-NPs, a PDA coating was deposited. PDA, which is formed by the self-polymerization of DA in alkaline aqueous media, is an efficient adhesive material that can be deposited onto virtually any type of substrate including nanoparticulate systems. Importantly, the antioxidant properties of PDA rendered Hb-NPs that were able to scavenge the $O_2^{\bullet-}$ and H_2O_2, which are two of the most harmful ROS in our body.[25-27] Additionally, these ROS-scavenging properties obtained by the PDA coating translated into minimizing the autoxidation of the encapsulated Hb into metHb.

However, PDA coatings display also important drawbacks. For example, PDA degrades in physiological conditions and this degradation is, so far, an uncontrollable process. This is a result of the complex redox processes that are involved in the formation of PDA, which makes the exact mechanisms of PDA formation and disintegration still not fully understood.[28–33] This uncontrolled

degradation is an important limitation in the context of HBOCs which, in order to fulfil the high O_2 demands of our body, are expected to stay in circulation for extended periods of time.

Thus, to avoid the limitations of PDA and push forward the development of small Hb-NPs fully made of Hb with antioxidant properties, we herein report a simple, rapid and one-step coating method based on the self-assembly of coordination complexes.[34,35] Specifically, as shown in **Scheme 4.1**, the Hb-NPs prepared by desolvation precipitation are coated by MPNs, which are supramolecular network structures consisting of metal ions coordinated to phenolic ligands. Such a process is completed in minutes and can be conducted in aqueous solution and at ambient temperature. As the polyphenol and the metal crosslinker, tannic acid (TA) and Fe^{3+} were chosen, respectively. These compounds were chosen since TA is already approved by the US Food and Drug Administration (FDA) while iron ions are generally recognized as safe by the FDA. Importantly, TA is an antioxidant polyphenol with reported ability for the scavenging of free radicals.

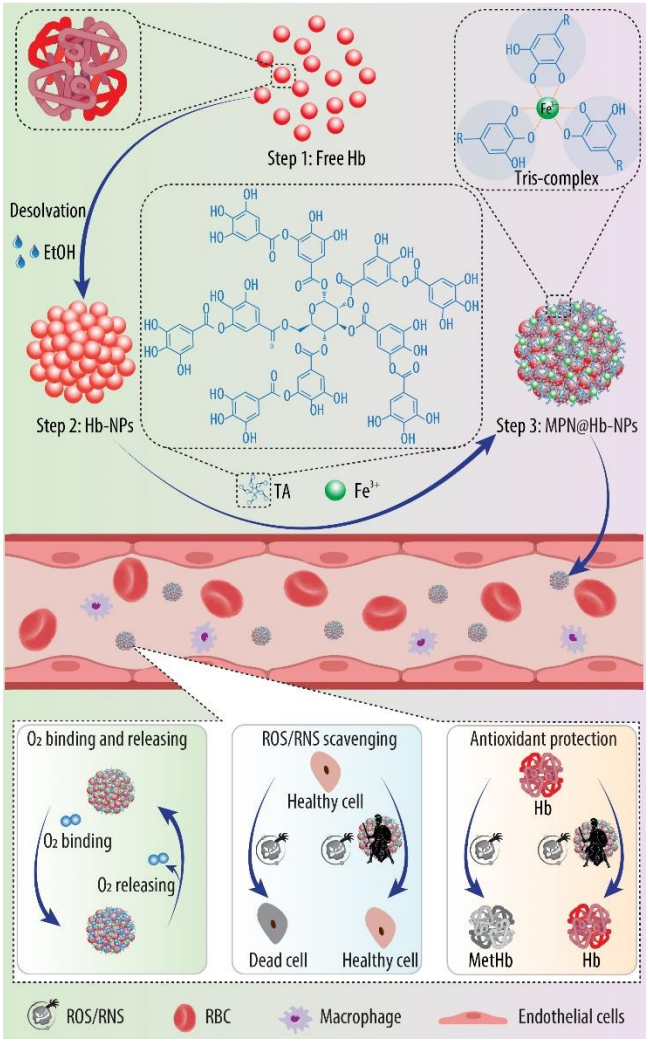

Scheme 4.1. Schematic illustration of the assembly process. Hemoglobin (Hb) nanoparticles (NPs) were fabricated by desolvation precipitation in ethanol (EtOH). A metal-phenolic network (MPN) coating was deposited via the interaction of tannic acid and iron III (Fe^{3+}). The resulting MPN@Hb-NPs were evaluated by their ability to bind and release oxygen (O_2), to deplete reactive oxygen (ROS) and nitrogen (RNS) species and their potential to minimize the oxidation of Hb into non-functional methemoglobin (metHb).

4.2. Materials and methods

4.2.1. Materials

EtOH, tannic acid (TA), iron (III) chloride hexahydrate ($FeCl_3 \cdot 6H_2O$), TRIS, SDT, H_2O_2, PBS, HCl, trolox, cell proliferation reagent WST-1, HRP, XO from bovine milk, xanthine, EDTA solution, 2,2-diphenyl-1-picrylhydrazyl ($DPPH^{\bullet}$), 2,2'-azino-bis(3-ethylbenzothiazoline-6-sulfonic acid) diammonium salt (ABTS), KO_2, potassium persulfate ($K_2S_2O_8$), nitrotetrazolium

blue chloride (NBT), potassium hexacyanoferrate ($K_3[Fe(CN)_6]$), trypsin, penicillin/streptomycin, HUVEC, DMEM D5796 and FBS were bought from Merck Life Science A/S (Søborg, DK). BCA protein assay kit, Pierce™ coomassie plus assay kit, Amicon Ultra (10 Kda), PrestoBlue cell viability reagent and Amplex Red reagent were purchased from Thermo Fisher Scientific (Roskilde, DK). The Hb used was extracted from bovine blood bought from SSI Diagnostica A/S (Hillerød, DK). Human blood was withdrawn from healthy donors in DTU-Health Technology at the University of Denmark (Kgs. Lyngby, DK). The blood withdrawal procedure was performed following approval and in accordance with the guidelines from the Regional Research Ethics Committees for the Capital Region of Denmark. The RAW 264.7 cell line was obtained from the European Collection of Authenticated Culture Collections (ECACC, Wiltshire, UK). ECM, 1% penicillin/streptomycin solution, 5% FBS and 1% endothelial cell growth supplement were obtained from Innoprot (Derio-Biskaia, ES). The HEK-293 and Hep G2 cells were obtained from American Type Culture Collection (ATCC, Manassas, Virginia, US).

4.2.2. Hb Extraction

Hb was obtained by from bovine blood following our previous protocol.[10] In detail, the same volume of saline (NaCl, 0.9%) and bovine blood was gently mixed and spun down (1500 g, 20 min) using a centrifuge (ThermoScientific, SL16R centrifuge, Langenselbold, DE). After removing the supernatant, the pellet containing the RBCs was washed with saline (NaCl, 0.9%) (2×, 1500g, 20 min) followed by the addition of a solution of MQ and toluene at a 1:0.4 volume ratio. The suspension was thoroughly mixed and allowed to separate in the different phases using a separatory funnel overnight and at 4 °C. The bottom phase containing a clear stroma-free Hb suspension was collected, placed in a falcon tube and spun down (8000g, 20 min). The Hb-containing supernatant was filtered through dust-free paper and stored in a freezer (−80 °C). The concentration of Hb was confirmed by a BCA assay.

4.2.3. Fabrication and Characterization of MPN-coated Hb-NPs (MPN@Hb-NPs)

4.2.3.1. MPN@Hb-NPs assembly.

First, Hb-NPs were fabricated following our previous protocol.[24] In brief, EtOH absolute (3 mL, 4 °C) was added dropwise to a Hb suspension in MQ (2 mL, 15.0 mg mL^{-1}, 4 °C), placed in an ice bath and under continuous stirring at 420 rpm using a magnetic stirring apparatus. The resulting turbid suspension (980 µL) was transferred to a 1.5 mL-Eppendorf tube and a TA solution (10 µL, 40 mg mL^{-1} in MQ) was rapidly added and vortexed for 5 sec. Next, $FeCl_3 \cdot 6H_2O$ (10 µL, 2.5 mg mL^{-1} in MQ) was rapidly added and the turbid suspension was vortexed by an additional 5 sec. The resulting dark red turbid suspension was spun down (3000g, 5 min, 4 °C) and washed in MQ (3×, 3000g, 5 min, 4 °C) using a bench-top centrifuge (Eppendorf, centrifuge 5804R, Hamburg, DE). Lastly, the obtained MPN@Hb-NPs were sonicated for 10 min by using an ultrasonic bath (EMERSON, St. Louis, USA) and stored at 4 °C until further use.

4.2.3.2. Characterization.

4.2.3.2.1. Size, PDI and zeta (ζ)-potential.

The size, PDI, and ζ-potentials of the Free Hb and MPN@Hb-NPs were evaluated by a Zetasizer nano ZS instrument (Malvern Instruments Ltd, Malvern, UK).

4.2.3.2.2. Hb content and concentration of MPN@Hb-NPs.

The Hb content within the MPN@Hb-NPs was determined as a weight percentage: Hb in the MPN@Hb-NPs (mg)/MPN@Hb-NPs (mg) × 100. To determine the amount of MPN@Hb-NPs, a known volume of MPN@Hb-NPs (in MQ) was lyophilized and weighted. For the amount of Hb in the MPN@Hb-NPs, the MPN@Hb-NPs were destroyed using HCl and the released Hb was purified by Amicon Ultra filter, then a Bradford assay was perfomed to determine the protein content. Due to the high Hb content of the MPN@Hb-NPs, the MPN@Hb-NPs concentration was also determined by using the Bradford assay as described above.

4.2.3.2.3. Scanning electron microscopy (SEM).

For the SEM micrographs, droplets of suspensions of MPN@Hb-NPs were added onto a glass slide and after 1 h of drying in the fume hood, the glass was mounted on a metal stub. Next, gold was sputtered onto the surface of the sample under vacuum and the coated samples were imaged using an FEI Quanta FEG 250 ESEM (FEI Company, Hillsboro, USA) at an operating voltage of 20 kV.

4.2.3.2.4. Hb's structure.

FTIR spectroscopy and circular dichroism (CD) studies. FTIR analysis was conducted using a PerkinElmer Spectrum 100 FT-IR spectrometer (PerkinElmer Inc., Wellesley, MA, USA). Free Hb and free MPN were set as control groups. CD spectra were obtained using a Jasco J-815 spectropolarimeter (JASCO, Essex, UK).

4.2.4. Oxygen Transporting Properties

4.2.4.1. Oxygen binding and releasing study.

The functionality of Hb entrapped within the MPN@Hb-NPs was evaluated by conducting an O_2-binding and releasing assay. For that, suspensions of free Hb (3 mL, 0.5 mg mL^{-1} in MQ) and MPN@Hb-NPs (3 mL, 0.5 mg mL^{-1} in MQ) were purged with compressed air or N_2 gas for 10 min in a closed system. The spectra of the suspensions were recorded using a UV-2600 UV-vis Spectrophotometer (Shimadzu, Kyoto, JP) in the wavelength range of 350–650 nm. When purging with N_2, a pinch of SDT was added to the solution to remove any residual O_2 before recording the spectrum.

4.2.4.2. Assessment of oxygen releasing.

The O_2 releasing ability of free Hb and MPN@Hb-NPs was next evaluated by measuring the O_2 concentration (μM) before and after the addition of $K_3[Fe(CN)_6]$, which reacts with the hem group of oxy-Hb and releases the bound O_2. In detail, 600 μL of free Hb (1–2.5 mg mL^{-1} in PBS) or MPN@Hb-NPs (1–2.5 mg mL^{-1} in PBS) were transferred to a glass vial tightly closed with a rubber cap, followed by the insertion of the O_2 probe needle. Next, the O_2 concentration before

and after the addition of 50 µL of 10% $K_3[Fe(CN)_6]$ was recorded with an O_2 meter (PreSens, Regensburg, DE).

4.2.4.3. Oxygen dissociation curve (ODC).

The ODCs of free Hb and MPN@Hb-NPs were obtained using a Hemox analyser (TSC Scientific Corp., New Hope, USA). For that, 3 mL of free Hb or MPN@Hb-NPs (1 mg mL^{-1} in PBS) were used for measuring (TCS Scientific Corp., New Hope, USA). The suspensions were purged with compressed air and N_2 to obtain oxygenized and deoxygenized Hb, respectively. After heating the samples to 37 ℃ and purging with compressed air to obtain oxygenized Hb, the samples deoxygenized with N_2 while simultaneously recording the ODCs. The Adair constants were calculated using linear iteration, after which the partial pressure of oxygen (pO_2) at which Hb is 50% saturated with oxygen (p50) and Hill coefficient (Hill-n) were obtained.

4.2.5. Free-Radical Scavenging

4.2.5.1. $O_2^{\bullet-}$ scavenging.

The scavenging of $O_2^{\bullet-}$ was evaluated by the NBT assay. For that, 150 µL of a mixture containing NBT (50 µL, 300 µM), riboflavin (50 µL, 80 µM), methionine (50 µL, 60 mM) all in PBS was added to a 96-well plate, followed by the addition of either free Hb (50 µL, 0.04–1 mg mL^{-1}), MPN@Hb-NPs (50 µL, 0.04–1 mg mL^{-1}) or trolox (50 µL, 0.04–1 mg mL^{-1}) all in PBS. Next, the well plate was illuminated with UV light for 10 sec at room temperature (RT) using a UV lamp (Omnicure series 1000, Lumen dynamics, Mississauga, CA) and the absorbance (Abs) readings due to the oxidized NBT (i.e., NBT-formazan) were recorded at 560 nm using a plate reader (Tecan Group Ltd., Männedorf, CH). A mixture containing only riboflavin, methionine and NBT placed in the dark or after UV exposure for 10 sec were used as negative and positive control, respectively. The normalized Abs (nAbs) was calculated using the following formula:

nAbs (%) = ((Abs of sample – Abs of negative control)/(Abs of positive control – Abs of negative control)) × 100.

4.2.5.2. H_2O_2 scavenging.

The scavenging of H_2O_2 was evaluated by the Amplex Red assay. For that, H_2O_2 (10 µL, 0.2 mM) was added to a suspension of free Hb (200 µL, 2.5×10^{-3}–1×10^{-2} mg mL^{-1}) or MPN@Hb-NPs (200 µL, 2.5×10^{-3}–1×10^{-2} mg mL^{-1}) all in TRIS 2 buffer. The samples were incubated using a thermoshaker (1400 rpm, 37 ℃) for 30 min, spun down (3000g, 5 min) and 180 µL of the supernatants were transferred to a new test tube and incubated for 5 min at 37 ℃ with HRP (10 µL, 2 U mL^{-1}) and Amplex Red (10 µL, 0.1 mM), all in TRIS 2 buffer. The mixtures (180 µL) were transferred to a black 96-well plate and the FI (λex/λem = 530/586 nm) was measured using the plate reader. A mixture of TRIS 2 (180 µL) and HRP (10 µL, 2 U mL^{-1}) and Amplex Red (10 µL, 0.1 mM) with and without the addition of H_2O_2 (10 µL, 0.2 mM) were used as positive and negative controls, respectively. The nFI was calculated with this formula:

nFI (%) = ((FI of sample - FI of negative control)/(FI of positive control - FI of negative control)) × 100.

4.2.5.3. $DPPH^{\bullet}$ scavenging.

The scavenging of $DPPH^{\bullet}$ was evaluated by mixing $DPPH^{\bullet}$ (200 µL, 0.042 mg mL^{-1} in EtOH) with either free Hb (10 µL, 0.04–1 mg mL^{-1}), MPN@Hb-NPs (10 µL, 0.04–1 mg mL^{-1}) or trolox (10 µL, 0.04–1 mg mL^{-1}) all in PBS in 96-well plate and incubated for 20 min at RT after which the Abs was recorded at 520 nm using the plate reader. PBS only and a mixture of PBS and $DPPH^{\bullet}$ solution were used as negative and positive controls, respectively. The nAbs was calculated as shown in Section 2.5.1.

4.2.5.4. ABTS free-radical ($ABTS^{\bullet+}$) scavenging.

The long-lived $ABTS^{\bullet+}$ was obtained by mixing $K_2S_2O_8$ (5 mL, 2.45 mM) and ABTS (5 mL, 2 mM) in PBS and letting it react in the dark for 4 h at RT. Next, the obtained $ABTS^{\bullet+}$ was diluted (4×) in PBS to an Abs reading of 0.9 at 734 nm. Then 100 µL of the $ABTS^{\bullet+}$ solution was incubated with either free Hb (10 µL, 0.04-1 mg mL^{-1}), MPN@Hb-NPs (10 µL, 0.04–1 mg mL^{-1}) or trolox (10 µL, 0.04–1 mg mL^{-1}) all in PBS for 5 min at RT and the Abs was recorded at 734 nm using the plate reader. PBS only and a mixture of PBS and $ABTS^{\bullet+}$ solution was used as negative and positive controls, respectively. The nAbs was calculated as shown in Section 2.5.1.

4.2.6. Biocompatibility

4.2.6.1. Hemolysis rate.

Donor blood was collected in heparin-coated tubes and washed in PBS (3×, 1000g, 4 °C, 15 min). Then, washed RBCs obtained from 1 mL of donor blood were resuspended into 50 mL PBS and 200 μL of these diluted RBCs were mixed with the MPN@Hb-NPs (300 μL, 1.28×10^{-3}–4 mg mL^{-1} in PBS). MQ (300 μL) and PBS (300 μL) were also added to the diluted RBCs and set as positive and negative controls, respectively. The obtained mixtures were incubated in a thermoshaker (gently shaking, 37 °C, 60 min) and spun down (1000g, 10 min, to obtain RBCs pellets). The supernatants were collected and spun down again (13 000g, 10 min, to obtain NPs pellets). The new supernatants were transferred to a 96-well plate and the Abs at 540 nm was recorded using the plate reader. The hemolysis rate was calculated with this formula:

Hemolysis rate (%) = ((Abs sample − Abs negative control)/(Abs positive control − Abs negative control)) × 100

Each condition was evaluated in triplicate in, at least, two independent experiments. The RBCs pellets collected after the first centrifugation step were re-suspended in PBS, then the morphology of the blood cells were assessed by using the Olympus Inverted IX83 microscope (bright field, 60× oil-immersion objective).

4.2.6.2. Cell culture.

DMEM containing penicillin/streptomycin (1% v/v, 10 000 U mL^{-1} and 10 μg mL^{-1}, respectively) and FBS (10% v/v) were used to culture RAW 264.7 cells, HEK-293 and Hep G2 cells, while ECM containing penicillin/streptomycin (1% v/v, 10 000 U mL^{-1} and 10 μg mL^{-1}, respectively), FBS (5% v/v) and endothelial cell growth supplements (1% v/v) was used to culture HUVEC cells. Both cell lines were cultured in T75 culture flasks by using a humidified incubator (5% CO_2, 37 °C). The cell culture medium was changed 2−3 times a week and cells were split when ∼80% confluence was reached. A cell scraper was used to detach RAW 264.7 cells while trypsin was used for the HUVEC cells. At subculture ratios of 1:5 for RAW 264.7 and 1:3 for HUVEC cells, the cells were resuspended in fresh cell culture media and transferred to new T75 culture flasks.

Only cell passages up to 18 for RAW 264.7 cells and up to14 for HUVECs were considered for the experiments.

4.2.6.3. Cell viability.

For the cell viability experiments, 30 000 RAW 264.7, 15 000 HUVEC, 10 000 Hep G2 or 20 000 HEK-293 per well were seeded in a 96-well plate and incubated for 24 h to allow cell attachment. PBS was used to wash the cells (2×, 150 μL) and following incubation with increasing concentrations of MPN@Hb-NPs (i.e., 200 μL, 1.28×10^{-3}–2 mg mL^{-1} in cell media) for another 4 h. Next, the cells were washed in PBS (2×, 150 μL) and incubated for 1 h in a PrestoBlue solution (100 μL, 10% v/v in cell media). The supernatants were collected and transferred to a 96-well plate to measure the FI (λex/λem: 535/615 nm). Media only and cells only were set as negative and positive controls, respectively. The nCV was calculated with the following formula:

nCV (%) = ((FI sample – FI negative control)/(FI positive control − FI negative control)) × 100

Each condition was evaluated in triplicate in at least three independent experiments.

4.2.7. H_2O_2 Scavenging in the Presence of Cells

4.2.7.1. H_2O_2 scavenging in the presence of RBCs.

To assess the hemolysis rate promoted by H_2O_2 concentration screening, washed RBCs obtained from 1 mL of donor blood (see Section 2.6.1 for details) were resuspended in 50 mL PBS. Then the diluted RBCs (200 μL) were incubated with H_2O_2 (300 μL at 50–800 mM in PBS) in a thermoshaker (gently shaking, 37 °C, 4 h). MQ and PBS (300 μL) were also added to the diluted RBCs and set as positive and negative controls, respectively. Next, the suspensions were spun down (1000g, 10 min, to obtain RBCs pellets), the supernatants were collected and centrifuged again (13 000g, 10 min, to obtain NPs pellets). The new supernatants were transferred to a 96-well plate and the Abs was recorded at 540 nm using the plate reader. The hemolysis rate was calculated as shown in Section 2.6.1.

The H_2O_2 scavenging by the MPN@Hb-NPs in the presence of RBCs was assessed by incubating washed and diluted RBCs (200 μL) with H_2O_2 (150 μL, 1600 mM) and MPN@Hb-NPs (150 μL, 0.5–4 mg mL^{-1}) all in PBS, for 4 h in a thermoshaker (gently shaking, 37 °C). Washed and diluted

RBCs (200 μL) incubated with only MQ (300 μL) was set as the positive control. And washed and diluted RBCs (200 μL) incubated with H_2O_2 (300 μL, 800 mM in PBS) was set as the H_2O_2 only group. After incubation, the samples were centrifuged (1000g, 10 min), the supernatants were collected and further spun down (13 000g, 10 min). The new supernatants were transferred to a 96-well plate, the Abs was recorded and the hemolysis rate was calculated as shown in Section 2.6.1. Each condition was evaluated in triplicate in at least two independent experiments.

4.2.7.2. H_2O_2 screening with RAW 264.7 and HUVEC cells.

RAW 264.7 (30 000) and HUVEC cells (15 000) were seeded in a 96-well plate and allowed to attach for 24 h. Next, PBS was used to wash the cells (2×, 150 μL) and the cells were then incubated for 4 h with increasing concentrations of H_2O_2 (200 μL, 25–1600 μM in cell media). Next, the cells were washed in PBS (2×, 150 μL) and incubated for another 24 h followed by washes in PBS (2×, 150 μL) and incubated for 1 h in a PrestoBlue solution (100 μL, 10% v/v in cell media). The supernatants were collected and transferred to a 96-well plate to measure the FI (λex/λem: 535/615 nm). Media only and cells only were set as negative and positive controls, respectively. The nCV was calculated as shown in Section 2.6.3. Each condition was evaluated in triplicate in at least three independent experiments.

4.2.7.3. H_2O_2 scavenging in the presence of RAW 264.7 and HUVEC cells.

RAW 264.7 (30 000) and HUVEC cells (15 000) were seeded in a 96-well plate and allowed to attach for 24 h. Next, PBS was used to wash the cells (2×, 150 μL) and the cells were then incubated for 4 h with increasing concentrations of MPN@Hb-NPs (100 μL, 16×10^{-8}–16×10^{-3} mg mL^{-1} in cell media) and H_2O_2 (100 μL, 200 μM for RAW 264.7 and 1600 μM for HUVEC, both in cell culture media). Cells in the presence of H_2O_2 but without MPN@Hb-NPs were also considered. Next, the cells were washed in PBS (2×, 150 μL) and incubated for another 24 h followed by washes in PBS (2×, 150 μL) and incubated for 1 h in a PrestoBlue solution (100 μL, 10% v/v in cell media). The supernatants were collected and transferred to a 96-well plate to measure the FI (λex/λem: 535/615 nm). Media only and cells only were set as negative and positive controls, respectively. The nCV was calculated as shown in Section 2.6.3. Each condition was evaluated in triplicate in at least three independent experiments.

4.2.8. Assessment of metHb content

H_2O_2 (30 µL, 1 M) was added to a suspension of free Hb or MPN@Hb-NPs (3 mL, 0.5 mg mL^{-1}) all in PBS. The Soret peak height over time was recorded at 416 nm using the UV-vis spectrometer. As controls, the Soret peak heights of free Hb and MPN@Hb-NPs without addition of H_2O_2 were recorded. The normalized Soret peak height was calculated with the following formula:

Normalised Soret peak height (%) =Abs sample with H_2O_2/Abs sample without H_2O_2 × 100

4.2.9. Statistics

A one-way ANOVA (confidence level of 95%, $\alpha = 0.005$) using Tukey's multiple comparisons test (*$p \leq 0.05$; **$p \leq 0.01$; ***$p \leq 0.001$; ****$p \leq 0.0001$) was employed to analysis the statistical difference between different groups, by using GraphPad Prism (9.1.2 (226)) software.

4.3. Results and discussion

4.3.1. Fabrication and Characterization of MPN@Hb-NPs

We, and others, have recently reported the fabrication of small, solid Hb-NPs by desolvation precipitation.[24,36] To obtain small and monodisperse NPs with this method, it is important to stop the growth of the NPs and to limit particle−particle interactions. For that, the Palmer group employed GA and oxidized Dex to stabilize the NPs through protein crosslinking, while in our group we coated the resulting Hb-NPs with PDA through the self-polymerization of DA.[24,36] While covalent modification of Hb with crosslinkers will inevitably alter Hb's conformation which will, in turn, affect its ability to bind and release O_2, PDA coatings also come with important limitations. These include an uncontrollable degradation behaviour in physiological conditions or potential neurotoxicity issues.[28,29,37,38] Thus, in this study we explore an alternative approach based on the complexation of polyphenols with Fe^{3+} through coordination bonds. Polyphenols such as TA contain the pyrogallol chemical group which is able to chelate with metal ions in a simple, rapid

and robust manner to form MPNs in a process that lasts only several minutes.[35,39] Although the use of MPNs represents an interesting alternative to PDA that is gaining popularity as shown by the wide range of nanocarriers that have been already coated (e.g., ZIF-8, PLGA NPs, $CaCO_3$ NPs, mesoporous silica NPs or gold NPs); thus far, MPN coatings have not been considered in the context of HBOCs.[35,40–44] Thus, herein, we advance the concept by fabricating, for the first time, an MPN-coated HBOC. The Hb-NPs were first formed by desolvation precipitation following our previously reported protocol.[24] After addition of EtOH, which was used as the antisolvent to create Hb-NPs, the MPN coating was deposited by simply adding the TA and a Fe^{3+} solution to the suspension. The colour of the suspension immediately turned dark red, indicating that the MPN coating to render MPN@Hb-NPs had been formed instantaneously (**Figure 4.1A**). SEM micrographs show monodisperse and spherical MPN@Hb-NPs (Figure 4.1B) with an average hydrodynamic diameter of ~250 nm with a relatively narrow size distribution (PDI < 0.1) (Figure 4.1C). The MPN@Hb-NPs have a 98.9% Hb content and display a positive ζ-potential (i.e., of 13.65 mV) resulting from the underlying positively charged Hb-NPs at solution pH (the isoelectric point of Hb is 6.8).[34] We would like to note that Hb-NPs without the MPN coating were not characterized (not here, nor in following experiments) since they cannot be isolated due to their lack of stability in aqueous media. However, the different size (i.e., of 6.7 nm) and ζ-potential (i.e., of -6.9 mV) of free Hb as shown in Figure S4.1 do further demonstrate that the MPN coating to render MPN@Hb-NPs had been formed instantaneously.

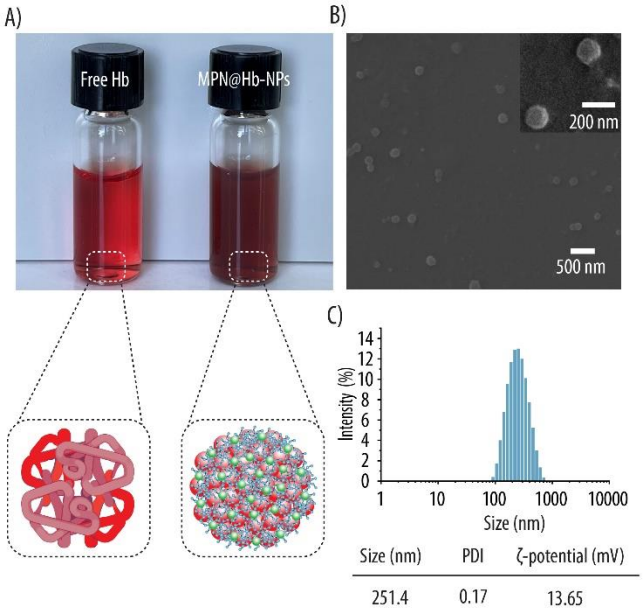

Figure 4.1. A) Photographic images of free Hb and Hb-NPs coated with a metal-phenolic network (MPN@Hb-NPs). B) Scanning electron microscopy and C) Size distribution, average size, polydispersity index (PDI) and zeta (ζ)-potential of the as-prepared MPN@Hb-NPs.

Next, FTIR was used to confirm the coordination between TA and Fe^{3+} and to rule out any potential effects of the MPN coating onto the chemical structure of the underlying Hb. This is an important aspect since the structure of proteins is closely related to their functionality. In proteins, the Amide I band (1600–1700 cm^{-1}) originates from the stretching vibrations of the C=O group and gives information about the conformation of the backbone while, the Amide II band (1510–1580 cm^{-1}), results from the in-plane N-H bending and C-N stretching vibrations. **Figure 4.2A** shows the FTIR spectra of MPN, free Hb and the MPN@Hb-NPs. The free Hb and the MPN@Hb-NPs displayed the characteristic bands of Amide I (at 1648 cm^{-1}) and Amide II (at 1533 cm^{-1}) showing that the chemical structure of Hb was preserved within MPN@Hb-NPs. Both the MPN and the MPN@Hb-NPs show the corresponding bands for the phenolate groups of the aromatic rings of TA at 1324 cm^{-1} and 1085 cm^{-1}, while the slightly shifted band at 1204 cm^{-1} indicates the interaction of phenolate groups with the Fe^{3+} center. Also, the absorption peak at 1439 cm^{-1} could further be attributed to the stretching vibration of the benzene ring skeleton.[45] Thus, once the successful assembly of Fe–TA film and preservation of Hb's chemical structure had been confirmed, we assessed any potential changes in the secondary structure by CD (Figure 4.2B). The spectra for both free Hb and MPN@Hb-NPs show the typical α-helical secondary structure with a maximum

at 195 nm and two minima at 208 nm and 222 nm. However, while both spectra display a similar band shape, the MPN@Hb-NPs have a clear reduction in molar ellipticity intensity which we attribute to the loss of α-helix structure for some of the Hb molecules upon being in contact with EtOH during the desolvation process.[26] Due to the chiral nature of TA and the tris complexes formed around Fe^{3+}, the MPN is expected to have a CD signal. Here MPN alone gave a CD signal with a weaker intensity of both positive and negative sign in the UV region. It is possible that the CD contribution of the MPN is altered when assembled in the MPN@Hb-NPs with contact to the chiral environment of Hb. Thus the deviation in CD between native Hb and the MPN@Hb-NPs could also stem from the spectral contribution of MPN.

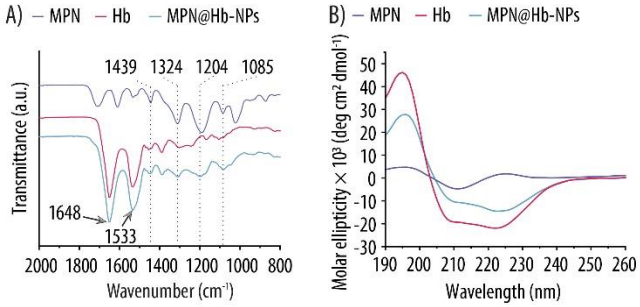

Figure 4.2. A) Fourier-transform infrared spectra of a metal phenolic network (MPN) resulting from the coordination between tannic acid and the iron ion, free Hb and the MPN-coated Hb-NPs (MPN@Hb-NPs). B) Circular dichroism spectra of free Hb, MPN and MPN@Hb-NPs.

4.3.2. Oxygen Transporting Ability

An ever-present concern when the secondary structure of a protein is altered is whether this will affect its functionality. Thus, we next assessed whether the Hb entrapped within the MPN@Hb-NPs preserved the ability to transport O_2. Hb has a characteristic UV-vis Abs spectrum that varies depending on the ligand state of the hem group. Hence, oxy-Hb displays a main band at 414 nm (known as the Soret peak) and two additional ones at 542 and 576 nm which are known as the Q-bands. In contrast, the characteristic Soret peak of deoxygenated Hb (deoxy-Hb) is located at 430 nm and the Q-band consists of a single peak at 554 nm. Thus, we assessed the ability of Hb to reversibly bind and release O_2 by monitoring the shifts of both the Soret peak and Q-band following a cycle of deoxygenation and re-oxygenation. **Figure 4.3A** shows that both free Hb and MPN@Hb-NPs display the expected Abs peaks of oxy-Hb (i.e., a Soret peak at 414 nm and the

two Q-bands at 541 and 576 nm). Following purging with N_2, both the free and the Hb entrapped within the MPN@Hb-NPs experienced the expected shifts towards the distinctive wavelengths of deoxy-Hb, as shown by the Soret peak at 429 nm and the single Q-band at 553 nm. Additional purging with compressed air promoted the expected shift back to the typical Abs spectra of oxy-Hb. Thus, these results indicate that, despite the reduced α-helical intensity observed by CD, the encapsulated Hb still maintained its ability to reversibly bind and release O_2. The amount of O_2 bound to Hb within the MPN@Hb-NPs was also evaluated by means of an O_2 electrode and compared to that of free Hb (Figure 4.3B). The amount of O_2 bound to both free Hb and Hb within MPN@Hb-NPs was concentration dependent since more O_2 was detected the higher the concentration of Hb. Although the amount of O_2 bound was always lower for the MPN@Hb-NPs as compared to free Hb (i.e., ~8–14 μM of O_2 less was bound to Hb entrapped within the MPN@Hb-NPs), ~70% of the encapsulated Hb remained functional. To get a deeper understanding of the O_2-binding abilities of the encapsulated Hb, the ODCs of free Hb and the MPN@Hb-NPs were evaluated. The ODC is determined by the ratio shift of signal in the visible region (at 560 and 570 nm) upon deoxygenation. Interestingly, this assessment could not be performed on our previous reported PDA-coated Hb-NPs (Hb/PDA-NPs) due to insufficient signal at these wavelengths.[24] This could either indicate loss of protein signal or signal shielding due to the PDA coating, making the newely developed MPN@Hb-NPs an improved system to assess the Hb's functionality. Figure 4.3C shows that, similarly to free Hb, the ODC of MPN@Hb-NPs displays the characteristic sigmoidal shape indicating that the binding of O_2 takes place in a positively cooperative manner. Throughout the body, Hb is exposed to different pO_2 and the amount of O_2 bound to Hb is related to this pO_2. In the lungs, where the pO_2 is high, the O_2 molecules readily bind to Hb promoting a change in conformation towards oxy-Hb. As a result of this conformational change, Hb's affinity for O_2 is enhanced and this promotes the binding of subsequent O_2 molecules, which results in Hb being saturated with O_2. Thus, for high pO_2, the ODC shows a plateau indicating complete saturation. In contrast, when blood transits to other body tissues with decreased pO_2, another change of conformation takes place promoting the release of O_2 to obtain deoxy-Hb. The O_2 equilibrium parameter p50, which indicates the pO_2 at which Hb is 50% saturated with O_2, it is almost identical for free Hb and MPN@Hb-NPs (i.e., 20.29 and 19.89 mmHg for free Hb and MPN@Hb-NPs, respectively) and very close the p50 of human Hb (~18.6 mmHg) and human blood (~23.8 mmHg for human Hb within RBCs).[46] This is an important

aspect since the p50 it is a good indicator of Hb's affinity for O_2 and it is considered as an important parameter for assessing different HBOCs. The Hill-n values for free Hb and MPN@Hb-NPs were calculated as 1.98 and 1.78, respectively. This is only a slight decrease in Hill-n following encapsulation, where the cooperativity of Hb is still well maintained (n > 1).

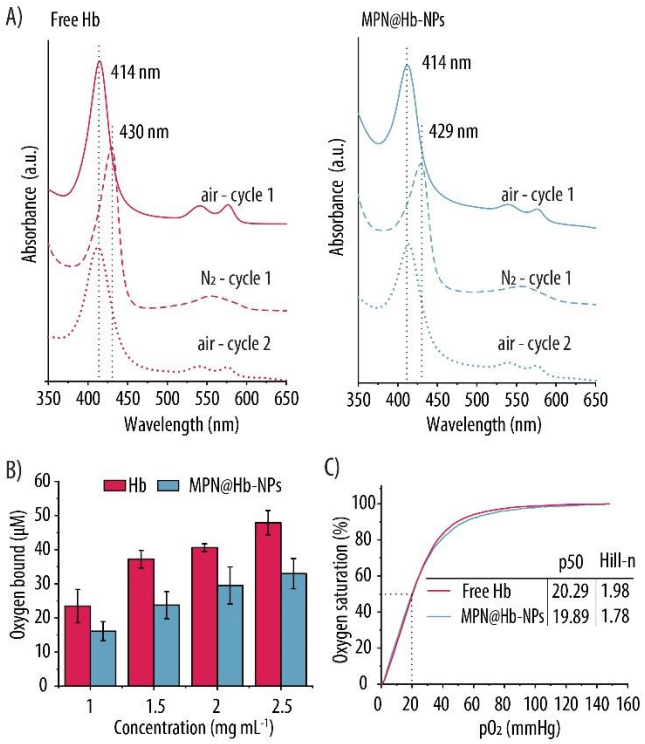

Figure 4.3. A) UV-vis spectra of free Hb and metal phenolic network (MPN)-coated Hb-NPs (MPN@Hb-NPs) after preparation and following purging with nitrogen gas (N_2) and compressed air. The wavelengths of the Soret peak are indicated. B) Oxygen released from free Hb and MPN@Hb-NPs. C) Oxygen dissociation curves of free Hb and MPN@Hb-NPs showing the relationship between the oxygen saturation of Hb and the partial oxygen pressure (pO_2) of the solution. The p50 (i.e., pO_2 at which 50% of Hb is saturated with oxygen) and Hill coefficient (Hill-n) values are also shown.

4.3.3. Scavenging Properties towards Reactive Oxygen and Nitrogen Species

Over time, Hb gets oxidized into metHb. Specifically, within RBCs 3% of Hb gets converted into metHb every 24 h.[3] However, this process is reverted by a set of endogenous antioxidant enzymes (i.e., CAT, SOD) with outstanding free radical scavenging capacities. Thus, herein, we explore the antioxidant protection rendered by the MPN coatings with the goal to eliminate, or at least minimize, Hb's conversion into metHb. Polyphenols such as TA are a class of organic compounds

with prominent antioxidant properties. They have the ability to neutralize harmful free radicals avoiding cellular damage and decreasing the risk of cancer, diabetes or heart disease.[47] Hence, as a first step we assess the ability of the as-prepared MPN@Hb-NPs to scavenge both ROS and reactive nitrogen species (RNS). To assess the effectiveness of the various assays, a trolox control was always added as a potent and well-known scavenger.

The ROS scavenging activity was investigated towards two representative ROS, namely $O_2^{\bullet-}$ and H_2O_2. **Figure 4.4A** shows the $O_2^{\bullet-}$ scavenging properties of both free Hb and the MPN@Hb-NPs, as evaluated by their ability to inhibit the photoreduction of NBT. With this assay, the $O_2^{\bullet-}$, which is produced by exposing riboflavin and methionine to UV radiation for 10 sec, is either consumed by NBT or by the antioxidant compound (i.e., MPN@Hb-NPs). For the former, NBT is oxidized into formazan, which displays a characteristic Abs signal at 560 nm. Thus, a decrease in the Abs signal indicates enhanced $O_2^{\bullet-}$ scavenging. Trolox, which is a water-soluble analogue of vitamin E (a well-known antioxidant), was used as the positive control. Figure 4.4Ai shows a significant decrease in nAbs by free Hb, MPN@Hb-NPs and trolox, which was concentration dependent. Specifically, at the lowest studied concentration (i.e., 0.04 mg mL^{-1}), the three compounds promoted a similar decrease in nAbs of ~25–30%. This result confirms $O_2^{\bullet-}$ scavenging properties for trolox, MPN@Hb-NPs and for free Hb, which oxidises into metHb in the presence of ROS.[24] However, upon increasing the concentration, the results where different and both MPN@Hb-NPs and trolox promoted a more pronounced decrease in nAbs than free Hb. These results where more evident for the highest studied concentration (i.e., 1 mg mL^{-1}) where MPN@Hb-NPs and trolox promoted a ~77 and ~100% decrease in nAbs, respectively (as compared to only a ~55% decrease for free Hb). Hence, these results indicate that MPN@Hb-NPs display higher $O_2^{\bullet-}$ scavenging properties than free Hb, probably resulting from the antioxidant MPN coating. The enhanced $O_2^{\bullet-}$ scavenging of MPN@Hb-NPs as compared to free Hb, could be ascribed to the ability of TA to transform $O_2^{\bullet-}$ into more stable H_2O_2 or O_2 by the transfer of hydrogen atoms or electrons, respectively.[48–50]

Following on, the scavenging ability towards H_2O_2 was evaluated by the Amplex Red assay (Figure 4.4Aii). With this assay, Amplex Red gets oxidized by H_2O_2 and HRP into resorufin, which can be detected at 586 nm by fluorescence measurements. Thus, scavenging of H_2O_2 will result in less resorufin product and in a decrease of the FI signal. Incubation of free Hb, MPN@Hb-NPs and trolox promoted a decrease in nFI and, such a decrease, was also concentration dependent.

However, the H_2O_2 scavenging properties of the three compounds were very different. As such, for the lowest studied concentration, free Hb promoted only a ~5% decrease in nFI, while the decrease in nFI was of ~28 and ~67% for MPN@Hb-NPs and trolox, respectively. As expected, higher concentrations resulted in higher H_2O_2 scavenging as shown by a ~63% and 97% decrease in nFI for Trolox and MPN@Hb-NPs (at 1×10^{-2} mg mL^{-1}), respectively. In contrast, free Hb resulted in only a ~40% decrease in nFI. Interestingly, when compared to the Hb/PDA-NP we developed in our previous study,[24] under the same exposure time (30 min), similar concentration (5 000 NPs μL^{-1}) of the Hb/PDA-NP (equal to 7.5×10^{-3} mg mL^{-1} of Hb inside the Hb/PDA-NP) promoted a ~35% decrease in nFI, while only 5×10^{-3} mg mL^{-1} of the MPN@Hb-NPs promoted a ~55% decrease in nFI, which means the MPN coating displays a better H_2O_2 scavenging capacity compared to the PDA coating.

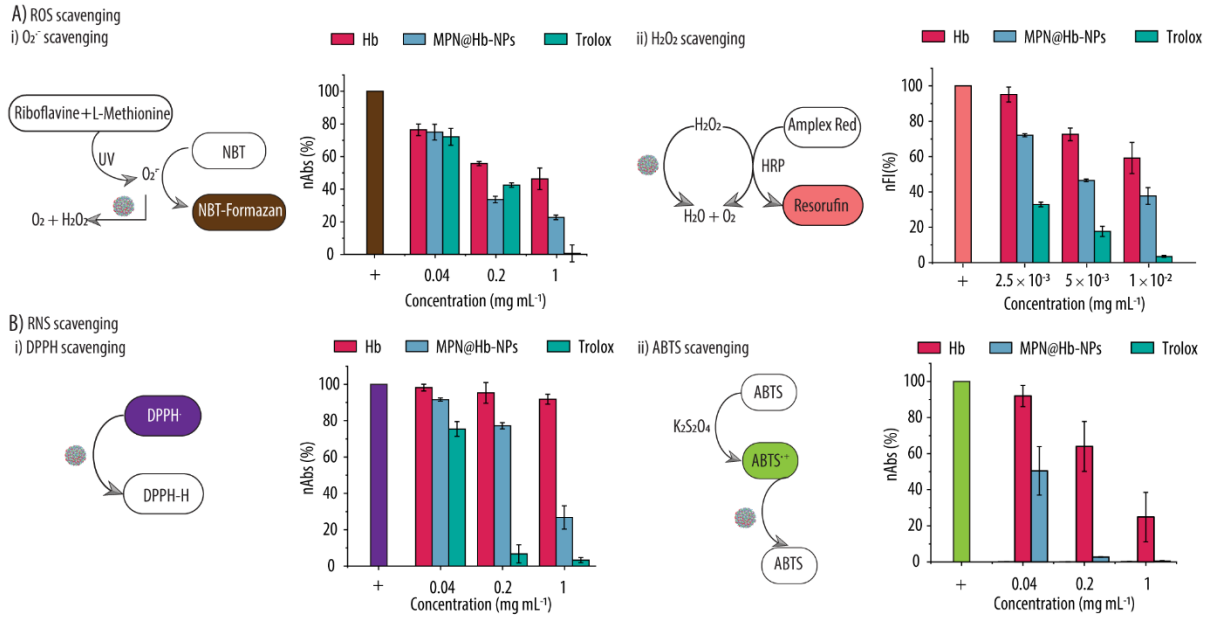

Figure 4.4. A) Scavenging of reactive oxygen species (ROS) by free Hb, metal phenolic network (MPN)-coated Hb-NPs (MPN@Hb-NPs) and trolox. i) Scavenging of the superoxide radical anion ($O_2^{\bullet-}$) which is generated by exposing riboflavin and methionine to UV radiation. $O_2^{\bullet-}$ can oxidise nitro blue tetrazolium (NBT) into the NBT-formazan which can be detected by absorbance (Abs) at 560 nm. The normalized Abs (nAbs) readings of free Hb, MPN@Hb-NPs and trolox incubated with $O_2^{\bullet-}$ and NBT are shown. ii) Scavenging of hydrogen peroxide (H_2O_2) which, in the presence of the enzyme horseradish peroxidase (HRP), can oxidise the Amplex Red reagent into resorufin which can be detected by fluorescence intensity (FI) measurements at 586 nm. The normalized FI (nFI) readings of free Hb, MPN@Hb-NPs and trolox incubated with H_2O_2, HRP and Amplex are shown. B) Scavenging of reactive nitrogen species (RNS). i) 1,1-Diphenyl-2-picryl-hydrazyl radical (DPPH$^{\bullet}$), which has a characteristic Abs band at 520 nm, can be reduced into 1,1-Diphenyl-2-picrylhydrazine ($DPPH_2$). The nAbs readings of free Hb, MPN@Hb-NPs and trolox incubated with DPPH$^{\bullet}$ are shown. ii) 2,2′-azinobis (3-ethylbenzothia-zoline-6-sulfonic acid) diammonium salt (ABTS) is oxidized into a stable radical ($ABTS^{\bullet+}$) by potassium persulfate ($K_2S_2O_8$) which has a characteristic Abs band at 734 nm. The nAbs readings of free Hb, MPN@Hb-NPs and trolox incubated with $ABTS^{\bullet+}$ are shown. In each assay, three different concentrations were assessed.

Next, the free-radical-scavenging properties towards RNS were evaluated. For that, we used DPPH$^{\bullet}$ and $ABTS^{\bullet+}$ since they are two typical nitrogen free radicals used to assess the RNS scavenging ability of nanomaterials.[18,48] Specifically, DPPH$^{\bullet}$ is a stable RNS which displays a characteristic Abs band at 517 nm. Thus, the scavenging of DPPH$^{\bullet}$ results in a decrease in the nAbs signal. Figure 4.4Bi shows how free Hb promotes a very slight decrease in nAbs when compared to MPN@Hb-NPs and trolox. Also, similarly as for ROS scavenging, the scavenging of this RNS is concentration dependent. For the highest studied concentration (i.e., 1 mg mL^{-1}), only a ~10% decrease in nAbs is observed for free Hb, while MPN@Hb-NPs and trolox promoted a ~72% and ~98% decrease in nAbs, respectively. This enhanced DPPH$^{\bullet}$ scavenging activity of

MPN@Hb-NPs as compared to free Hb, can be ascribed to the TA, which provide hydrogen atoms to scavenge $DPPH^{\bullet}$. Figure 4.4.Bii shows the scavenging properties towards $ABTS^{\bullet+}$ which is another stable RNS. $ABTS^{\bullet+}$ can be obtained by oxidating ABTS with $K_2S_2O_8$ and displays a strong Abs peak at 734 nm. Thus, $ABTS^{\bullet+}$ scavenging also results in a decrease of the Abs signal. In this case, the results show that the MPN@Hb-NPs displayed a very strong scavenging ability, since the middle and higher studied concentrations were able to reduce the nAbs by almost 100%. These results highlight the strong free radical scavenging properties towards both ROS and RNS rendered to Hb-NPs as a result of the MPN coating.

4.3.4. Biocompatibility

To ensure the normal physiological function of the body, the biocompatibility of the newly developed MPN@Hb-NPs was evaluated in terms of hemocompatibility and cell viability assays. Thus, the impact of MPN@Hb-NPs onto human RBCs was assessed by a hemolysis test. For that, increasing concentrations of MPN@Hb-NPs (i.e., up to 4 mg mL^{-1}) were incubated with RBCs for 1 h and the hemolysis rate was calculated by quantification of the released Hb. **Figure 4.5A** shows that up to a concentration of 2 mg mL^{-1}, the hemolysis rates are below 5%. Since, according to ISO/TR 7406, nanomaterials promoting a hemolysis rate below 5% can be considered non-hemolytic, we consider that MPN@Hb-NPs display good hemocompatibility at concentrations up to 2 mg mL^{-1}. Thus, only concentrations of 2 mg mL^{-1} or below will be considered in the upcoming experiments. Figure 4.5B shows the photographic images of the different RBCs suspensions incubated with MPN@Hb-NPs at the different studied concentrations as well as of the negative (0% lysis) and the positive (100% lysis) controls. The results are in agreement with the hemolysis rate results, since only the positive control displays the characteristic bright red colour of free Hb. The samples with MPN@Hb-NPs concentrations of 2 mg mL^{-1} or below are as colourless as the negative control. Figure 4.5C shows how the blood cells also retained their shape following incubation for 1 h with MPN@Hb-NPs at a concentration of 2 mg mL^{-1}. While similar low hemolysis rates were obtained for the MPN@Hb-NPs (0.97% at 3.2×10^{-2} mg mL^{-1}) compared to our previously reported Hb/PDA-NPs (<1%) at similar concentrations (highest concentration, 30 000 NPs μL^{-1}, equal to 4.5×10^{-2} mg mL^{-1} of Hb inside the Hb/PDA-NPs),[24] we could reach much

higher NPs concentrations (up to 2 mg mL^{-1}) for the new MPN@Hb-NPs before obtaining hemolysis values above 5%.

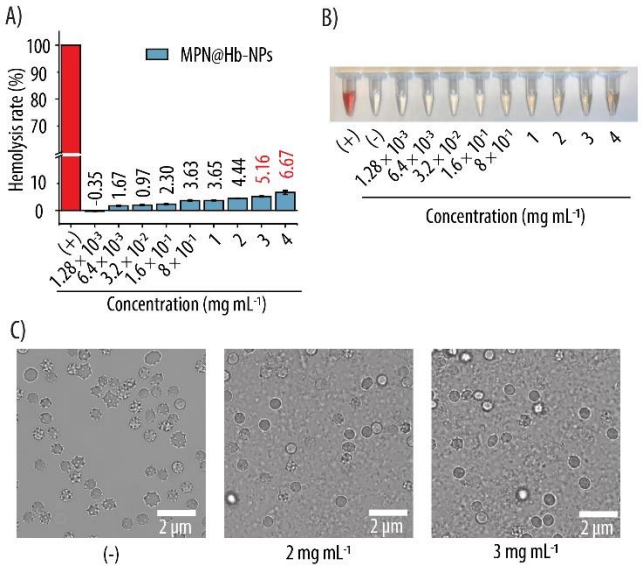

Figure 4.5. A) Hemolysis rate resulting from incubating increasing concentrations of metal phenolic network (MPN)-coated Hb-NPs (MPN@Hb-NPs) with red blood cells (RBCs) for 1 h at different concentrations. B) The photographic images of the corresponding supernatants are shown. C) Bright-field images of the negative control and RBCs incubated with MPN@Hb-NPs at two different concentrations. RBCs incubated with PBS and MQ only have been used as negative (−) and positive (+) controls, respectively.

After identifying the maximum concentration where the MPN@Hb-NPs can be considered as non-hemolytic, we further assessed their biocompatibility in terms of in vitro cell viability. For that, four relevant cell lines in the context of intravenous drug delivery were considered, namely the RAW 264.7 cell line as model of macrophages, the HUVEC cell line as a model of endothelial cells, the HEK-293 cell line as model of kidney cells and the Hep G2 cell line as model of liver cells. **Figure 4.6** shows the nCV readings for increasing concentrations of MPN@Hb-NPs incubated for 4 h with the four cell lines. First, the biocompatibility on HUVEC and RAW 264.7 cells were assessed as model for two cell types present in the intraveneous environment. For both cell lines, good cell viability data was obtained for all studies concentrations. The new developed MPN@Hb-NPs furthermore perform as good as our previous developed Hb/PDA-NPs (the highest test concentration, 30 000 NPs μL^{-1}, equal to 4.5×10^{-2} mg mL^{-1} of Hb inside the Hb/PDA-NPs) on RAW 264.7 cell line and HUVEC cell line.[24] Interestingly, a slight increase in nCV (up to ~115%)

could be detected for RAW 264.7 cells incubated with the highest concentrations of MPN@Hb-NPs (i.e., 3.2×10^{-2}–2 mg mL^{-1}). Next, to get insight in the effect of the MPN@Hb-NPs on the metabolic organs of our body, HEK-293 and Hep G2 cells were assessed. Even up to concentrations of 2 mg mL^{-1} MPN@Hb-NPs, no effect on the cell viability was observed. Thus importantly, no decrease in nCV could be detected for any of the studied concentrations independently of the cell line studied.

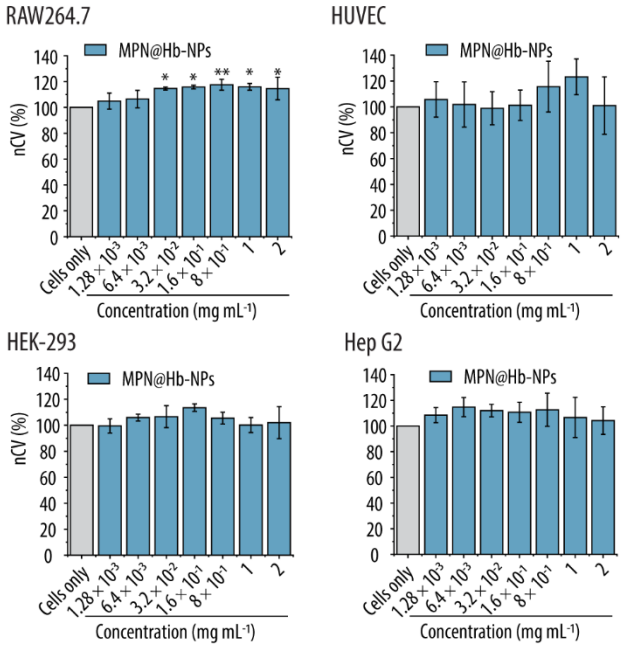

Figure 4.6. Normalized cell viability readings (nCV) after incubating increasing concentrations of metal phenolic network (MPN)-coated Hb-NPs (MPN@Hb-NPs) with RAW 264.7, HUVEC, HEK-293 and Hep G2 cells for 4 h. *p ≤ 0.05; **p ≤ 0.01. MPN@Hb-NPs vs cells only.

4.3.5. Antioxidant Activity in the Presence of Cells

Since the as-prepared MPN@Hb-NPs are expected to deplete free radicals in the body, we next evaluated their activity in the presence of cells. For this, we continued with the RBCs, RAW 264.7 and HUVECs as cell models, due to the main interaction of the MPN@Hb-NPs with these cell types upon intraveneous administration. H_2O_2 was further chosen as a representative free-radical. Despite the relevance of such an experiment, to assess the antioxidant properties of HBOCs, very few reports have taken into consideration the biological environment.[25,51] To show the protective effect of our newly developed MPN@Hb-NPs, we first evaluated the hemolysis rate upon

incubating RBCs with increasing concentrations of H_2O_2 (**Figure S4.2A**, Supporting Information). To demonstrate the potential of our system, the H_2O_2 concentrations chosen where in the mM range which are much higher than normally found in the body,[52] thereby inducing hemolytic conditions. Increasing amounts of MPN@Hb-NPs were incubated with a suspension of RBCs and H_2O_2 at a concentration of 800 mM, which produced a high hemolysis rate of ~85%. **Figure 4.7A** shows how incubation with MPN@Hb-NPs promoted a substantial decrease in the hemolysis rate and such a decrease was concentration dependent. The lowest studied concentration (i.e., 0.25 mg mL^{-1}) promoted a decrease to ~62% in hemolysis rate while for the highest one (i.e., 2 mg mL^{-1}), only a ~20% hemolysis rate was detected. These result shows the protective effect of our newly developed MPN@Hb-NPs towards RBCs, presumably due to their ROS scavenging ability.

Next, we evaluated whether the MPN@Hb-NPs where also able to promote a beneficial effect towards RAW 264.7 and HUVEC cells due to their ROS depletion ability. Thus, we incubated both cell lines with MPN@Hb-NPs and H_2O_2 for 4 h and assessed the nCV. As controls, only H_2O_2 without the NPs and cells only were considered. A H_2O_2 concentration of 800 μM and 100 μM was selected for HUVEC and RAW 264.7, respectively, since these two concentrations fall within the physiological range and promotes a marked decrease in nCV (see **Figure S4.2B** and C, Supporting Information). Figure 4.7B and 7C show the significant decrease in nCV for cells incubated with H_2O_2 only. Specifically, incubation with H_2O_2 resulted in a nCV of only ~43% and 20% for RAW 264.7 and HUVEC, respectively. However, upon incubation with MPN@Hb-NPs, already a marked increase in nCV (up to 50% and 35% for RAW 264.7 and HUVEC, respectively) was observed for the two cell lines at the lowest studied concentration (i.e., 8×10^{-8} mg mL^{-1}). Interestingly, the highest studied concentration (i.e., 8×10^{-3} mg mL^{-1}), promoted a 100% recovery in nCV for RAW cells and an improved nCV for the HUVEC cell line (i.e., a nCV of ~120% was observed in this case) as compared to the control of cells only. It is worth mentioning that the studied concentrations are well below the maximum tolerated by the RBCs (i.e., a concentration of 2 mg mL^{-1} which can be considered as non-hemolytic).

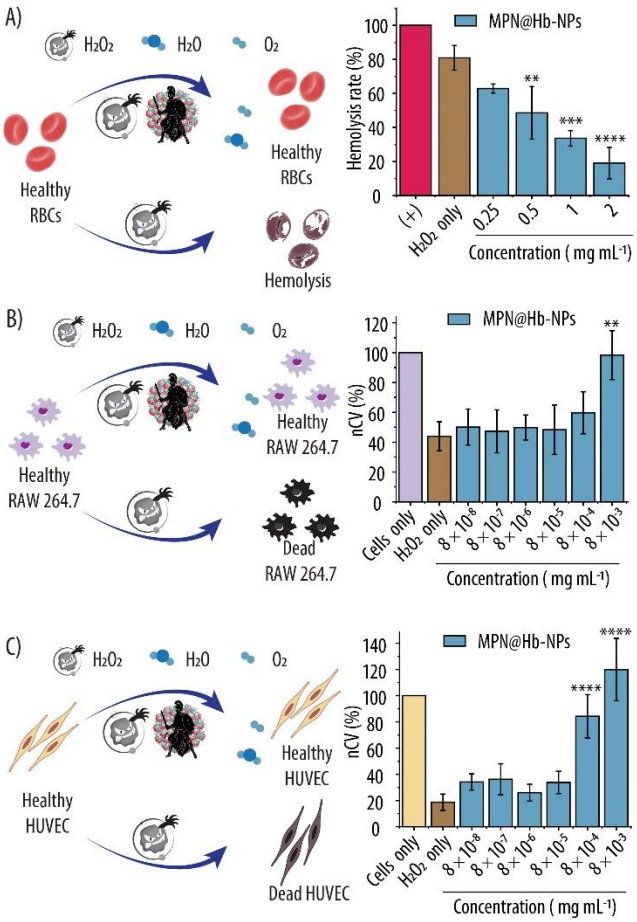

Figure 4.7. A) Hemolysis rate resulting from incubating red blood cells (RBCs) with hydrogen peroxide (H_2O_2) and increasing concentrations of metal phenolic network (MPN)-coated Hb-NPs (MPN@Hb-NPs) for 4 h. Normalized cell viability readings (nCV) after incubating RAW 264.7 (B) and HUVEC cells (C) with H_2O_2 and increasing concentrations of MPN@Hb-NPs for 4 h. $^{**}p \leq 0.01$; $^{***}p \leq 0.001$; $^{****}p \leq 0.0001$, MPN@Hb-NPs vs H_2O_2 only.

Thus, all in all, these results highlight that the strong antioxidant properties of the MPN@Hb-NPs resulting from the incorporated polyphenol-based coating translate into an important protective effect towards three relevant cell types that had been exposed to physiologically relevant concentrations of a prominent ROS, that is H_2O_2.

4.3.6. Antioxidant Protection towards Conversion into MetHb

Considering these very promising free-radical scavenging ability, we next assessed whether these antioxidant properties resulting from the MPN coating, also translated into reduced metHb conversion. Hence, we incubated both free Hb and MPN@Hb-NPs in a H_2O_2 solution to accelerate

the Hb's oxidation as monitored by the height of the oxy-Hb Soret peak over time (**Figure 4.8**). An instant ~11% decrease in normalized peak height was observed for free Hb. In contrast, the decrease in Soret peak height for MPN@Hb-NPs was four times less pronounced, with only a ~3% decrease. The differences in metHb content depending on the MPN coating were also obvious at the end of the incubation period where only a ~7% decrease in Soret peak height was observed for MPN@Hb-NPs as compared to the ~12% decrease for free Hb. This is an important achievement, since the unavoidable autoxidation of Hb is a crucial limitation for the successful implementation of HBOCs.

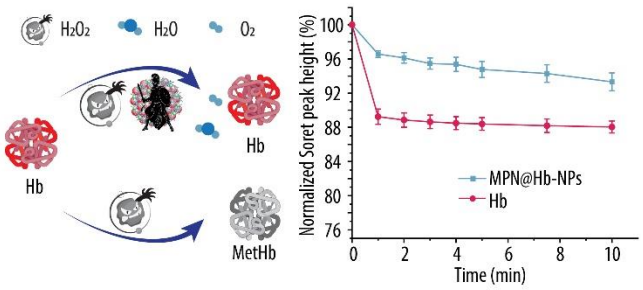

Figure 4.8. Normalized Soret peak height over time of free Hb and metal phenolic network (MPN)-coated Hb-NPs (MPN@Hb-NPs) in the presence of a 10 mM hydrogen peroxide (H_2O_2) solution.

4.4. Conclusions

In summary, we have fabricated small, solid Hb-NPs by desolvation precipitation with antioxidant properties resulting from an MPN coating. These newly reported MPN@Hb-NPs had an average hydrodynamic diameter of ~250 nm and a PDI < 0.1. These values indicate that the MPN@Hb-NPs are suitable for pharmaceutical applications. Preservation of Hb's functionality has been demonstrated by an O_2 binding and releasing assay, and the amount of released O_2 has been quantified using an O_2 electrode. Important parameters such as the p50 and Hill-n are further similar to the ones obtained for free Hb. Broad-spectrum free-radical scavenging properties have also been shown since the MPN@Hb-NPs are able to successfully scavenge both ROS and RNS. Furthermore, these antioxidant properties rendered by the MPN coating translate into a protective effect towards three relevant cell types (i.e., RBCs, RAW 264.7 cells and HUVECs) that had been exposed to various concentrations of H_2O_2, which is a prominent ROS. The as-prepared

MPN@Hb-NPs are also biocompatible as shown by hemolysis rate and cell viability studies. Finally, the MPN coating is able to slow down the oxidation of the entrapped Hb into metHb when exposed to H_2O_2.

4.5. Author information and associate content

Corresponding Author * Email: leri@dtu.dk

Funding Sources.This work has been supported by the Danish Council for Independent Research (Grant No. 6111-00298B) and by the European Research Council under the European Union's Horizon 2020 research and innovation programme (Grant No. 101002060).

Supporting information. Size distribution, average size, polydispersity index and zeta -potential of free Hb; H_2O_2 concentration screening on RBCs, RAW cell line, and HUVEC cell line.

Notes. The authors declare no competing financial interests.

4.6. References

(1) Jahr, J. S.; Guinn, N. R.; Lowery, D. R.; Shore-Lesserson, L.; Shander, A. Blood Substitutes and Oxygen Therapeutics: A Review. *Anesth. Analg.* **2020**, *132* (1) 119-129. https://doi.org/10.1213/ANE.0000000000003957.

(2) Jansman, M. M. T.; Hosta-Rigau, L. Recent and Prominent Examples of Nano- and Microarchitectures as Hemoglobin-Based Oxygen Carriers. *Adv. Colloid Interface Sci.* **2018**, *260*, 65–84. https://doi.org/10.1016/j.cis.2018.08.006.

(3) Coll-Satue, C.; Bishnoi, S.; Chen, J.; Hosta-Rigau, L. Stepping Stones to the Future of Haemoglobin-Based Blood Products: Clinical, Preclinical and Innovative Examples. *Biomater. Sci.* **2021**, *9* (4), 1135–1152. https://doi.org/10.1039/D0BM01767A.

(4) Sen Gupta, A.; Doctor, A. Oxygen Carriers. In Damage Control Resuscitation: Identification and Treatment of Life-Threatening Hemorrhage; Spinella, P. C., Ed.; *Springer International Publishing: Cham.* **2020**; pp 197–222. https://doi.org/10.1007/978-3-030-20820-2_11.

(5) Sen Gupta, A. Bio-Inspired Nanomedicine Strategies for Artificial Blood Components. *WIREs Nanomed. Nanobiotechnol.* **2017**, *9* (6), e1464. https://doi.org/10.1002/wnan.1464.

(6) Sen Gupta, A. Hemoglobin-Based Oxygen Carriers: Current State-of-the-Art and Novel Molecules. *Shock* **2019**, *52* (1S), 70–83. https://doi.org/10.1097/SHK.0000000000001009.

(7) Shellington, D. K.; Du, L.; Wu, X.; Exo, J.; Vagni, V.; Ma, L.; Janesko-Feldman, K.; Clark, R. S. B.; Bayir, H.; Dixon, C. E.; Jenkins, L. W.; Hsia, C. J. C.; Kochanek, P. M. Polynitroxylated Pegylated Hemoglobin: A Novel Neuroprotective Hemoglobin for Acute Volume-Limited Fluid Resuscitation after Combined Traumatic Brain Injury and Hemorrhagic Hypotension in Mice. *Crit. Care Med.* **2011**, *39* (3), 494–505. https://doi.org/10.1097/CCM.0b013e318206b1fa.

(8) Davis, J. M.; El-Haj, N.; Shah, N. N.; Schwartz, G.; Block, M.; Wall, J.; Tidswell, M.; DiNino, E. Use of the Blood Substitute HBOC-201 in Critically Ill Patients during Sickle Crisis: A Three-Case Series. *Transfusion* **2018**, *58* (1), 132–137. https://doi.org/10.1111/trf.14386.

(9) Matton, A. P. M.; Burlage, L. C.; van Rijn, R.; de Vries, Y.; Karangwa, S. A.; Nijsten, M. W.; Gouw, A. S. H.; Wiersema-Buist, J.; Adelmeijer, J.; Westerkamp, A. C.; Lisman, T.; Porte, R. J. Normothermic Machine Perfusion of Donor Livers without the Need for Human Blood Products. *Liver Transplant.* **2018**, *24* (4), 528–538. https://doi.org/10.1002/lt.25005.

(10) Jansman, M. M. T.; Coll-Satue, C.; Liu, X.; Kempen, P. J.; Andresen, T. L.; Thulstrup, P. W.; Hosta-Rigau, L. Hemoglobin-Based Oxygen Carriers Camouflaged with Membranes Extracted from Red Blood Cells: Optimization and Assessment of Functionality. *Biomater. Adv.* **2022**, *134*, 112691. https://doi.org/10.1016/j.msec.2022.112691.

(11) Buehler, P. W.; D'Agnillo, F.; Schaer, D. J. Hemoglobin-Based Oxygen Carriers: From Mechanisms of Toxicity and Clearance to Rational Drug Design. *Trends Mol. Med.* **2010**, *16* (10), 447–457. https://doi.org/10.1016/j.molmed.2010.07.006.

(12) Bunn, H. F.; Esham, W. T.; Bull, R. W. The Renal Handling of Hemoglobin: I. Glomerular Filtration. *J. Exp. Med.* **1969**, *129* (5), 909–924. https://doi.org/10.1084/jem.129.5.909.

(13) Coll-Satue, C.; Jansman, M. M. T.; Thulstrup, P. W.; Hosta-Rigau, L. Optimization of Hemoglobin Encapsulation within PLGA Nanoparticles and Their Investigation as Potential Oxygen Carriers. *Pharmaceutics* **2021**, *13* (11), 1958. https://doi.org/10.3390/pharmaceutics13111958.

(14) Rameez, S.; Alosta, H.; Palmer, A. F. Biocompatible and Biodegradable Polymersome Encapsulated Hemoglobin: A Potential Oxygen Carrier. *Bioconjug. Chem.* **2008**, *19* (5), 1025–1032. https://doi.org/10.1021/bc700465v.

(15) Sakai, H.; Sou, K.; Horinouchi, H.; Kobayashi, K.; Tsuchida, E. Review of Hemoglobin-Vesicles as Artificial Oxygen Carriers. *Artif. Organs* **2009**, *33* (2), 139–145. https://doi.org/10.1111/j.1525-1594.2008.00698.x.

(16) Liu, X.; Jansman, M. M. T.; Hosta-Rigau, L. Haemoglobin-Loaded Metal Organic Framework-Based Nanoparticles Camouflaged with a Red Blood Cell Membrane as Potential Oxygen Delivery Systems. *Biomater. Sci.* **2020**, *8* (21), 5859–5873. https://doi.org/10.1039/D0BM01118E.

(17) Gu, X.; Palmer, A. F. ZIF-8 Metal–Organic Framework Nanoparticles Loaded with Hemoglobin as a Potential Red Blood Cell Substitute. *ACS Appl. Nano Mater.* **2022**, *5* (4), 5670–5679. https://doi.org/10.1021/acsanm.2c00608.

(18) Baidukova, O.; Wang, Q.; Chaiwaree, S.; Freyer, D.; Prapan, A.; Georgieva, R.; Zhao, L.; Bäumler, H. Antioxidative Protection of Haemoglobin Microparticles (HbMPs) by PolyDopamine. *Artif. Cells, Nanomedicine, Biotechnol.* **2018**, *46* (sup3), S693–S701. https://doi.org/10.1080/21691401.2018.1505748.

(19) Eich, R. F.; Li, T.; Lemon, D. D.; Doherty, D. H.; Curry, S. R.; Aitken, J. F.; Mathews, A. J.; Johnson, K. A.; Smith, R. D.; Phillips George N.; Olson, J. S. Mechanism of NO-Induced Oxidation of Myoglobin and Hemoglobin. *Biochemistry* **1996**, *35* (22), 6976–6983. https://doi.org/10.1021/bi960442g.

(20) Balla, J.; Jacob, H. S.; Balla, G.; Nath, K.; Eaton, J. W.; Vercellotti, G. M. Endothelial-Cell Heme Uptake from Heme Proteins: Induction of Sensitization and Desensitization to Oxidant Damage. *Proc. Natl. Acad. Sci.* **1993**, *90* (20), 9285–9289. https://doi.org/10.1073/pnas.90.20.9285.

(21) Motterlini, R.; Foresti, R.; Vandegriff, K.; Intaglietta, M.; Winslow, R. M. Oxidative-Stress Response in Vascular Endothelial Cells Exposed to Acellular Hemoglobin Solutions. *Am. J. Physiol. Circ. Physiol.* **1995**, *269* (2), H648–H655. https://doi.org/10.1152/ajpheart.1995.269.2.H648.

(22) Alayash, A. I. Oxygen Therapeutics: Can We Tame Haemoglobin? *Nat. Rev. Drug Discov.* **2004**, *3* (2), 152–159. https://doi.org/10.1038/nrd1307.

(23) Alayash, A. I. Blood Substitutes: Why Haven't We Been More Successful? *Trends Biotechnol.* **2014**, *32* (4), 177–185. https://doi.org/10.1016/j.tibtech.2014.02.006.

(24) Chen, J.; Jansman, M. M. T.; Liu, X.; Hosta-Rigau, L. Synthesis of Nanoparticles Fully Made of Hemoglobin with Antioxidant Properties: A Step toward the Creation of Successful Oxygen Carriers. *Langmuir* **2021**, *37* (39), 11561–11572. https://doi.org/10.1021/acs.langmuir.1c01855.

(25) Liu, X.; Jansman, M. M. T.; Li, W.; Kempen, P.; Thulstrup, P. W.; Hosta-Rigau, L. Metal–Organic Framework-Based Oxygen Carriers with Antioxidant Protection as a Result of a Polydopamine Coating. *Biomater. Sci.* **2021**, *9* (21), 7257–7274. https://doi.org/10.1039/D1BM01005K.

(26) Liu, X.; Jansman, M. M. T.; Thulstrup, P. W.; Mendes, A. C.; Chronakis, I. S.; Hosta-Rigau, L. Low-Fouling Electrosprayed Hemoglobin Nanoparticles with Antioxidant Protection as Promising Oxygen Carriers. *Macromol. Biosci.* **2020**, *20* (2), 1900293. https://doi.org/10.1002/mabi.201900293.

(27) Jansman, M. M. T.; Liu, X.; Kempen, P.; Clergeaud, G.; Andresen, T. L.; Thulstrup, P. W.; Hosta-Rigau, L. Hemoglobin-Based Oxygen Carriers Incorporating Nanozymes for the Depletion of

Reactive Oxygen Species. *ACS Appl. Mater. Interfaces* **2020**, *12* (45), 50275–50286. https://doi.org/10.1021/acsami.0c14822.

(28) Hao, Y.-N.; Zheng, A.-Q.; Guo, T.-T.; Shu, Y.; Wang, J.-H.; Johnson, O.; Chen, W. Glutathione Triggered Degradation of Polydopamine to Facilitate Controlled Drug Release for Synergic Combinational Cancer Treatment. *J. Mater. Chem. B* **2019**, *7* (43), 6742–6750. https://doi.org/10.1039/C9TB01400D.

(29) Chen, X.; Yang, W.; Zhang, J.; Zhang, L.; Shen, H.; Shi, D. Alkalinity Triggered the Degradation of Polydopamine Nanoparticles. *Polym. Bull.* **2021**, *78* (8), 4439–4452. https://doi.org/10.1007/s00289-020-03312-2.

(30) Godoy-Gallardo, M.; Portolés-Gil, N.; López-Periago, A. M.; Domingo, C.; Hosta-Rigau, L. Multi-Layered Polydopamine Coatings for the Immobilization of Growth Factors onto Highly-Interconnected and Bimodal PCL/HA-Based Scaffolds. *Mater. Sci. Eng. C* **2020**, *117*, 111245. https://doi.org/10.1016/j.msec.2020.111245.

(31) Godoy-Gallardo, M.; Portolés-Gil, N.; López-Periago, A. M.; Domingo, C.; Hosta-Rigau, L. Immobilization of BMP-2 and VEGF within Multilayered Polydopamine-Coated Scaffolds and the Resulting Osteogenic and Angiogenic Synergy of Co-Cultured Human Mesenchymal Stem Cells and Human Endothelial Progenitor Cells. *Int. J. Mol. Sci.* **2020**, *21* (17), 6418. https://doi.org/10.3390/ijms21176418.

(32) Rahim, Md. A.; Kristufek, S. L.; Pan, S.; Richardson, J. J.; Caruso, F. Phenolic Building Blocks for the Assembly of Functional Materials. *Angew. Chemie Int. Ed.* **2019**, *58* (7), 1904–1927. https://doi.org/10.1002/anie.201807804.

(33) d'Ischia, M.; Napolitano, A.; Ball, V.; Chen, C.-T.; Buehler, M. J. Polydopamine and Eumelanin: From Structure–Property Relationships to a Unified Tailoring Strategy. *Acc. Chem. Res.* **2014**, *47* (12), 3541–3550. https://doi.org/10.1021/ar500273y.

(34) Hirotaka, E.; J, R. J.; Kang, L.; P, B. J.; P, van K. M.; K, S. G.; Jiwei, C.; Frank, C. One-Step Assembly of Coordination Complexes for Versatile Film and Particle Engineering. *Science* **2013**, *341* (6142), 154–157. https://doi.org/10.1126/science.1237265.

(35) Liu, P.; Shi, X.; Zhong, S.; Peng, Y.; Qi, Y.; Ding, J.; Zhou, W. Metal-Phenolic Networks for Cancer Theranostics. *Biomater. Sci.* **2021**, *9* (8), 2825–2849. https://doi.org/10.1039/D0BM02064H.

(36) Hickey, R.; Palmer, A. F. Synthesis of Hemoglobin-Based Oxygen Carrier Nanoparticles By Desolvation Precipitation. *Langmuir* **2020**, *36* (47), 14166–14172. https://doi.org/10.1021/acs.langmuir.0c01698.

(37) Cagnin, M.; Ozzano, M.; Bellio, N.; Fiorentino, I.; Follo, C.; Isidoro, C. Dopamine Induces Apoptosis in APPswe-Expressing Neuro2A Cells Following Pepstatin-Sensitive Proteolysis of APP in Acid Compartments. *Brain Res.* **2012**, *1471*, 102–117. https://doi.org/10.1016/j.brainres.2012.06.025.

(38) Michel, P. P.; Hefti, F. Toxicity of 6-Hydroxydopamine and Dopamine for Dopaminergic Neurons in Culture. *J. Neurosci. Res.* **1990**, *26* (4), 428–435. https://doi.org/10.1002/jnr.490260405.

(39) Guo, J.; Ping, Y.; Ejima, H.; Alt, K.; Meissner, M.; Richardson, J. J.; Yan, Y.; Peter, K.; von Elverfeldt, D.; Hagemeyer, C. E.; Caruso, F. Engineering Multifunctional Capsules through the Assembly of Metal–Phenolic Networks. *Angew. Chemie Int. Ed.* **2014**, *53* (22), 5546–5551. https://doi.org/10.1002/anie.201311136.

(40) Zhang, L.; Wan, S.-S.; Li, C.-X.; Xu, L.; Cheng, H.; Zhang, X.-Z. An Adenosine Triphosphate-Responsive Autocatalytic Fenton Nanoparticle for Tumor Ablation with Self-Supplied H_2O_2 and Acceleration of Fe(III)/Fe(II) Conversion. *Nano Lett.* **2018**, *18* (12), 7609–7618. https://doi.org/10.1021/acs.nanolett.8b03178.

(41) Li, L.; Yang, Z.; Fan, W.; He, L.; Cui, C.; Zou, J.; Tang, W.; Jacobson, O.; Wang, Z.; Niu, G.; Hu, S.; Chen, X. In Situ Polymerized Hollow Mesoporous Organosilica Biocatalysis Nanoreactor for Enhancing ROS-Mediated Anticancer Therapy. *Adv. Funct. Mater.* **2020**, *30* (4), 1907716. https://doi.org/10.1002/adfm.201907716.

(42) Zeng, T.; Zhang, X.; Guo, Y.; Niu, H.; Cai, Y. Enhanced Catalytic Application of Au@polyphenol-Metal Nanocomposites Synthesized by a Facile and Green Method. *J. Mater. Chem. A* **2014**, *2* (36), 14807–14811. https://doi.org/10.1039/C4TA02831G.

(43) Liu, T.; Zhang, M.; Liu, W.; Zeng, X.; Song, X.; Yang, X.; Zhang, X.; Feng, J. Metal Ion/Tannic Acid Assembly as a Versatile Photothermal Platform in Engineering Multimodal Nanotheranostics for Advanced Applications. *ACS Nano* **2018**, *12* (4), 3917–3927. https://doi.org/10.1021/acsnano.8b01456.

(44) Ping, Y.; Guo, J.; Ejima, H.; Chen, X.; Richardson, J. J.; Sun, H.; Caruso, F. PH-Responsive Capsules Engineered from Metal–Phenolic Networks for Anticancer Drug Delivery. *Small* **2015**, *11* (17), 2032–2036. https://doi.org/10.1002/smll.201403343.

(45) Chu, H.; Zheng, H.; Yao, J.; Sun, N.; Yan, G.; Deng, C. Magnetic Metal Phenolic Networks: Expanding the Application of a Promising Nanoprobe to Phosphoproteomics Research. *Chem. Commun.* **2020**, *56* (76), 11299–11302. https://doi.org/10.1039/D0CC04615A.

(46) Chu, Z.; Wang, Y.; You, G.; Wang, Q.; Ma, N.; Li, B.; Zhao, L.; Zhou, H. The P50 Value Detected by the Oxygenation-Dissociation Analyser and Blood Gas Analyser. *Artif. Cells, Nanomedicine, Biotechnol.* **2020**, *48* (1), 867–874. https://doi.org/10.1080/21691401.2020.1770272.

(47) Xie, W.; Guo, Z.; Zhao, L.; Wei, Y. Metal-Phenolic Networks: Facile Assembled Complexes for Cancer Theranostics. *Theranostics* **2021**, *11* (13), 6407–6426. https://doi.org/10.7150/thno.58711.

(48) Wei, Z.; Wang, L.; Tang, C.; Chen, S.; Wang, Z.; Wang, Y.; Bao, J.; Xie, Y.; Zhao, W.; Su, B.; Zhao, C. Metal-Phenolic Networks Nanoplatform to Mimic Antioxidant Defense System for Broad-Spectrum Radical Eliminating and Endotoxemia Treatment. *Adv. Funct. Mater.* **2020**, *30* (49), 2002234. https://doi.org/10.1002/adfm.202002234.

(49) Losada-Barreiro, S.; Bravo-Díaz, C. Free Radicals and Polyphenols: The Redox Chemistry of Neurodegenerative Diseases. *Eur. J. Med. Chem.* **2017**, *133*, 379–402. https://doi.org/10.1016/j.ejmech.2017.03.061.

(50) Nimse, S. B.; Pal, D. Free Radicals, Natural Antioxidants, and Their Reaction Mechanisms. *RSC Adv.* **2015**, *5* (35), 27986–28006. https://doi.org/10.1039/C4RA13315C.

(51) York-Duran, M. J.; Godoy-Gallardo, M.; Jansman, M. M. T.; Hosta-Rigau, L. A Dual-Component Carrier with Both Non-Enzymatic and Enzymatic Antioxidant Activity towards ROS Depletion. *Biomater. Sci.* **2019**, *7* (11), 4813–4826. https://doi.org/10.1039/C9BM00913B.

(52) de Gracia Lux, C.; Joshi-Barr, S.; Nguyen, T.; Mahmoud, E.; Schopf, E.; Fomina, N.; Almutairi, A. Biocompatible Polymeric Nanoparticles Degrade and Release Cargo in Response to Biologically Relevant Levels of Hydrogen Peroxide. *J. Am. Chem. Soc.* **2012**, *134* (38), 15758–15764. https://doi.org/10.1021/ja303372u.

4.7. Supporting information

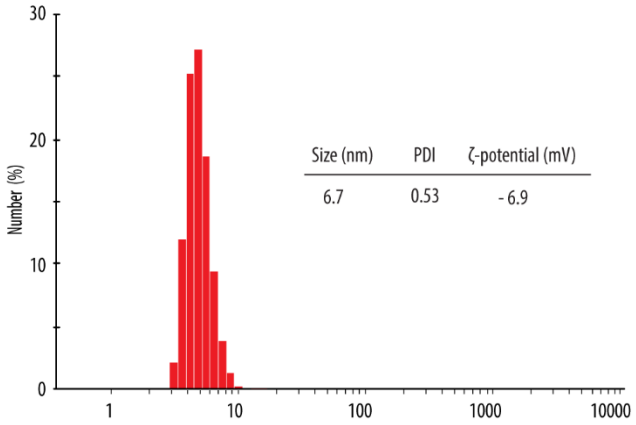

Figure S4.1 Size distribution, average size, polydispersity index (PDI) and zeta (ζ)-potential of free Hb

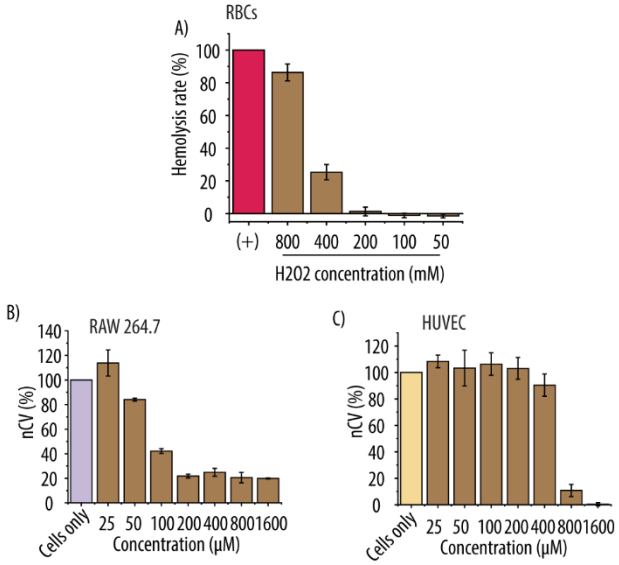

Figure S4.2. H_2O_2 concentration screening on A) RBCs, B) RAW, and C) HUVEC.

Chapter 5

Conclusions and Outlook

5.1. Conclusions

HBOCs with high Hb content and antioxidant properties were explored in this thesis. Specifically, in chapter 3, by using the desolvation technique and optimized parameters (using a 4.4 mg mL^{-1} Hb concentration, a 0.9× desolvation ratio and 40 sec of sonication with an amplitude of 30) during the desolvation process, Hb-NPs with a size of ~568 nm and a PDI of ~0.2 were fabricated. Then, by reacting with DA solution (1 mg mL^{-1} in TRIS 1) for 30 min, an antioxidant PDA coating was deposited on the surface of the Hb-NPs to further improve the stability of this system. The as-prepared Hb/PDA-NPs showed remarkable O_2 binding and releasing properties, and displayed ROS (e.g., $O_2^{\bullet-}$ and H_2O_2) scavenging capacity. More importantly, the PDA with antioxidant properties can shield the Hb inside the Hb/PDA-NPs from H_2O_2 damage, which can protect the Hb from being oxidized to unfunctional metHb. Finally, both the Hb-NPs and Hb/PDANPs show negligible cytotoxicity for two studied cell lines (i.e., RAW 264.7 cells and HUVECs) even at the highest studied concentration (i.e., 30 000 NPs μL^{-1}). At the same time, the hemolysis assay results show that both types of NPs display a hemolysis rate of less than 1% even at the highest studied concentration (i.e., 30 000 NPs μL^{-1}). Which suggests the as-prepared HBOC are biocompatible and hemocompatible.

In chapter 4, by a further optimization of the desolvation procedure which was conducted at 4 °C to minimize the autoxidation of Hb, a smaller, solid, and MPN-coated Hb-NPs were fabricated. The obtained MPN@Hb-NPs had a size of ~250 nm and a PDI of ~0.1. Such a size and PDI are regarded as suitable for pharmaceutical applications. The O_2 binding and releasing assay and O_2 electrode were used to determine the O_2 delivery capacity of MPN@Hb-NPs, which shows that ~70% of the function of Hb in the MPN@Hb-NPs was well preserved. Due to the remarkable antioxidant properties of MPN (i.e., derived from the TA), the MPN@Hb-NPs displayed broad-spectrum ROS/RNS (e.g., $O_2^{\bullet-}$, H_2O_2, $DPPH^{\bullet}$, and $ABTS^{\bullet+}$) scavenging properties as compared to the same concentration of free Hb. What is more, the ROS/RNS scavenging properties resulting from the MPN coating where able to promote a decrease in the rate of metHb conversion (i.e., only a ~7% decrease in Soret peak height was observed for MPN@Hb-NPs as compared to the ~12% decrease for free Hb). Further, MPN@Hb-NPs were able to protect three cell lines (i.e., RBCs, RAW 264.7 cells, and HUVECs) from H_2O_2-induced damage, that is, the highest studied concentration of MPN@Hb-NPs (2 mg mL^{-1}) can decrease the hemolysis rate caused by H_2O_2

from ~85% to ~20%, and the highest studied concentration of MPN@Hb-NPs (i.e., 8×10^{-3} mg mL^{-1}) can promote a 100% recovery in nCV for RAW cells and an improved nCV for the HUVEC cell line (i.e., a nCV of ~120%) as compared to the control of cells only group. Finally, the cell viability and hemolysis studies showed that the MPN@Hb-NPs displayed remarkable biocompatibility even at the highest studied concentration (2 mg mL^{-1}).

5.2. Outlook

In this PhD project, I have presented a novel way of fabricating HBOCs with high Hb content and antioxidant properties to accelerate the development of HBOCs. However, future work is needed to further explore these O_2 carriers.

5.2.1. Further improvement of the percentage of functional Hb.

Hb content is one of the important characteristics of HBOCs, which means high Hb content indicates a great O_2 delivery potential. In this PhD project, the Hb content of the novel-designed HBOC reached up to 98.9% which is very promising. However, the percentage of functional Hb in the HBOCs is another important issue that needs to be put into consideration. In Chapter 4, the released O_2 was measured by the O_2 electrode. Compared to the same concentration of free Hb, ~70% of the encapsulated Hb in the MPN@Hb-NPs remained functional. This means ~30% of Hb lost their function during the fabrication process. Nikolaidis et. al reported that EtOH can irreversibly denature whey protein,[1] so we hypothesized that the ~30% loss of Hb's function could be attributed to some of the Hb molecules being in contact with EtOH during the desolvation process. Therefore, it would be interesting to further optimize the desolvation parameters, for instance, decrease the desolvation time to minimize the interaction between Hb and EtOH and further decrease the amount of dysfunctional Hb.

5.2.2. Further exploration of the MPN coating process.

In this thesis, the Fe^{3+}-TA based MPN was used as a multifunctional surface coating for the as-formed Hb-NPs, including offering antioxidant properties to this system and acting as the surface crosslinking agent. The concentration of $FeCl_3 \cdot 6H_2O$ and TA should be high enough to form the MPN which can stabilize the Hb-NPs, but we found that a too high concentration of Fe^{3+} and TA results in aggregation for the resulting MPN@Hb-NPs, which cannot fulfil the requirement of the pharmaceutical application. Then, a balanced concentration of Fe^{3+} and TA was used in this thesis (i.e., 40 mg mL^{-1} of TA, 2.5 mg mL^{-1} of $FeCl_3 \cdot 6H_2O$), followed by MPN@Hb-NPs with a size

of ~250 nm, a PDI of ~0.1 and a yield of ~4%. It would be interesting to further assess different MPN coating (consisting of other polyphenol/metal ions) and to see if they have the potential in obtaining a higher yield of MPN@Hb-NPs, which can bring more possibility for future scaling up.

5.2.3. Incorporation of the stealth properties of HBOCs.

In this thesis, both PDA and MPN were used as an end surface coating since the in vitro studies showed that both of them display remarkable biocompatibility. However, as mentioned in Section 1.3.4, designing HBOCs with stealth properties to obtain a long circulation time in vivo is crucial. Unfortunately, I did not address this issue due to the time limitation of this PhD project. Thus, it would be interesting to perform serval strategies in future studies. Firstly, a PEG-modified polyphenol can be used for the MPN fabrication,[2] which could result in PEGylated MPN@Hb-NPs displaying long circulating times. Secondly, RBC-membrane was used for the end coating for HBOCs in our group. Specifically, both Hb-loaded MOF-NP,[3] and PLGA-NPs had been coated by membranes extracted from native human RBCs.[4] The post-RBC-membrane coating enabled the novel HBOCs to decrease the uptake by endothelial cells and macrophages. Thus, such an approach could be another choice for the post-modification of the Hb/PDA-NPs and MPN@Hb-NPs. Thirdly, Peng et al. reported albumin corona-coated PHBHHx NPs which showed a longer blood circulation time.[5] Besides, Ju et al. reported MPN capsules that were coated by a protein corona by simply incubating the MPN capsules with the human serum to enhance the targeting specificity of cancer cells.[6] Thus, it would be interesting to further explore the specifically selected protein corona modification to improve the stealth properties of Hb/PDA-NPs and MPN@Hb-NPs.

5.3.4. Further *in vitro* and *in vivo* investigations.

Upon the remarkable O_2 delivery capacity of the Hb/PDA-NPs and MPN@Hb-NPs shown in vitro, it would be interesting to further evaluate the capacity of these HBOCs to decrease the effect of hypoxia on cells. Specifically, cells (e.g., HUVEC) can be cultured under hypoxia for a period of time and, afterwards, the HBOCs can be added and keep the hypoxic condition for a particular

time, and then the cell viability can be measured to determine the O_2 delivery capacity on cells. Besides, immunogenicity test and anticoagulation test on the HBOCs need to be performed. Furthermore, it would be interesting to perform preclinical animal studies in the future to further evaluate the in vivo O_2 delivery capacity. For example, a hemorrhagic shock animal model can be established.[7] Specifically, the blood of mice will be withdrawn gradually until a critical level of the mean arterial pressure (MAP) (35 mmHg) is reached, then after a period of time (e.g., 10 min), the solution of Hb/PDA-NPs or MPN@Hb-NPs will be administrated and the MAP will be monitored and compared with the whole blood administration group.[7]

5.3.5. Investigate the application in cancer therapy.

Lastly, while the NPs fabricated in this thesis were designed to act as RBCs substitutes, these O_2 carriers should also be explored for different medical applications. For example, by delivering O_2 to a hypoxic tumor microenvironment and followed by killing the tumor cells, HBOCs can act as an O_2 therapeutic platform to target hypoxia in tumor therapy.[8] The Hb/PDA-NPs and MPN@Hb-NPs developed in this thesis showed remarkable O_2 delivery capacity in vitro, it would be interesting to investigate the use of Hb/PDA-NPs and MPN@Hb-NPs in cancer therapy. For example, the Hb/PDA-NPs can be used as a multifunctional platform for cancer therapy, where the Hb-NPs are responsible for the O_2 therapeutic and PDA act as a photothermal material. And for the MPN@Hb-NPs, we can expect a 3-in-1 platform for cancer therapy. That is, chemotherapeutic agents (e.g., DOX) can be co-loaded when fabricating the Hb-NPs by desolvation, then the post-MPN coating (consisting of PEGylated TA) can keep the as-formed drug delivery system stable in physiological condition (pH 7.4). However, when these NPs reached tumor tissues where there is an acidic microenvironment (pH 5.7–6.8),[9] due to the pH-responsive properties of MPN mentioned in Section 1.4.3.2, the MPN coating can be disassembled gradually and release the three therapeutic compounds, where the Hb is responsible for O_2 therapeutic, the DOX act as a chemotherapeutic agent, and the released TA act as a nature-derived anti-cancer compound..

5.4. References

(1) Nikolaidis, A.; Moschakis, T. On the Reversibility of Ethanol-Induced Whey Protein Denaturation. *Food Hydrocoll* **2018**, *84*, 389–395. https://doi.org/https://doi.org/10.1016/j.foodhyd.2018.05.051.

(2) Ju, Y.; Cui, J.; Müllner, M.; Suma, T.; Hu, M.; Caruso, F. Engineering Low-Fouling and PH-Degradable Capsules through the Assembly of Metal-Phenolic Networks. *Biomacromolecules* **2015**, *16* (3), 807–814. https://doi.org/10.1021/bm5017139.

(3) Liu, X.; Jansman, M. M. T.; Hosta-Rigau, L. Haemoglobin-Loaded Metal Organic Framework-Based Nanoparticles Camouflaged with a Red Blood Cell Membrane as Potential Oxygen Delivery Systems. *Biomater Sci* **2020**, *8* (21), 5859–5873. https://doi.org/10.1039/D0BM01118E.

(4) Jansman, M. M. T.; Coll-Satue, C.; Liu, X.; Kempen, P. J.; Andresen, T. L.; Thulstrup, P. W.; Hosta-Rigau, L. Hemoglobin-Based Oxygen Carriers Camouflaged with Membranes Extracted from Red Blood Cells: Optimization and Assessment of Functionality. *Biomaterials Advances* **2022**, *134*, 112691. https://doi.org/https://doi.org/10.1016/j.msec.2022.112691.

(5) Peng, Q.; Wei, X.-Q.; Yang, Q.; Zhang, S.; Zhang, T.; Shao, X.-R.; Cai, X.-X.; Zhang, Z.-R.; Lin, Y.-F. Enhanced Biostability of Nanoparticle-Based Drug Delivery Systems by Albumin Corona. *Nanomedicine* **2015**, *10* (2), 205–214. https://doi.org/10.2217/nnm.14.86.

(6) Ju, Y.; Dai, Q.; Cui, J.; Dai, Y.; Suma, T.; Richardson, J. J.; Caruso, F. Improving Targeting of Metal–Phenolic Capsules by the Presence of Protein Coronas. *ACS Appl Mater Interfaces* **2016**, *8* (35), 22914–22922. https://doi.org/10.1021/acsami.6b07613.

(7) Zhuang, J.; Ying, M.; Spiekermann, K.; Holay, M.; Zhang, Y.; Chen, F.; Gong, H.; Lee, J. H.; Gao, W.; Fang, R. H.; Zhang, L. Biomimetic Nanoemulsions for Oxygen Delivery In Vivo. *Advanced Materials* **2018**, *30* (49), 1804693. https://doi.org/https://doi.org/10.1002/adma.201804693.

(8) Spiess, B. D. Oxygen Therapeutic Agents to Target Hypoxia in Cancer Treatment. *Curr Opin Pharmacol* **2020**, *53*, 146–151. https://doi.org/https://doi.org/10.1016/j.coph.2020.09.009.

(9) Ping, Y.; Guo, J.; Ejima, H.; Chen, X.; Richardson, J. J.; Sun, H.; Caruso, F. PH-Responsive Capsules Engineered from Metal–Phenolic Networks for Anticancer Drug Delivery. *Small* **2015**, *11* (17), 2032–2036. https://doi.org/https://doi.org/10.1002/smll.201403343.